

Distribution Agreement

In presenting this thesis or dissertation as a partial fulfillment of the requirements for an advanced degree from Emory University, I hereby grant to Emory University and its agents the non-exclusive license to archive, make accessible, and display my thesis or dissertation in whole or in part in all forms of media, now or hereafter known, including display on the world wide web. I understand that I may select some access restrictions as part of the online submission of this thesis or dissertation. I retain all ownership rights to the copyright of the thesis or dissertation. I also retain the right to use in future works (such as articles or books) all or part of this thesis or dissertation.

DocuSigned by:
Signature: *Alishah Lakhani*
5A311439BB36448...

Alishah Lakhani
Name

10/17/2024 | 11:47 AM EDT
Date

Title Exploring homeostatic regulation in neuronal systems: Insights from cortical cultures, embryonic chick spinal cord, and the Fmr1 KO mouse model

Author Alishah Lakhani

Degree Doctor of Philosophy

Program Biological and Biomedical Sciences
Neuroscience

Approved by the Committee

Signed by:

33988437DE0F4E7...

Peter Wenner
Advisor

DocuSigned by:

63FF90548572448...

Nicholas Au Yong
Committee Member

Signed by:

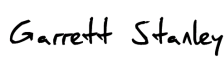
80F33F01F01E491...

Malavika Murugan
Committee Member

DocuSigned by:

3686AEF627D5496...

Astrid Prinz
Committee Member

DocuSigned by:

464AA8AEE1754F9...

Garrett Stanley
Committee Member

Committee Member

Accepted by the Laney Graduate School:

Kimberly Jacob Arriola, Ph.D, MPH
Dean, James T. Laney Graduate School

Date

Exploring homeostatic regulation in neuronal systems: Insights from cortical cultures, embryonic chick spinal cord, and the *Fmr1* KO mouse model

By

Alishah Lakhani
B.S., Davidson College, 2018

Advisor:
Pete Wenner, Ph.D.

An abstract of
A dissertation submitted to the Faculty of the James T. Laney School of Graduate Studies of Emory
University in partial fulfillment of the requirements for the degree of
Doctor of Philosophy

Graduate Division of Biological and Biomedical Science
Neuroscience

2024

Abstract

Exploring homeostatic regulation in neuronal systems: Insights from cortical cultures, embryonic chick spinal cord, and the *Fmr1* KO mouse model

By Alishah Lakhani

Homeostatic plasticity encompasses a set of mechanisms that are crucial for stabilizing various characteristics of neural activity despite any perturbations the nervous system might encounter. This dissertation explores homeostatic regulation and plasticity in three different systems: neuronal cortical cultures, the embryonic chick spinal cord, and the Fragile X Syndrome (FXS) mouse model. In the first study, we investigated the effects of GABAergic blockade on neuronal firing in mouse cortical cultures and motoneurons in the embryonic chick spinal cord. After conducting a comprehensive analysis of various spiking activity characteristics, we found that the response to GABAergic blockade was variable across many spiking features, including burst frequency and overall spike frequency. However, the spike rate within a burst consistently increased and then returned to baseline control levels within hours in both systems, suggesting that this feature is robustly homeostatically maintained. In the second study, we used a mouse model of FXS, the *Fmr1* KO mouse, to examine if there are impairments in homeostatic plasticity following unilateral whisker deprivation in layer 5/6 of the barrel cortex. Our results demonstrate significant deficits in the recruitment of excitatory and inhibitory neurons, both at baseline and following whisker deprivation. In addition, we observed a change in the sensitivity of excitatory neurons at a later developmental time point. Together, these two studies provide insights into how networks maintain stable activity levels through homeostatic plasticity mechanisms, and how perturbations affect normal spiking activity, in both *in vitro* and *in vivo* experimental models.

Exploring homeostatic regulation in neuronal systems: Insights from cortical cultures, embryonic chick spinal cord, and the *Fmr1* KO mouse model

By

Alishah Lakhani
B.S., Davidson College, 2018

Advisor:
Pete Wenner, Ph.D.

A dissertation submitted to the Faculty of the James T. Laney School of Graduate Studies of Emory University in partial fulfillment of the requirements for the degree of
Doctor of Philosophy

Graduate Division of Biological and Biomedical Science
Neuroscience

2024

Acknowledgments

This dissertation would not have been possible without the support of many people. First and foremost, I would like to thank my advisor, Dr. Pete Wenner, for your mentorship, training, and discussions that have been invaluable to my time in graduate school – I've become a much better scientist and writer with your guidance and feedback. Thank you for fostering an inclusive and welcoming lab environment, with our monthly First Fridays. Thank you for always listening and for making the lab feel like home. Your endless optimism has been refreshing, and I truly appreciate that. Thank you to Dr. April Ratliff, Washington Huang, and Dr. Carlos Gonzalez Islas for making the lab home. A very special thank you to Dr. Dobromila Pekala, who has always been my support system both inside and outside of lab.

I would also like to thank each one of my committee members. Dr. Garrett Stanley, thank you and your lab, specifically Dr. Caleb Wright, for advice on how to setup experimental paradigms, start the computational analyses, and the expertise you provided about the barrel cortex. Dr. Nicholas Au Yong, thank you for your help with setting up Kilosort and your professional guidance. Dr. Malavika Murugan, thank you for your insightful questions and feedback during the committee meetings. Dr. Astrid Prinz, thank you for your feedback on my first manuscript and for providing another homeostatic plasticity perspective. The dynamics of this committee were crucial to the completion of my degree.

In addition, thank you to Bill Goolsby for the design and construction of much of the equipment that I used for this dissertation. Thank you to Dr. Gary Bassell and his lab, specifically Jingsheng Gu, for providing us with animals to start our own mouse colony and helping with any difficulties with the animals. Finally, I could not have completed this dissertation without the support and guidance of Dr. Chris Rodgers. Since he arrived at Emory, Dr. Rodgers has been an integral part of the analysis of much of the data presented here, and has always been quick to help me when I've faced challenges.

Thank you to my undergraduate mentor, Dr. Barbara Lom, for sparking my initial interest in research and encouraging me to pursue a PhD. I am thankful for the Neuroscience Program at Emory for introducing me to some of my closest friends, Dr. Juliet Santiago, Sarah Blumenthal, and Dr. Maha Rashid, that have been on this journey with me from the very beginning and have always provided comfort in difficult times. I am incredibly grateful to have you all as my friends. I would also like to thank my brother, Abid Lakhani, for patiently listening to me talk about the research, grants, and papers, and for always believing in me. I would like to give a very special thank you to my partner, Ahmed Rahim, who has constantly helped me find a balance between graduate school and personal life, and has always lightened my mood in stressful times. Thank you to all my friends and family who have supported me in this journey in so many ways - I will forever be grateful for the love and support.

This dissertation is dedicated to my mom, Shamim Lakhani. My passion for learning and motivation to succeed are a direct reflection of her and the values she instilled in me. I know she would be incredibly proud of me.

Table of Contents

1	Introduction	1
1.1	Homeostatic plasticity	1
1.1.1	Homeostatic synaptic plasticity	2
1.1.2	Homeostatic intrinsic plasticity.....	3
1.1.3	Importance of homeostatic plasticity in neuron function and development .	4
1.1.4	Homeostatic plasticity in the embryonic chick spinal cord	5
1.1.5	Homeostatic regulation of spiking characteristics	8
1.1.6	Homeostatic plasticity in neurodevelopmental disorders	10
1.2	Fragile X Syndrome (FXS)	12
1.2.1	Genetic basis and prevalence	12
1.2.2	Anatomical, cognitive, and behavioral clinical manifestations	13
1.2.3	Current therapeutic approaches	15
1.2.4	Functions of FMRP in the nervous system	16
1.2.5	Experimental models of FXS	18
1.2.6	mGluR theory of FXS	19
1.2.7	Impaired baseline and homeostatic plasticity in FXS	21
1.3	Barrel Cortex	22
1.3.1	Overview of the whisker-responsive circuit	23
1.3.2	Deficits in the barrel cortex in FXS models	27
1.3.4	Importance of using sensory systems in studying plasticity	29
1.4	Dissertation aims and hypotheses	31
2	Homeostatic Regulation of Spike Rate within Bursts in Two Distinct Preparations	33
2.1	Abstract	33
2.2	Introduction	34
2.3	Results	35
2.3.1	SRWB is homeostatically restored following GABAergic blockade in cortical cultures	35
2.3.2	SRWB is homeostatically restored following GABAergic blockade in the isolated chick embryo spinal cord	47

2.4	Discussion	56
2.4.1	Variability in firing rate properties following GABAergic blockade	56
2.4.2	Homeostasis of SRWB in both preparations	58
2.5	Experimental Procedures	61
2.5.1	Cell culture	61
2.5.2	Spinal cord dissection	62
2.5.3	Electrophysiology recordings	62
2.5.4	Calcium imaging	63
2.5.5	Data analysis	64
2.5.6	Statistical analysis	67
3	Failure to homeostatically recruit layer 5/6 neurons during whisker stimulation in <i>Fmr1</i> KO mice	68
3.1	Abstract	68
3.2	Introduction	68
3.3	Results	70
3.3.1	P16 WT RS neurons respond to whisker stimulation more than KO RS neurons	71
3.3.2	P16 2-day whisker-deprived WT and KO neurons increased responsiveness, but only WT neurons increased neuronal recruitment	74
3.3.3	P21 KO RS neurons exhibit an increased threshold to whisker stimulation compared to WT neurons	77
3.3.4	P21 7-day whisker-deprived WT and KO neurons increased responsiveness, but only WT neurons increased neuronal recruitment	79
3.3.5	WT and KO FS neurons respond similarly to RS neurons at P16	81
3.4	Discussion	82
3.4.1	Baseline differences in WT and KO neurons	83
3.4.2	Plasticity in WT neurons	85
3.4.3	Plasticity in KO neurons	86
3.5	Experimental Procedures	88
3.5.1	Mice	88
3.5.2	Whisker deprivation	89
3.5.3	Electrophysiology recordings	90

3.5.4	Whisker stimulation	91
3.5.5	Histology	91
3.5.6	Analysis	91
3.5.7	Code and data availability	92
4	Discussions and Future Directions	94
4.1	General discussion and future directions for Chapter 2	94
4.1.1	Variability and degeneracy of firing properties	94
4.1.2	Significance of SRWB homeostasis	95
4.1.3	Future directions	97
4.2	General discussion and future directions for Chapter 3	101
4.2.1	Developmental changes in sensory processing in the <i>Fmr1</i> KO model ...	101
4.2.2	Impaired recruitment of neurons at baseline and following perturbations in the <i>Fmr1</i> KO	102
4.2.3	Future directions	105
4.3	What aspect of neuronal activity is homeostatically maintained	108
5	References	110

Chapter 1: Introduction

1.1 Homeostatic plasticity

Homeostatic plasticity represents a set of mechanisms that are thought to stabilize various functions of neural activity. When a neuron encounters a perturbation or change in its environment, it aims to maintain features of neural signaling through various mechanisms, which will be described later in this section. The first study to describe homeostatic plasticity was published in 1994 in lobster stomatogastric ganglion (STG) ¹. These neurons were isolated in a plated culture with no synaptic input and no neuromodulators, and during this time, demonstrated tonic firing. However, the normal rhythm of STG neurons is burst firing, and after several days in isolation, the neurons were able to recover this bursting ability. These results suggested that neurons have endogenous mechanisms, such as control over the constellation of their ion channels, that allow them to regulate firing rates and patterns ².

Neurons and networks have the capacity to maintain a certain firing rate set point or spiking activity feature. This can be achieved in two main ways, through synaptic compensations (homeostatic synaptic plasticity or HSP) and intrinsic compensations (homeostatic intrinsic plasticity or HIP). HSP is triggered by adjusting synaptic strength in a compensatory direction in response to spike or neurotransmission blockade. For instance, during periods of reduced activity, neurons may increase the number of AMPA receptors, while GABA receptors might be decreased. On the other hand, HIP regulates voltage-gated ion channels to control membrane excitability. For example, activity-deprived neurons can increase their intrinsic excitability by increasing the number or sensitivity of their voltage-gated sodium channels. These homeostatic adjustments are often referred to as occurring in a negative feedback loop to counteract excessive excitation or inhibition to

maintain optimal neural functioning. With this dynamic regulation, homeostatic plasticity ensures that neural circuits are stable for proper information processing and learning.

1.1.1 Homeostatic synaptic plasticity

Homeostatic synaptic plasticity (HSP) is one form of homeostatic plasticity that is employed by neurons to maintain stable neural activity levels within networks over prolonged periods. It adjusts the strength of synaptic connections in response to changes in overall neuronal activity, ensuring the stability and function of neural circuits ³.

The molecular mechanisms underlying synaptic scaling, a form of HSP, have been extensively studied in recent years, revealing a complex interplay of signaling pathways and cellular processes. One well-characterized mechanism involves the regulation of the number of postsynaptic receptors. This mechanism was first studied in cortical cultures, reported in a seminal paper from 1998 ⁴. The group measured miniature excitatory postsynaptic currents (mEPSCs), which are small, spontaneous currents that occur at the synapse in the absence of an action potential. These currents represent the smallest unit of synaptic transmission, typically resulting from the release of a single neurotransmitter vesicle. In this study, when neuronal activity was suppressed, the amplitude of mEPSCs increased, indicating an upscaling of synaptic strength, which is typically mediated by an increase in the number of postsynaptic receptors at excitatory synapses to restore activity levels. Conversely, when activity was enhanced, the mEPSC amplitude decreased, signifying downscaling thought to prevent excessive firing. Scaling is also observed at inhibitory synapses ⁵. These changes in synaptic strength were shown to be multiplicative (hence the name synaptic ‘scaling’), affecting all synapses on a neuron proportionally rather than selectively so that relative Hebbian differences are maintained. However, recent studies suggest that AMPAergic scaling is not multiplicative, but rather is nonuniform, across different synapses ⁶⁻⁸. These divergent scaling factors, although still moving towards a homeostatic goal, would affect some synapses more than others ⁷.

Another form of HSP that I would like to briefly mention is presynaptic homeostatic plasticity, which involves adjusting the presynaptic vesicle release in a compensatory manner. A good example of this occurs at the neuromuscular junction (NMJ). When postsynaptic receptors at the NMJ become less responsive after a perturbation, the presynaptic transmitter vesicle release increases so that the overall synaptic output is restored⁹. These different types of HSP work together to ensure that the strength of synaptic connections is appropriately adjusted following perturbations¹⁰.

1.1.2 Homeostatic intrinsic plasticity

Another form of homeostatic plasticity is homeostatic intrinsic plasticity (HIP). It involves regulating the excitability of the neuronal membrane in order to control the output of the cell. While the first study to show compensatory changes in intrinsic excitability was the study mentioned above², the first study to show this in a network of neurons was published in 1999¹¹. Experiments were conducted in visual cortical neurons in culture, where activity was blocked for 48 hours. These deprived neurons increased their sensitivity to incoming input by increasing their intrinsic excitability, specifically by changing the constellation of sodium and potassium conductances. Other studies have used computational modeling to demonstrate that despite the inherent variability in ion channel expression, homeostatic mechanisms can correlate ion channel conductances to the activity output of the cell^{12,13}. For example, the authors studied neurons in crab STG and found variability in the ion channels expressed, but the pattern of the firing rate of these neurons remained consistent. This consistency was achieved by homeostasis, where changes in the expression of one ion channel are compensated by adjustments in others. Using these methods, the neuron's overall electrical properties remain stable, allowing it to function reliably regardless of the variability.

It is also possible that HIP occurs through activity-independent mechanisms. Using the lobster STG once more, two key ion currents were monitored, a transient potassium current and a

hyperpolarization-activated inward current. Researchers discovered that when one of these currents was altered, the neuron adjusted the other current to compensate, ensuring consistent neuronal activity with this co-regulation^{14,15}. It is interesting to hypothesize how these activity-dependent and activity-independent HIP mechanisms work together.

1.1.3 Importance of homeostatic plasticity in neuron and network development and function

Together, experimental and computational studies suggest that homeostatic synaptic plasticity and homeostatic intrinsic plasticity are working in concert with one another in the neuron (Figure 1.1). Mathematical modeling demonstrates that the interaction between both HSP and HIP allows for the control of both the mean and variance of firing rates¹⁶. Neural circuits with different sets of ion channel conductances and synaptic strengths can produce nearly identical network activity patterns^{17,18}. A key insight from this study was the concept of "degeneracy" in neural circuits, meaning that multiple distinct configurations can yield the same network behavior. Because of this variability, an activity perturbation can affect one cell/network differently than another, as some are more dependent on certain conductances/synapses. This large degree of flexibility supports the idea that homeostatic compensation is occurring at multiple levels, in a unique way in different cells, and throughout development and adulthood¹⁹.

As neurons grow and form synaptic connections, homeostatic adjustments of synaptic strengths and ion channel expression occur to stabilize neuronal output. This ensures that neurons can respond appropriately to stimuli, and support learning and memory processes. For example, STG neurons and recordings from both young and adult lobsters demonstrate that despite the growth in size of the neurons, the motor patterns of individual neurons and the network remain consistent²⁰. In this case, homeostatic plasticity ensured the maintenance of the network output. Other studies in multiple model organisms have demonstrated that the diameters of neuronal processes increase as they increase in length, allowing for specific electrical properties, such as

resistance, to remain consistent as the neuron grows^{21,22}. By proportionally scaling the neural components and the density of ion channels, neurons ensure that the overall output of the cell is preserved.

Neurons and networks are under homeostatic regulation during development, and this helps define the synaptic strengths and voltage-gated conductances of the baseline circuit excitability. When the system encounters a perturbation, these homeostatic mechanisms are engaged, but can use different strategies to achieve homeostasis and therefore contribute to the variability that we observe across multiple individuals.

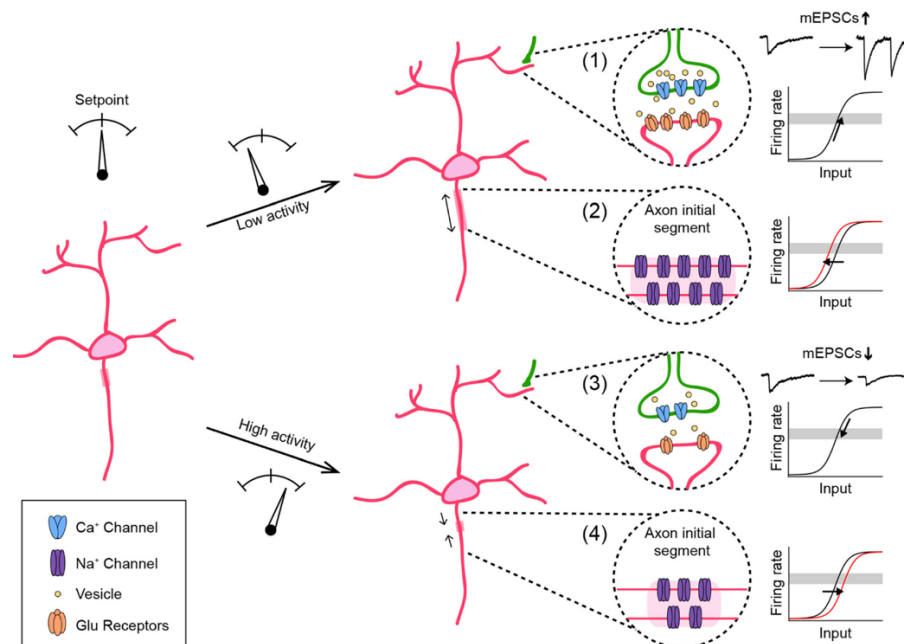


Figure 1.1. Homeostatic plasticity mechanisms that work in concert with one another in neurons. When the activity of a neuron is decreased, the neuron could homeostatically respond to this perturbation by either increasing synaptic strength, or mEPSCs (1), or increase the intrinsic excitability of the cell (2). Alternatively, when the activity of a neuron is increased, it can return to baseline levels by decreasing the amplitude of its mEPSCs (3) or decreasing its membrane excitability. Figure taken from Tien & Kerschensteiner 2018²³.

1.1.4 Homeostatic plasticity in the embryonic chick spinal cord

Using the embryonic chick to study homeostatic plasticity offers several advantages that make it an ideal model system for understanding the mechanisms of neural development and plasticity. One advantage is that the embryonic movements, or “kicks”, can be observed by opening the eggshell. In

this way, we can track how perturbations affect these movements and watch as the system homeostatically works to maintain this network activity. The chick embryo is also highly accessible for experimental manipulations; for example, researchers can pharmacologically and genetically manipulate the model organism *in ovo* and can also easily isolate parts of the chick embryo for *ex vivo* studies. In addition, the developmental stages of the chick embryo are well-documented and occur over a relatively short period, which gives investigators the ability to accurately target certain time periods²⁴. Finally, the embryonic chick spinal cord exhibits robust spontaneous network activity (SNA) that is important for motoneuron axons targeting their peripheral muscles²⁵⁻²⁷. SNA recruits the majority of neurons in network-wide bursts of activity called episodes, which last for several seconds up to one minute, and *in vivo*, drive embryonic limb movements (kicks) by recruiting motoneurons²⁸⁻³⁰. These episodes occur every 5-10 minutes *in vitro*, and each episode is composed of several bursts of depolarizations. This network is highly excitatory due in part to the fact that during this period in development, GABAergic chloride currents are also excitatory and depolarizing³¹⁻³⁴.

Our lab has taken advantage of the embryonic chick because we observed when homeostasis occurred behaviorally and then looked for the plasticity mechanisms that were engaged during this time. For instance, when various neurotransmitter antagonists were infused into the egg, embryonic limb movements were initially abolished, as observed through a window in the eggshell³⁵. However, after several hours, limb movements were seen to recover while the embryo was still in the presence of the neurotransmitter antagonists. These results demonstrate that there are homeostatic mechanisms triggered during this time that allowed for activity to return to baseline levels. One such mechanism could be that there were compensatory changes in synaptic strength. In order to test this, lidocaine, a sodium channel blocker, was infused into the egg for 2 days to block spiking activity and embryonic movements³⁶. Interestingly, the amplitude of both AMPAergic and

GABAergic mPSCs (miniature postsynaptic currents) was increased, suggesting an increase in synaptic strength. Since GABA is also depolarizing at this stage, this compensatory result makes sense because a reduction in activity should increase excitatory drive. Blocking GABAergic and glutamatergic receptors also resulted in the abolition of embryonic limb movements. However, the recovery in the kicks happened by 12 hours, but these changes in synaptic strength were not seen at the 12-hour time point, suggesting that there was potentially another mechanism responsible for the recovery³⁵. Thus, the lab also investigated the intrinsic excitability of neurons. GABA receptor blockade, but not glutamate receptor blockade, triggered an increase in cellular excitability at the 12-hour time point. This plasticity was mediated by an increase in sodium currents and a decrease in the fast-inactivating and calcium-activated potassium currents³⁷. Still, the recovery began within 2 hours of neurotransmitter blockade. Two important mechanisms have been identified that occur fast enough to contribute to this early recovery. First, a 10mV depolarization of the resting membrane potential was observed in motoneurons and interneurons after GABA or glutamate receptor blockade³⁸. Second, a rapid form of scaling was observed after NMDAR block in embryonic motoneurons⁶. Taken together, these results demonstrate that slow synaptic scaling does not mediate the *in ovo* recovery of embryonic movements following neurotransmitter blockade, but rapid scaling and changes in intrinsic excitability appear to, since these changes occur while the recovery occurs. On the other hand, we now favor the idea that slow synaptic scaling is there to ensure that the neuron is receiving sufficient synaptic input. In addition, these results suggest that GABA has a special importance in triggering homeostatic slow synaptic scaling.

The lab has established that homeostatic slow scaling was triggered after neurotransmitter blockade, but what are the mechanisms that mediate this synaptic strengthening? Our lab found that AMPAergic scaling occurs through the insertion of calcium permeable GluA2-lacking AMPA receptors, rather than GluA2-containing receptors³⁹. On the other hand, Clomeleon, a genetically

encoded chloride indicator, was used to determine what exactly was occurring during GABAergic scaling. There was an increase in the intracellular chloride concentration of the cell, which caused a depolarizing shift in the GABAergic reversal potential and increased the driving force for these currents^{40, 41}. These are just two examples of how homeostatic mechanisms are expressed to compensate for changes in the developing nervous system.

In summary, these studies from our lab investigating homeostatic plasticity in the embryonic chick have been crucial in uncovering several mechanisms and providing a timeline of mechanistic changes that could be compared to the actual homeostatic recovery of embryonic movements. However, the specific features of neural activity that are under homeostatic control have been incompletely defined over the past several years. Thus, one of my projects focused on identifying the specific features that are best homeostatically controlled in two different systems (see next section, 1.1.5, and Chapter 2).

1.1.5 Homeostatic regulation of spiking characteristics

Due to individual variability caused by homeostatic plasticity as discussed above, perturbations affect one cell or network differently than another, as some are more dependent on certain conductances or synapses than others. However, identifying the actual neural features that are homeostatically maintained has been elusive. By perturbing network activity and observing how different activity features are altered and homeostatically recovered, one can potentially begin identifying which features are more likely to be regulated. Past literature has shown that different systems have different homeostatic goals. For example, monocular deprivation experiments have shown that firing rate homeostasis took place at the level of the individual cell over the course of multiple days as monocular deprivation was still in effect^{42, 43}. Firing rates also changed after deprivation in response to a visual stimulus⁴⁴. However, another study in primary hippocampal cultures demonstrated that firing rate homeostasis following synaptic perturbations took place at the

population level, but not at the single-neuron level⁴⁵. This would suggest that the system places a greater importance on network-wide firing rates rather than individual firing rates. Finally, another study has suggested that networks are tuned to criticality, a computational concept that maximizes information capacity and transmission by balancing excitation and inhibition to optimize learning⁴⁶. Due to the importance of homeostatic plasticity in neuron growth and development, along with a potential role in neurodevelopmental disorders, it is critical that we come to a better understanding of the precise activity properties that are homeostatically regulated (ex: firing rate, firing pattern, burst duration, burst frequency).

An important question is – how does a neuron sense changes in neural features thus triggering homeostatic adjustments^{3,9,47}. There's a myriad of molecular pathways involved in this process, but since this work is outside the scope of my project, I will only describe two here⁴⁸. A prime example of a target molecule is calcium. When cells alter their spiking, this alters the calcium entering the cell and therefore downstream calcium signaling cascades, such as a calcium/calmodulin-dependent protein kinase, also known as CaMK^{49,50}. Experiments in rat cortical neurons show that a decrease in somatic calcium influx and reduced CaMKIV activation can trigger scaling⁵¹. Another example of a target molecule is brain-derived neurotrophic factor, or BDNF, which has been thought to be necessary for cortical development and different types of plasticity. Exogenous BDNF added to cortical cultures prevents the usual effects of activity blockade on pyramidal cells (upscaling)⁵². It is even possible that these different molecular pathways are connected at some point in the signaling cascade. Thus, detecting changes in activity levels, through whatever means, is crucial for maintaining set points of specific neural features.

Another important feature to understand is the time course of homeostatic recovery of firing rates in neural networks after activity perturbations. As mentioned earlier, the behavioral recovery of embryonic limb movements occurs around 12 hours following GABAergic or glutamatergic

receptor blockade. In the STG system, the behavioral recovery of the rhythmic firing pattern following the absence of neuromodulatory input occurs over the course of 1-4 days⁵³. However, this is the timing of the behavioral recovery; what about the timing of the homeostatic mechanisms that are linked to this recovery? Different mechanisms demonstrate different timescales. For instance, synaptic scaling has been thought to occur over the timescale of several hours to days⁴⁸, though rapid forms of scaling were more recently discovered^{6,51}. Changes in intrinsic excitability also can occur over hours to days^{11,54}. However, a more rapid form of intrinsic plasticity was uncovered when potassium currents acted to stabilize a central pattern generator network that was responsible for cardiac muscle contraction in crabs in just 60-90 minutes⁵⁵. These timescales of homeostatic plasticity mechanisms at the network and neuron level potentially suggest that different mechanisms can regulate different aspects of the recovery of behavior, or they can occur at different points in the recovery phase.

1.1.6 Homeostatic plasticity in neurodevelopmental disorders

Homeostatic plasticity plays a crucial role in shaping the development and functionality of neural circuits, often with significant implications for cognitive and behavioral outcomes.

Neurodevelopmental disorders, such as autism spectrum disorders (ASD) and intellectual disability, are characterized by disruptions in development that can lead to imbalances in excitation and inhibition (E/I ratio) within the brain^{56,57}. Furthermore, models of febrile seizures in the developing system have demonstrated alterations in ionic conductances that affect the E/I ratio⁵⁸. These imbalances can result from genetic mutations, environmental factors, or a combination of both, affecting the normal homeostatic mechanisms that regulate synaptic strength and neuronal excitability. Therefore, these impairments can play a role in the altered activity levels, often hyperexcitability, associated with these disorders.

Rett syndrome is a rare genetic neurological disorder caused by a mutation in the MecP2 gene, and it affects 7 in 100,000 females⁵⁹. Normally, a bicuculline-induced increase in activity leads to a decrease in the GluA2 subunit of the AMPA receptor in cortical slices through increasing MecP2 expression, which is a translational repressor of the GluA2 unit. However, in MecP2-deficient neurons, this activity-dependent synaptic scaling is impaired⁶⁰. In fact, there are homeostatic mechanisms in place, through the utilization of microRNAs, to balance MecP2 levels in response to changes in neuronal activity⁶¹. Fragile X Syndrome (FXS), another neurodevelopmental disorder, is often co-diagnosed with autism spectrum disorders. Again, many studies have found deficits in both homeostatic synaptic plasticity and intrinsic plasticity in FXS neurons⁶²⁻⁶⁵. More information on the specific impairments in homeostatic plasticity found in FXS models can be found in Section 1.2.7.

Targeting homeostatic plasticity represents a promising therapeutic strategy for treating neurodevelopmental disorders. Research has revealed that restoring E/I balance can ameliorate some of the symptoms associated with these conditions. Pharmacological approaches that target homeostatic mechanisms have shown potential in preclinical models. For example, mutations in the scaffolding protein Shank3 are strongly associated with autism spectrum disorders. Shank3-deficient neurons do not demonstrate synaptic scaling or homeostatic intrinsic plasticity. However, these deficits could be rescued by treating with lithium in slice, and in the mouse model, which also leads to a rescue of the behavioral deficits⁶⁶. Other studies in rodents have found that synaptic upscaling and downscaling can be elicited by ketamine and lithium, respectively⁶⁷. Blocking NMDA receptors with ketamine inhibits EF2 kinase and increases local protein synthesis, which triggers rapid and long-lasting anti-depressant effects⁶⁷. In conclusion, leveraging homeostatic plasticity mechanisms offers a targeted and potentially effective way to mitigate the neural imbalances that underlie many neurodevelopmental disorders.

1.2 Fragile X Syndrome

Fragile X Syndrome (FXS) is a neurodevelopmental disorder that is the leading monogenetic cause of autism spectrum disorder (ASD). ASD is specifically marked by deficits in social communication and repetitive behaviors, and it manifests differently for everyone. Autism can be caused by both genetic and environmental factors, and FXS is one of the genetic factors. FXS was first described in 1943 by Martin and Bell as an inherited form of intellectual disability that follows an X-linked inheritance pattern ⁶⁸. The association between the disorder and the specifically affected *Fmr1* allele was later confirmed in 1991 ⁶⁹. FXS is caused by a mutation in the *Fmr1* (Fragile X messenger ribonucleoprotein 1) gene on the X chromosome, which is responsible for translating a protein called Fragile X messenger ribonucleoprotein (FMRP). Some of the common clinical manifestations include developmental delays, intellectual disability, behavioral symptoms, and other health problems.

1.2.1 Genetic basis and prevalence

The *Fmr1* gene was the first example of a trinucleotide repeat expansion that resulted in a disorder. Within the 5' untranslated region of the *Fmr1* gene, there is an area that contains CGG repeats, which is typically around 30 repeats long in people who do not have FXS. In people who have the premutation for this neurodevelopmental disorder, there can be anywhere from 55-200 CGG repeats ⁷⁰. Individuals carrying this premutation may not display the full spectrum of FXS symptoms, but can still have subtle clinical features. They are also at risk for associated conditions like Fragile X-associated tremor/ataxia syndrome (FXTAS; characterized by problems with movement and cognition, usually late-onset) or primary ovarian insufficiency (POI; ovaries don't function normally) ^{71,72}. Premutations of the *Fmr1* gene generally occur in female carriers, and these alleles are particularly unstable during meiosis, during which the duplication and separation of genes leads to the formation of haploid eggs and sperm. Thus, it is possible, and likely, that during this process, the

CGG repeat length increases significantly, expanding into a full mutation in future generations ⁷³. The full mutation occurs in individuals who have 200 or more CGG repeats. When this happens, the locus is heavily methylated, leading to silencing of the gene, the absence of FMRP, and the characteristic clinical manifestations of the disorder ⁷³.

Knowing the prevalence rates of FXS is crucial to understanding the differences in clinical phenotypes and developing targeted approaches for individuals in both populations. The prevalence of the FXS full mutation in Europe and North America is 1/5000 males and 1/4000-8000 females ⁷⁴, ⁷⁵. This prevalence discrepancy is because males, having only one X chromosome, are more severely affected when they inherit the mutation. On the other hand, females, with two X chromosomes, often have milder symptoms due to the presence of a normal *Fmr1* gene on their second X chromosome, and these symptoms may be so mild that they do not even consider genetic testing. The number of individuals that carry the FXS premutation is higher, approximately 12/10000 males and 35/10000 females ⁷⁵. These differences between males and females, as well as the differences between individuals with the premutation and full mutation, are considered when developing therapeutic strategies.

1.2.2 Anatomical, cognitive, and behavioral clinical manifestations

There are many neuroanatomical signs of FXS in human brains. Dendritic spine abnormalities are one of the most prominent features, and this is thought to be due to the role of FMRP in regulating translation within dendrites (more information on FMRP function in section 1.2.4 below) ⁷⁶.

Furthermore, white matter tracts in infants with FXS are significantly diminished, specifically from subcortical regions to the prefrontal cortex and some corpus callosum pathways ⁷⁷. Changes have also been reported in the amygdala, striatum, and cerebellum ⁷⁸. Many of these neuroanatomical changes observed in the FXS brain align well with the clinical symptoms associated with FXS.

There is a wide range of clinical phenotypes associated with FXS. Initially, at birth, there are differences in weight, height, and head circumference, but these changes are usually subtle, which is why early diagnosis is difficult ⁷⁹. Within the first year, many of the major FXS symptoms begin to appear, especially in boys. These include mild motor delays, increased seizure susceptibility, hyperactivity, language delays, signs of autism and intellectual disability, poor eye contact, anxiety, and aggression ⁸⁰. With these signs, FXS is then typically diagnosed with a DNA test at approximately three years of age in boys, but may be later in girls ^{80,81}. As children with FXS develop into adults, more symptoms can become apparent, such as impulsivity, increased aggression, poor attention, loss of control, and eventually, cognitive decline and symptoms of Parkinson's disease in older age ⁸⁰.

Furthermore, there are differences between boys and girls that have FXS. Since females have two copies of the X chromosome and thus, typically have a normal *Fmr1* allele, there is a broader range of clinical symptoms. This range is in part due to X inactivation, where one of the X chromosomes is inactivated. Some cells have the paternal X chromosome inactivated while other cells have the maternal X chromosome inactivated. Therefore, FMRP will be expressed in a mosaic pattern, depending on which chromosome is expressed in that particular cell (full mutation *Fmr1* allele or the normal *Fmr1* allele) ⁸². Other differences that are apparent in boys and girls with FXS include comorbidities with psychiatric and neurological disorders. For instance, while approximately 30-50% of FXS males are co-diagnosed with ASD, only 25% of FXS females are diagnosed with ASD. Comorbidity with anxiety disorders is also lower in FXS females compared to males, and FXS females are generally less affected by impaired communication skills ⁸³.

The variability in clinical manifestations of FXS has many theories. It was previously thought that people with FXS that produce higher levels of FMRP are typically less cognitively affected than people that produce lower levels of FMRP or no FMRP ⁸⁴. In males that have the full mutation,

FMRP levels can range from 0 to 21% of the normal mean FMRP level, and the greater the FMRP level, the better the IQ score⁸⁵. However, more recent work has demonstrated that FMRP expression and IQ is only correlated in females, but not in males, with FXS⁸⁶. Furthermore, there is an interestingly near-normal distribution of IQ scores (shifted five standard deviations downward from typically developing individuals) in males with no or low FMRP expression⁸⁶. More work needs to be done to identify what biological and/or socio-economic and/or environmental factors contribute to this normal variation in IQ scores.

1.2.3 Current therapeutic approaches

Since there is no cure for FXS currently, treatment is limited to ameliorating the symptoms displayed by patients. Additionally, because of the wide range in symptoms, therapeutic approaches to FXS are often individualized based on the clinical manifestations, age, sex, and comorbidities (ASD/intellectual disability, ADHD, OCD).

In this section, I'll mention a couple drugs that have been effective in targeting FXS clinical phenotypes. Metformin, widely known as an antidiabetic drug, was initially shown to be successful in preclinical models. Treatment with this drug restored short-term memory, corrected excessive grooming and social behavior deficits, and decreased audiogenic seizures in FXS animal models⁸⁷. Metformin was then used in clinical trials to test its effectiveness on individuals with FXS. In a study of six adults and one child, metformin improved irritability, social responsiveness, hyperactivity, social avoidance, and communication skills⁸⁸. In another clinical trial, children between the ages of 2 and 7 were treated with metformin and they showed improvements in behavior and language development⁸⁹. Another drug that has been shown to be helpful against FXS symptoms is lovastatin, which is widely known to reduce cholesterol. In a mouse model of FXS, lovastatin corrected both excessive hippocampal protein synthesis and increased seizure susceptibility⁹⁰.

Chronic administration of lovastatin in human clinical trials with FXS patients was shown to improve behavioral symptoms, such as irritability, hyperactivity, and social avoidance ⁹¹.

Drugs are not the only therapeutic approach to treating FXS symptoms. For example, in one clinical trial, a speech therapy called Parent Implemented Language Intervention was delivered to patients, either with lovastatin or a placebo. In both groups, there was an improvement in spoken language and social impairments, and the amount of change in these measures was comparable, suggesting that just the language intervention was sufficient to improve FXS symptoms ⁹². Another behavioral intervention is discrete trial training, which is an intensive, highly structured program where reinforcement and guidance is provided as needed ⁹³. This alternative approach has been effective in identifying learning impairments and correcting behavioral abnormalities, such as social gaze ⁹⁴⁻⁹⁶.

Altogether, these pharmacological and behavioral interventions provide some improvements in the characteristic symptoms of FXS. However, due to the variability in how FXS manifests, the wide range of functions of FMRP in the brain, and our limited knowledge of the molecular pathways that are affected in FXS, there is currently no sufficient cure available. CRISPR/Cas9 genome editing technology holds some promise as another avenue to pursue ^{97,98}.

1.2.4 Functions of FMRP in the nervous system

In order to understand the functions of FMRP, it is first important to discuss the structure of the protein. FMRP contains three canonical RNA-binding domains: two central KH (ribonucleoprotein K homology) domains and one RGG (arginine–glycine–glycine) box ⁹⁹. A novel domain has been more recently discovered in the form of another KH domain on the amino terminus of the protein ¹⁰⁰. These domains allow FMRP to bind to specific mRNA targets, many of which are involved in synaptic function and plasticity. The protein also contains nuclear localization and nuclear export

signals to allow for FMRP to be shuttled between the nucleus and cytoplasm¹⁰¹. FMRP can also be phosphorylated at various sites, controlling the various functions of the protein.

The mRNAs that FMRP binds to have been well-documented over the past several decades, thus providing important information about their functional impact. A complex structure called the FMRP kissing complex on target RNAs allows FMRP to bind to polyribosomes and regulate translation¹⁰². This structure interacts with the coding region of transcripts that encode both presynaptic and postsynaptic proteins, as demonstrated by high-throughput sequencing of RNAs isolated by crosslinking immunoprecipitation¹⁰³. More recent work has shown that FMRP targets a wide variety of mRNAs, including those related to neurogenesis, intellectual disability, mTOR (mammalian target of rapamycin) pathway, and chromatin/chromosome organization and histone modifications¹⁰⁴. These studies provide evidence that FMRP targets include not only genes that encode neural/synapse development and function, but also epigenetic regulation and cell cycle regulation¹⁰⁵. Altogether, FMRP selectively binds to approximately 4% of the mRNA in the mammalian brain⁷³.

FMRP is also involved in the local synthesis of proteins at synapses. An important study from 2002 demonstrated that activity-dependent synaptic plasticity is impaired in the absence of FMRP¹⁰⁶. Metabotropic glutamate receptor (mGluR)-dependent long-term depression (LTD), which is important for learning and memory, was significantly enhanced in the hippocampal neurons of *Fmr1* knockout (KO) mice. This enhanced LTD was due to the increase in synthesis of proteins, suggesting that FMRP normally functions as a translational repressor at synapses (see section 1.2.6 for more information)¹⁰⁶. How does FMRP regulate this translation? FMRP reversibly stalls the ribosome on its target RNAs when it binds to them¹⁰³. It is thought that the phosphorylation state of FMRP might be a signal for whether FMRP is bound to actively translating or stalled ribosomes, with phosphorylated FMRP required for translational repression and dephosphorylated FMRP

triggering translation^{107, 108}. Thus, FMRP is an mRNA-binding protein that plays a profoundly important role in many different pathways in the nervous system.

Finally, there are non-canonical effects of FMRP that include direct protein-protein interactions. One such example is that FMRP binds to SK (small conductance calcium-activated potassium) channels. SK currents are reduced in FXS hippocampal cultures, leading to the hyperexcitability of pyramidal neurons¹⁰⁹. In addition, FMRP directly interacts with the HCN (hyperpolarization-activated cyclic nucleotide-gated) channel to regulate its current¹¹⁰. Altogether, FMRP can influence neuronal excitability, synaptic transmission, and synaptic plasticity by modulating the activity or expression of ion channels and receptors.

1.2.5 Experimental models of FXS

Animal models have been extensively used to study the function of FMRP and the pathology of FXS. Mice, in particular, are a strong model because 99% of mouse genes have homologous genes in humans¹¹¹. In addition, the mouse has several advantages as an experimental model – its genome can be edited relatively easily with current technology, they have short lifespans, and have biological similarities to humans. However, one of the main differences between human FXS and *Fmr1* KO mice relates to their genetics. In humans, the FMRP gene is expressed for a short period of time, until approximately the 10th week of gestation, before DNA methylation causes the silencing of the gene¹¹². On the other hand, KO mice never express any FMRP because many of the genetic models silence the *Fmr1* gene immediately¹¹³. Furthermore, the cortex is quite different in mice compared to humans. Mice have fewer cortical regions, less neocortical area, a relatively low density of neurons, and not as many association areas that integrate information¹¹³. These neuroanatomical differences make it more difficult to study cognitive aspects of FXS pathology. Thus, some researchers have turned toward rats, which perform better on learning and cognitive tasks, and display more social behaviors than mice. However, the dearth of genetic tools for rats prevents more widespread

experiments in this model organism ¹¹⁴. Additionally, experiments on zebrafish and drosophila have also contributed to our understanding of FXS ^{115,116}. Results in these models have been inconsistent, perhaps due to the differences in the sensory, molecular, and behavioral pathways compared to human FXS pathology. Furthermore, many of the cognitive symptoms of FXS are difficult to test and interpret in these animals, making it difficult to draw applicable conclusions.

Despite the abundance of research in the above-mentioned experimental models, there are no treatments that prevent the FXS phenotype. Thus, there are new emerging animal models to better understand FMRP and FXS. For example, one such model is the Mongolian gerbil ¹¹⁷. Gerbils have an auditory system (both auditory range and auditory circuit) that better recapitulates the human sensory system. In addition, gerbils are mostly diurnal like humans, unlike the other nocturnal rodents previously studied, and have better visual acuity. Finally, gerbils display more social behaviors, allowing us to better study the social impairments in FXS ¹¹⁷. Another emerging model to study FXS pathology is the chick embryo. Work in the chick embryo has shown that FMRP binds to targets in the chick auditory system (which is more comparable to humans than rodents), and has demonstrated novel roles for FMRP ^{118,119}. Overall, animal models have been crucial to our understanding of FMRP function and FXS pathology, and these emerging animal models, along with the use of nonhuman primates, could help uncover novel therapeutic areas.

1.2.6 mGluR theory of FXS

The mGluR theory of FXS was first proposed by Mark Bear and colleagues in 2004. The theory explains the role of group 1 metabotropic glutamate receptors (mGluRs), particularly mGluR5, in the pathology of FXS. It states that the loss of FMRP results in exaggerated signaling through mGluR5, a receptor involved in synaptic plasticity and protein synthesis ¹²⁰. Under normal conditions, mGluR signaling leads to the translation of specific mRNAs at the synapse, which is crucial for processes like LTD, a form of synaptic plasticity that weakens synapses. FMRP acts as a

negative regulator of this protein synthesis to ensure that it occurs in a controlled manner. However, in the absence of FMRP, mGluR5-induced protein synthesis is unchecked, leading to excessive protein synthesis and exaggerated LTD¹²⁰.

Several key preclinical studies led scientists to believe that this finding would significantly explain the behavioral phenotypes of FXS. For example, *Fmr1* KO mice demonstrate increased sensory responses, such as high seizure susceptibility, perhaps due to increased mGluR signaling¹²¹. When an mGluR5 antagonist (an anticonvulsant) raised the threshold for these audiogenic seizures in mice by reducing excitatory synaptic transmission, it suggested that the increased mGluR signaling may be the main problem¹²². In another example, the corticostriatal pathway, which is important for forming motor and cognitive patterns, was found to have excessive mGluR5 signaling, leading to an obsessive-compulsive disorder (OCD) phenotype, which is often co-diagnosed with FXS^{123, 124}. These studies, along with many others, demonstrated the detrimental impact of increased mGluR activation.

By identifying mGluR5 as a key player in FXS, researchers then focused on developing drugs that modulate mGluR5 activity. The first mGluR inhibitor, fenobam, was tested in a single-dose clinical trial of 12 participants with FXS. Some participants in the study showed varying levels of improvements in anxiety and hyperactivity, and there were no adverse effects of the drug, but the small sample size limited the ability to draw definitive conclusions from this trial¹²⁵. Another mGluR antagonist, acamprosate, was given to 3 patients, over the course of at least 16 weeks, starting with daily to 3 times per day. Each participant improved their communication capabilities, which included more complex grammar and vocabulary¹²⁶. However, despite the strong preclinical evidence for targeting mGluR5 activity and some of the earlier promising clinical trials, many clinical trials have not shown improvements in FXS symptoms¹²⁷. One potential reason for this is tolerance to the drugs after chronic administration¹²⁸. Some other reasons include differences between mice and

humans, genetic variability in FXS patients, simultaneous use of multiple medications for co-diagnoses, and perhaps the fact that these drugs may need to be delivered at an earlier age to see therapeutic results, as FXS is a neurodevelopmental disorder ¹²⁹.

Although clinical trials of the mGluR theory of FXS have faced challenges, the theory still provides information for understanding some of the molecular and synaptic impairments associated with the absence of FMRP. In fact, the theory has also been applied to other neurological and psychiatric disorders, such as epilepsy, schizophrenia, anxiety, and depression, where similar mechanisms and dysregulation might exist for mGluR5 signaling ¹³⁰⁻¹³³.

1.2.7 Impaired baseline and homeostatic plasticity in FXS

FXS neurons have a different baseline level of activity compared to WT neurons across various model systems. For instance, multiple studies have established that FXS excitatory neurons are more intrinsically excitable at baseline, both in the hippocampus and the cortex ^{64, 65, 134}. Additionally, changes in the cortical circuit demonstrate that UP states, which are persistent periods of activity that generate synchronous firing, are longer in *Fmr1* KO cortical slices ¹³⁴. Finally, experiments in the intact FXS mouse report changes in the whisker-evoked response. Both excitatory and inhibitory cells in L2/3 of the whisker-responsive barrel cortex demonstrate a decreased response to whisker stimulation compared to the WT, and spontaneous activity of inhibitory cells is also decreased in the KO mouse ¹³⁵. These results suggest that FXS neurons have a different baseline activity compared to WT neurons, which could suggest they may be more sensitive to challenges or perturbations.

This altered baseline activity suggests that homeostatic plasticity could be disrupted in FXS, leading to some of the cognitive and behavioral deficits that are characterized by this disorder. Many studies have demonstrated that homeostatic synaptic plasticity, along with synapse development, is impaired ¹³⁶. Normally, a loss of synaptic activity leads to the translation of retinoic acid, a molecule that activates the synthesis and insertion of post-synaptic AMPA receptors in the dendrite ¹³⁷.

However, in *Fmr1* KO mice, although retinoic acid synthesis still occurs following the blockade of synaptic activity, the translation of new AMPA receptors is impaired, preventing upscaling⁶². This result was also confirmed in FXS patient-derived induced pluripotent stem cells (iPSCs), and repairing the *Fmr1* gene rescued homeostatic synaptic scaling, suggesting the importance of FMRP in synaptic plasticity¹³⁸. In the other direction, downscaling is also impaired in *Fmr1* KO hippocampal neurons. For instance, FMRP normally modulates the expression of the tumor suppressor gene, p53, and a ubiquitin E3 ligase, Nedd4-2, and without their proper regulation, synaptic strength does not change following activity perturbation¹³⁹.

FXS models have also shown that there are deficits in homeostatic intrinsic plasticity. For example, a study from our lab demonstrated that in *Fmr1* KO cortical cultures, after blocking activity/NMDARs with TTX/APV, single-spiking neurons failed to convert to a multi-spiking phenotype, as the WT neurons did. In addition, the *Fmr1* KO multi-spiking neurons demonstrate exaggerated plasticity, potentially due to an overexpression of sodium channels⁶³. In another study done in hippocampal neurons, after the addition of KCl to increase activity, *Fmr1* KO neurons demonstrated an exaggerated decrease in the number of action potentials fired compared to WT neurons⁶⁴.

These results suggest that there are bidirectional deficits in both synaptic scaling and homeostatic intrinsic plasticity. Research on FMRP and its role in homeostatic plasticity mechanisms continues to grow, and a deeper understanding of this relationship should prove useful in the development of more targeted and effective therapies for FXS and related disorders that have impaired plasticity.

1.3 Barrel Cortex

The term “barrel cortex” was first coined by Woolsey and Van der Loos in 1970 to describe a distinct region of the cortex where there was an interesting arrangement of cell bodies in layer 4

(L4). In this original study, the histological technique of Nissl staining was used to study the organization more closely. The scientists named the cell-dense regions in the mouse brain “barrels,” which ranged from 100-400 μm in diameter. The consistent cortical architecture corresponded well to individual whiskers on the mouse's snout. Along with previously established microelectrode recordings and the analysis of cortical maps based on whisker-evoked potentials, Woolsey and Van der Loos suggested that one barrel represents one whisker, and that these barrels are responsible for the functional organization of cortical columns ¹⁴⁰.

1.3.1 Overview of the whisker-responsive circuit

Whiskers, or vibrissae, are often compared to human fingertips, in the sense that we use our fingers to both actively and passively discriminate shapes and objects in our environment ¹⁴¹. Whiskers are specialized hair follicles that are located on the snouts of mice and rats. They are split into two categories – macrovibrissae and microvibrissae. The macrovibrissae (more caudal) are longer and are actively used for long-distance discrimination, while the microvibrissae (more rostral) are shorter and have a more passive role in sensing the environment ¹⁴². The thickness at the base of the whisker vs the thinness of the whisker towards the end, along with the shape of the whisker, plays an important role in allowing rodents to measure object distance and force. In fact, these characteristics of individual whiskers are so crucial that when a whisker is shed and grows back, it has highly similar features ¹⁴³. Rodents use their whiskers for a wide range of tactile and learning behaviors, including spatial navigation, object recognition, and social interactions ^{144, 145}.

Information obtained through the whiskers is then transmitted to the brain. The whisker follicles are packed with nerve endings, such that when a whisker encounters an object, the mechanoreceptors in the sensory neurons transduce the mechanical signal (ex: bending, vibrations, displacement of whiskers) into a neural signal. There are many classes of sensory neurons that innervate an individual whisker. This includes about 6-7 morphological types and 2 main

electrophysiological types (rapidly adapting (RA) and slowly adapting (SA))¹⁴⁶. Whereas the RA neurons have a low amplitude threshold, the SA neurons have a low velocity threshold, and there are even some neurons that show mixed properties¹⁴⁷. From here, the axons for these sensory neurons travel through the trigeminal nerve to the principal trigeminal nucleus in the brainstem. The neurons in this nucleus are somatotopically arranged into barrelettes, similar to the barrel cortex architecture described earlier (section 1.3). Excitatory output from the brainstem then reaches the ventral posterior medial (VPM) nucleus of the thalamus. In the VPM, a topographic map of the whisker pad (termed barreloids) is once again maintained¹⁴⁴. The thalamus, a major relay station, filters and refines the sensory inputs before it reaches the barrel cortex. Within the barrel cortex, layer 4 (L4) primarily receives this input, and the stereotypical barrel map is established here, the last discrete somatotopically defined location for preserving the spatial organization of inputs (secondary somatosensory cortex, S2, contains a continuous band for each row, but not each whisker)¹⁴⁸. The information flow described above is known as the lemniscal pathway. Another pathway that transmits whisker information to the barrel cortex is known as the paralemniscal pathway. In this path, information flows from the spinal trigeminal nucleus in the brainstem to the posterior medial (POM) nucleus of the thalamus, which in turn innervates L1 and L5A of the barrel cortex¹⁴⁷. A recent study suggested that while the lemniscal pathway is crucial for transmitting sensory information, the paralemniscal pathway might play a more modulatory role rather than directly channeling sensory input. This indicates that the paralemniscal pathway influences the processing and integration of sensory information¹⁴⁹.

Within the cortex, the canonical pathway for information flow is from L4 -> L2/3 -> L5/6 in the same barrel column (Figure 1.2). However, this is an oversimplified circuit, and one that is still not entirely clear in the field. For instance, one study suggests that information from the VPM actually gets transmitted to L4 and L5B simultaneously, bypassing the conventional sensory

processing circuit ¹⁵⁰. Another study suggests that some projections from VPM also terminate in L3 and L6 ¹⁵¹. Perhaps these widespread connections serve a role in the function of each of these layers. L2/3 projects mainly to neocortical regions, whereas L5/6 projects to both cortical and subcortical regions that are action-related and higher-order areas ¹⁵⁰. Since all layers have access to most of the same information, the many projection patterns can differentially alter behavior.

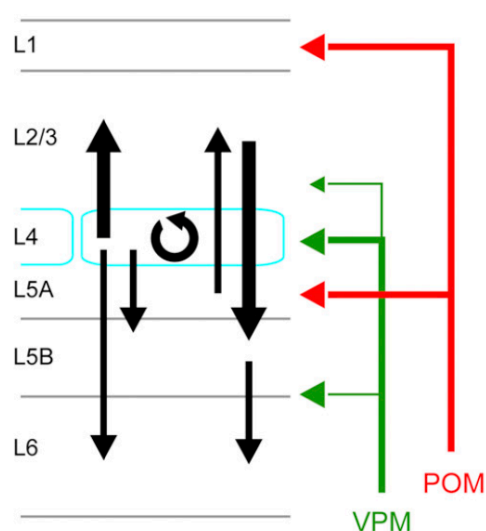


Figure 1.2. Barrel cortex circuitry. The black lines represent the main excitatory connections in the barrel cortex between all the layers. The green and red arrows represent input coming from the thalamus into the barrel cortex (ventral posteromedial nucleus, VPM, and posteromedial nucleus, POM, respectively). Taken from Petersen & Crochet 2013 ¹⁵².

In general, each cortical layer has unique cell types that correspond relatively well to the output projections for that layer. Starting with L4, the excitatory neuron types include stellate cells and pyramidal cells. The dendrites and axons of stellate cells are restricted to L4, which likely form the barrel columns ¹⁵³. On the other hand, L4 pyramidal cells typically have dendritic arbors that extend into neighboring columns and more superficial layers ¹⁴¹. L2/3 excitatory neurons are sparse-coding pyramidal neurons that project to primary somatosensory cortices outside of the barrel cortex, motor cortex (M1), and whisker secondary somatosensory cortex (S2). L5 consists of regular spiking (RS) cells and intrinsically bursting (IB) cells. This layer is often divided into L5A and L5B due to the differences in output projections. For example, L5A projects robustly to L1-3, while L5B

has strong projections to the POM and superior colliculus, and both parts of L5 likely project to whisker M1 and whisker S2 ¹⁴¹. Finally, L6 has cortico-thalamic cells that receive input from L4-L6 and project primarily to the thalamus, while the cortico-cortical cells have dense axonal arbors and long-range projections to many brain regions ¹⁴¹. In contrast to these layer-specific excitatory cells, there are two main types of inhibitory cells across all layers. Parvalbumin (PV) cells make up about 40% of the inhibitory cells, and one of their main functions is to provide rapid inhibitory feedback to excitatory cells. This ensures that the local microcircuit is quickly balanced and sharply conveys information, resulting in the sparse coding of whisker information such that only about 10% of excitatory neurons fire action potentials in response to each whisker stimulation ^{144, 154}. Somatostatin (STT) cells are another inhibitory cell type. They make up about 30% of the inhibitory neurons, and play a role in perception, synchronization, and modulation of activity ¹⁴¹. Collectively, these cell types (and others not mentioned here for simplicity) play a fundamental role in the barrel cortex and the processing of whisker information.

It is important to note that a key feature of the barrel cortex is the heterogeneity of the whisker response, which is commonly known as a salt-and-pepper organization. Neurons in one barrel may not respond best to the whisker that is associated with that barrel. It is even possible that neurons right next to each other are more responsive to different whisker stimulations ¹⁵⁵. Furthermore, previous literature also suggests that there are small local clusters of neurons in barrels that are perhaps co-tuned to the same whisker, whether that be the corresponding whisker of the barrel or a different whisker ¹⁵⁶. Thus, more experiments need to be conducted to determine how this salt-and-pepper layout and local clusters affect decoding in downstream processes.

Briefly, the regions between barrels in L4 are known as septa. These are regions that are not neuronally dense, and are primarily innervated by POM neurons ¹⁵¹. While barrel-related circuits are thought to encode spatiotemporal information of whiskers contacting objects, septal-related circuits

are thought to encode frequency and other kinetic information of whisker movements¹⁵¹. Septa are also more prominent in rats than mice, and further studies are warranted to elucidate the differences in sensory processing between the two species and brain regions.

In conclusion, whiskers are an incredibly important sensory modality for rodents. There are multiple pathways that transmit sensory input from the mechanosensory neurons at the whisker follicle to the barrel cortex. Each layer and cell type in the cortex serves a fundamental function in the processing, integration, and transmitting of tactile information from the environment to produce specific behaviors.

1.3.2 Deficits in the barrel cortex in FXS models

In FXS rodents, the barrel cortex exhibits several changes in anatomical structure, synaptic function, and sensory processing. For instance, the dendrites of FXS stellate cells near the barrel wall were shown to extend toward the septa more than WT cells. However, the dendritic projections towards the middle of the barrel remain the same, indicating that FMRP may be responsible for the normal pruning and removal of these projections¹⁵⁷. In another study, L5 neurons in the barrel cortex were imaged to track dendritic spine characteristics over the span of 1-4 weeks to examine potential developmental changes. Researchers discovered that there was an increase in spine length and density at 1 week of age, but that by 4 weeks, these changes were much less pronounced¹⁵⁸. These transient differences suggest that FMRP plays an important role in the normal development of spines at an earlier time point. Furthermore, *Fmr1* KO L5 pyramidal neurons demonstrated an increase in dendritic spine formation and elimination, and that these spines were not as responsive to whisker trimming as the WT neurons¹⁵⁹. These results suggest that the synaptic circuits in the *Fmr1* KO mice are not being tuned to sensory stimulation as responsively as in the WT. These changes in dendritic spine morphology would impact synaptic connectivity, plasticity, and sensory learning, which will be discussed throughout this section.

In addition to neuroanatomical differences in FXS mice, changes in the excitability and synaptic connectivity of neurons have also been observed. For example, the intrinsic excitability of L4 and L2/3 *Fmr1* KO excitatory neurons is increased compared to WT neurons^{65, 134, 135}. There is also reduced connectivity of L4 excitatory neurons to inhibitory neurons^{65, 134}. However, there are mixed observations about how the absence of FMRP impacts short-term plasticity in the barrel cortex. While one study found that there was no change in inhibitory postsynaptic currents (IPSCs) from inhibitory cells to excitatory cells, another found that there was more short-term depression in L4 of the *Fmr1* KO^{65, 134}. More studies need to be conducted to evaluate if/how short-term plasticity changes, which can impact sensory and information processing. Another circuit-level defect in *Fmr1* KO mice is that the connection from L4 to L3 is altered in multiple ways. The strength of this connection is reduced (caused by a lower neuronal connection probability), the L4 axons in L2/3 are more spatially diffuse in the KO than in the WT, and whisker trimming does not elicit a decrease in the strength of this connection as it does in the WT¹⁶⁰. It is interesting to note that the morphological differences were only transiently present during the second postnatal week, and that by the third week, the KO L4 to L2/3 connection was comparable to the WT, although experience-dependent plasticity was not measured again so we do not know if plasticity had recovered as well¹⁶⁰. Additionally, another study found that the critical period for L4 synaptic plasticity is delayed, showing yet another instance of developmental delay in FXS¹⁶¹. This idea of delayed maturation of the cellular and synaptic properties of neurons fits well with the idea of developmental delays as a clinical phenotype for FXS.

Finally, I want to briefly highlight some of the sensory processing deficits in FXS animal models. *Fmr1* KO L2/3 excitatory neurons and L2/3 inhibitory neurons, but not L4 excitatory neurons, demonstrated a decrease in the whisker-evoked firing rate¹³⁵. In addition, KO mice exhibit a broadening of the L2/3 receptive fields, but the L4 receptive fields stayed the same in response to

whisker stimulation¹⁶². These differences point to layer-specific changes that occur in the barrel cortex, and the effects of some of these changes can be observed in behavior. For example, *Fmr1* KO L2/3 neurons show deficits in neuronal adaptation to repetitive whisker stimulation, which may lead to tactile defensiveness often seen in autism¹⁶³. Tactile behavioral tasks also demonstrate that *Fmr1* KO mice are not as successful as WT mice in performing tasks that require solely whisker input, suggesting that there is a deficit in sensory processing¹⁶⁴. Interestingly, one study demonstrated that whisker stimulation results in increased translation of FMRP, supporting a strong role for FMRP in experience-dependent synaptic plasticity and learning¹⁶⁵.

Altogether, these studies demonstrate that barrel cortex anatomy and circuitry is impaired in FXS rodent models. FMRP is crucial for dendritic spine morphology and development, circuit function, and sensory processing. Without FMRP, FXS models can show either reduced or increased neural activity depending on the location. With this observation, one logical question to ask would be: why did homeostatic plasticity not correct for these changes in baseline activity? Is it possible that homeostatic plasticity itself is impaired in FXS? These studies and questions pave the way for my use of the FXS mouse barrel cortex in studying possible impairments in homeostatic plasticity.

1.3.3 Importance of using sensory systems in studying plasticity

Studying sensory systems, such as the visual, auditory, and somatosensory systems, have been crucial for understanding plasticity. There has already been extensive research on the anatomical structures and the topographic organization throughout the circuit. Thus, manipulating the sensory systems, in terms of deprivation or enrichment or stimulation, can help us better understand the triggers and mechanisms of plasticity, and the impact that plasticity has on sensory processing disorders like autism.

First, I would like to briefly highlight some plasticity studies in the visual cortex, since the initial plasticity experiments focused on critical periods and plasticity during visual development¹⁶⁶. An early study found that two days of monocular deprivation (MD) resulted in upscaling of mEPSC amplitudes in L4 neurons during a critical period, but outside of this period, there was no change, suggesting that scaling happens in an age- and layer- dependent manner¹⁶⁷. In another study, after just one day of MD, inhibitory neurons demonstrated a transient decrease in firing rates while pyramidal neurons showed no change in firing rates⁴⁴. A similar result was discovered by another group of researchers, where inhibitory neurons were the first cell type to alter their firing rates and rebound following MD, followed by changes in the excitatory neurons, suggesting the existence of cell-specific changes associated with deprivation⁴². It is also possible that different forms of homeostatic plasticity are in effect at different developmental stages, as studies have found that synaptic scaling could be triggered in the adult mouse brain, but homeostatic intrinsic plasticity could not^{168,169}. Thus, the visual cortex has been crucial in understanding how sensory perturbations at different timepoints affect specific layers and cell types.

The whisker-responsive barrel cortex has also become an increasingly valuable model for understanding tactile processing and the plasticity responses associated with perturbations. However, because scientists perform different types of deprivations (unilateral deprivation, row deprivation, checkerboard deprivation, single whisker experience), it is important to keep in mind how and when each of these variations affect the neural response. For the sake of clarity, I will only mention unilateral whisker deprivation studies in this section, since this is the experimental paradigm that I used to trigger homeostatic plasticity. Unilateral whisker deprivation removes the competition-based Hebbian plasticity that would occur with the other types of deprivation mentioned earlier. One study found that deprivation before P14 disrupted the receptive fields of L2/3 neurons, but not L4 neurons, suggesting that the critical period plasticity window for L2/3 neuronal development is

P12-P14¹⁷⁰. L2/3 neurons also demonstrated a delay in the maturation of the spiking properties when whisker deprivation was performed, thus establishing the importance of sensory input to the development of intrinsic excitability properties¹⁷¹. In another study, whisker deprivation from P9-P21 increased intercolumnar inputs to L2/3 neurons from neighboring columns, while also changing the intercolumnar inputs to L5 neurons, suggesting that sensory input is also necessary for the proper development of synaptic connections in multiple layers^{172,173}. However, deprivation in the adult mouse results in an interesting timeline of neural responses. Immediately following deprivation, there is a decrease in the L2-L4 neuron's firing rate after whisker stimulation, but by 3-4 days of deprivation, the neurons' firing rates return to baseline levels, and after 7 days, the firing rates potentiate above the baseline¹⁷⁴. The above results show that unilateral deprivation at different ages leads to unique layer- and timeline-specific changes in the barrel cortex.

There are multiple shared mechanisms of homeostatic plasticity in the rodent visual and barrel cortex. For instance, in both systems, rapid disinhibition occurs immediately after deprivation, whether that be through synaptic changes or intrinsic excitability changes^{175,176}. In addition, a slower firing rate homeostasis occurs over several days through homeostatic synaptic scaling, which serves to stabilize activity levels more long-term in a correlative study¹⁷⁵. The similarities in sensory systems suggest that although the plasticity mechanisms can selectively affect different layers and cells, there are common pathways that regulate overall excitability, such as synaptic strength, synaptic connectivity, and intrinsic excitability. Understanding both these separate and overlapping mechanisms would help us understand the role of homeostatic plasticity in neurodevelopmental and neuroplasticity-related disorders.

1.4 Dissertation aims and hypotheses

In summary, homeostatic plasticity plays an important role in stabilizing a neuron and/or network's firing rates and activity patterns. However, the neural features that are actually homeostatically

maintained have not been fully uncovered, since different systems might have different homeostatic goals. Chapter 2 discusses the homeostatic regulation of spiking characteristics in two distinct preparations – cortical neuronal cultures and the embryonic chick spinal cord. We blocked GABA receptor activity and conducted a comprehensive analysis of various spiking activity characteristics. We had hypothesized that there would be at least one feature that would be homeostatically maintained in both preparations, and found that this was in fact true. The spike rate within bursts showed a consistent initial increase and then homeostatic recovery following GABAergic blockade. Findings from this work demonstrate that individual cells and networks homeostatically restore spike rate during synaptic bursts, suggesting that this is an important spiking characteristic to maintain following perturbations. This work has already been published in *eNeuro*¹⁷⁷.

The second part of my research, discussed in Chapter 3, focuses on how impairments in homeostatic plasticity can be observed in neurodevelopmental disorders, such as FXS. In order to examine the homeostatic capacity of FXS neurons, I performed unilateral whisker deprivation on mice during a critical developmental window (P14-P21) to perturb the sensory system and trigger homeostatic plasticity. I then analyzed the whisker-evoked responses of L5/6 neurons in the barrel cortex to determine if cortical sensitivity to whisker input was altered. I had initially hypothesized that homeostatic plasticity would be severely impaired in the FXS mouse model (*Fmr1* KO). We found that the KO mouse exhibits deficits in the recruitment of excitatory and inhibitory L5/6 somatosensory neurons, both at baseline and after sensory deprivation. In addition, we observed a change in the sensitivity of excitatory neurons at a later developmental stage. This compromised excitatory and inhibitory function in development could influence sensory processing and long-term cortical organization. This work has been submitted to *Cell Reports*.

Chapter 2: Homeostatic Regulation of Spike Rate within Bursts in Two Distinct Preparations ¹⁷⁷

2.1 Abstract

Homeostatic plasticity represents a set of mechanisms thought to stabilize some function of neural activity. Here, we identified the specific features of cellular or network activity that were maintained after the perturbation of GABAergic blockade in two different systems: mouse cortical neuronal cultures where GABA is inhibitory and motoneurons in the isolated embryonic chick spinal cord where GABA is excitatory (male and female combined in both systems). We conducted a comprehensive analysis of various spiking activity characteristics following GABAergic blockade. We observed that most features were highly variable after blocking GABA_A receptors (e.g. burst frequency, burst duration, and overall spike frequency in culture). These results are consistent with the idea that neuronal networks achieve activity goals using different strategies (degeneracy). On the other hand, some features were consistently altered after receptor blockade in the spinal cord preparation (e.g. overall spike frequency). Regardless, these features did not express strong homeostatic recoveries when tracking individual preparations over time. One feature showed a consistent change and homeostatic recovery following GABA_A receptor block. We found that spike rate within a burst (SRWB) increased after receptor block in both the spinal cord preparation and cortical cultures, and then returned to baseline within hours. These changes in SRWB occurred at both single cell and population levels. Our findings indicate that the network prioritizes the spiking dynamics within a burst, which appear to be variable under tight homeostatic regulation. The result is consistent with the idea that networks can maintain an appropriate behavioral response in the face of challenges.

2.2 Introduction

Neuronal activity patterns can be highly stereotyped and invariant, even though the ion channels and synaptic inputs that drive such activity can vary widely^{17, 178-180}. For instance, in the crab stomatogastric ganglia, neurons expressing the same activity pattern can show a threefold variation in channel conductances^{13, 178}. This variation arises as cells homeostatically maintain some feature of activity, but achieve this in different ways (degeneracy). Because of this variability, an activity perturbation will affect one cell/network differently than another, as some are more dependent on certain conductances/synapses^{178, 181, 182}. Both this variability and the activity feature that is homeostatically maintained can be observed by perturbing network activity and observing how different activity features are altered and homeostatically recover.

However, identifying the actual neural characteristics that are homeostatically maintained has been elusive. Different studies have identified different homeostatic goals. Studies have found evidence supporting overall firing rate homeostasis at the level of the individual cell^{42, 43}, at the network population level⁴⁵, in response to a sensory stimulus⁴⁴, and in terms of criticality that maximizes information capacity⁴⁶. Due to the importance of homeostatic plasticity in neural disorders, it is critical that we come to a better understanding of the multiple activity properties that may be homeostatically regulated. With the idea that individual preparations achieve similar activity using different strategies and that different spiking features are homeostatically regulated, our goal was twofold. First, we assessed variability of firing properties in individual preparations following a synaptic perturbation. Second, we examined which properties were best homeostatically regulated^{183, 184}, and have done this using two very different developing systems.

We and others have demonstrated that the addition of CNQX, an AMPA receptor (AMPA) antagonist, to cortical cultures results in a wide range of changes in overall firing rates, and that homeostatic recovery of the spike rates did not occur within 24 hours^{45, 185}. In the current

study, we blocked GABA_A receptor (GABAR) activation in cortical cultures. Our primary objective was to identify the specific spiking features that undergo homeostatic regulation in response to perturbation. To assess the generality of our observations in culture in a more intact system, we also chose the isolated embryonic chick spinal cord preparation. This system expresses several homeostatic plasticity mechanisms, both *in vivo* and *in vitro*^{6,27,35,36}. Previous work has suggested that GABAR blockade *in ovo*, during a developmental stage when GABA is depolarizing and excitatory, leads to the abolition of embryonic movements that are then recovered 12 hours after drug application³⁵. Nevertheless, the precise features of activity that were homeostatically regulated in motoneurons were unknown. Thus, the current study aimed to understand how activity features are altered and homeostatically restored in response to GABAR blockade in two systems: one in which GABA is inhibitory (cortical culture), and the other in which GABA is excitatory (isolated spinal cord).

Following GABAergic blockade, we assessed overall spike rate, burst frequency and duration, spike rate within a burst (SRWB), and inter-burst spike rate. As predicted due to degeneracy, we observed variability in both preparations after perturbation. On the other hand, we found that SRWB was most consistently altered (increased) and was also most reliably returned to pre-perturbation levels in both systems. Our findings suggest that both cells and the network actively and homeostatically restore spike rate during synaptic bursts, thus preventing long-term hyperexcitability.

2.3 Results

2.3.1 *SRWB is homeostatically restored following GABAergic blockade in cortical cultures*

Previous work from our lab has shown that AMPA receptor blockade (CNQX) in cortical cultures changed the firing rates and burst frequencies in a highly variable manner¹⁸⁵. Both the degree to which firing/burst rates were reduced and the 24-hour homeostatic recovery were variable in these

different cultures. We wondered if such variability would similarly be observed if we attempted to increase activity. GABAR blockade in cortical cultures has been shown to increase certain features of spiking acutely^{4, 186, 187}. In order to assess the variability of this response and to determine the timing of such a recovery, we disinhibited cortical cultures and monitored various firing rate characteristics following this perturbation. To this end, we plated mouse cortical cultures on 64-channel MEAs and allowed for circuit development for 10-14 DIV. We observed typical network burst activity, with bursts involving relatively synchronous spikes across multiple channels in semi-regular intervals. Then, we analyzed overall spike rate, burst duration and frequency, inter-burst interval spike rate (IBI, spike rate outside of bursts), and spike rate within a burst (SRWB) (Figure 2.1). Baseline activity was recorded for several hours before the drug was introduced, and spiking features were then monitored for 24 hours after the addition of the GABAR antagonist bicuculline (20 μ M) or in untreated control cultures.

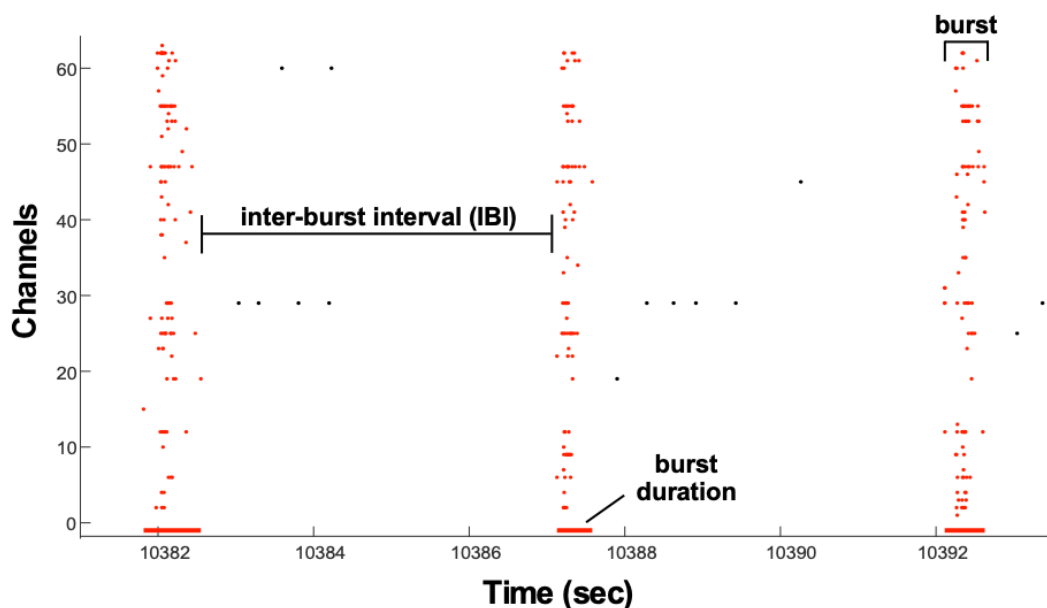


Figure 2.1. Firing rate characteristics analyzed in cortical cultures. Raster plot of network burst activity across all channels in the MEA. Inter-burst interval (IBI) spike rate is the spiking that occurred outside of the bursts (spikes are black dots). SRWB is the spike rate that occurs within the burst (spikes are red dots). Burst duration is shown by the red lines below raster plot.

Overall spike rate

Previously, it was observed that overall spike rate increased shortly after bicuculline addition, although it did not reach significance¹⁸⁸. Here, we tracked overall spiking across individual cultures over a 24 hr period. On average (thick black line – Figure 2.2A, Figure 2.3A), this parameter increased following bicuculline, and then 24 hours after GABAergic blockade, it had recovered to the level of control cultures at 24 hours. However, looking at individual cultures tells a different story, as we observed strikingly distinct responses to bicuculline in each culture (shown as different colors in Figure 2.2A). While most cultures showed a clear increase in overall spiking, one briefly increased and then was reduced, one was unchanged, and two others were profoundly reduced. By 24 hours, cultures appeared to be above, below, or at untreated control levels (Figure 2.2A). The two cultures that were reduced from the onset of bicuculline remained low for the entire 24 hours (showed no homeostatic tendency). Consistent with degeneracy, it was clear that following disinhibition, there was dramatic variability in both overall spike rate as well as in the homeostatic recovery of this feature. In addition, pre-bicuculline values (not normalized) for all parameters are shown in Table 2.1.

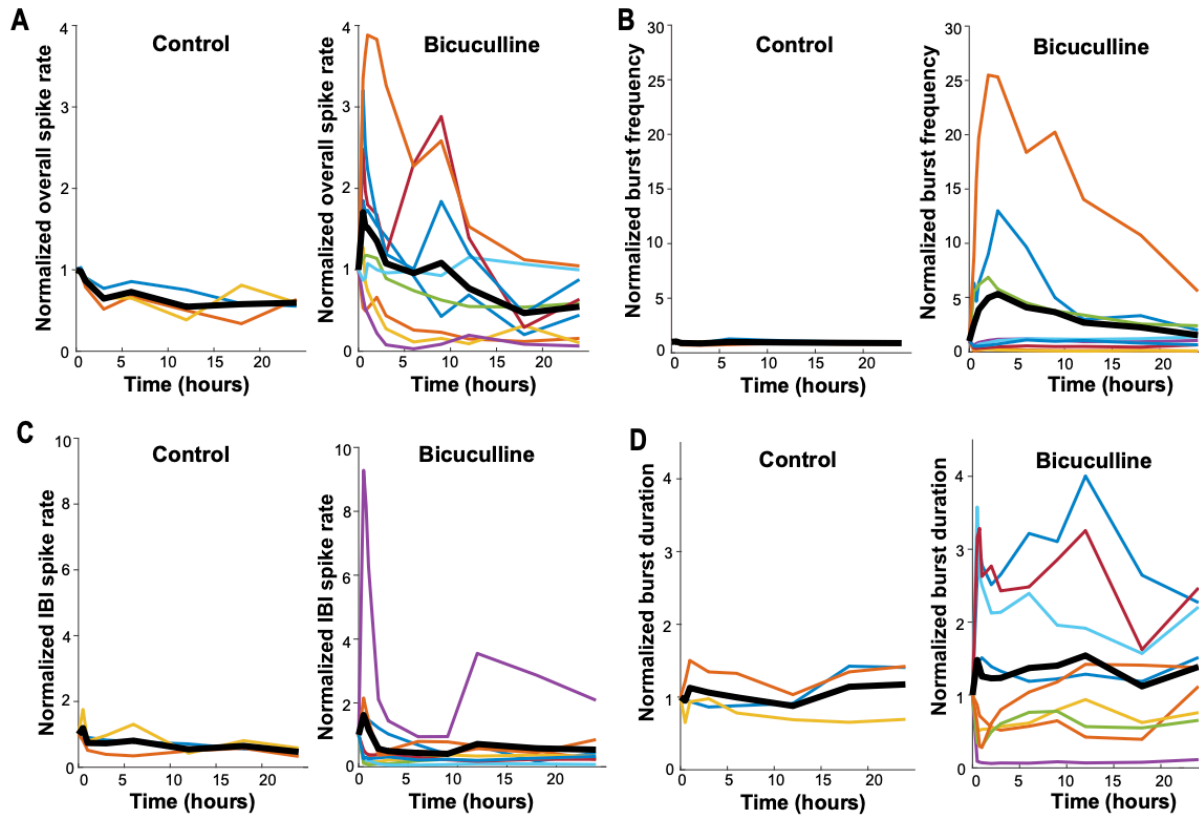


Figure 2.2. Burst dynamic parameters measured following GABAR blockade (bicuculline) in cortical cultures. **A)** Normalized overall spike rate **B)** Normalized burst frequency **C)** Normalized inter-burst interval (IBI) spike rate and **D)** Normalized burst duration displayed over a 24-hour period for control and bicuculline-treated cultures. Values at each time point are normalized to baseline (pre-drug) condition. Each color line represents a single culture, with the thick black line representing the mean of all cultures. The data shown in A and B are the same data as in our previous publication (Gonzalez-Islas et al., 2024), however here we follow individual cultures over time. Estimation statistics comparing bicuculline-treated and control cultures at each of the time points establish that none are significantly different. This is likely due to the dramatic variability.

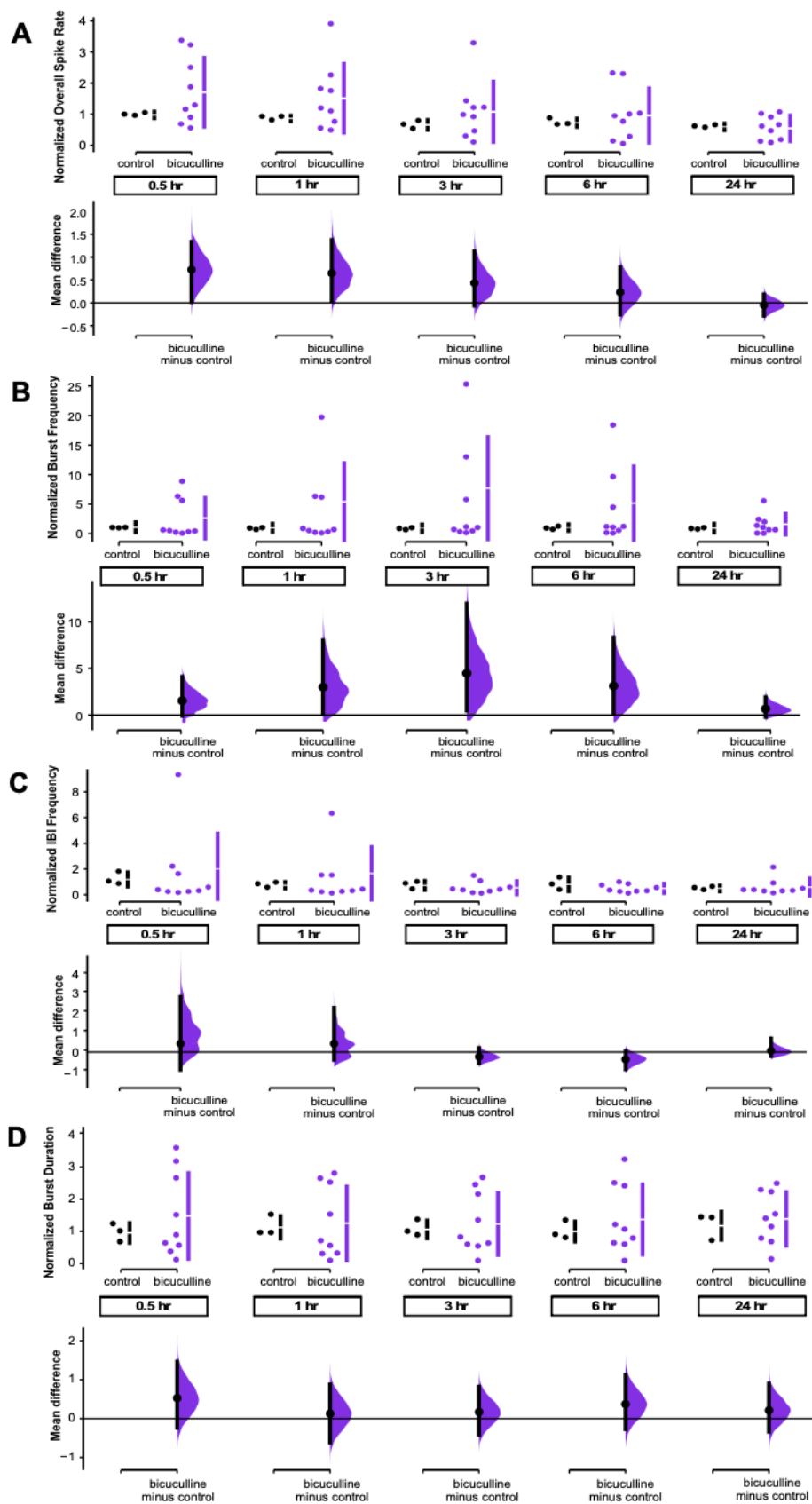


Figure 2.3. Estimation statistics of burst dynamics parameters from bicuculline-treated cultures for **A**) overall spike rate **B**) burst frequency **C**) inter-burst interval (IBI) spike rate and **D**) burst duration. The mean differences at each time point are compared to control and displayed in Cumming estimation plots. Upper panel shows raw data from single spinal cord recordings (filled circles), where the mean value is represented by the gap in the vertical bars and the SD is represented by the vertical bars. Lower panel shows mean differences between control and treated groups as a bootstrap sampling distribution (mean difference is represented by filled circle and the 95% CIs are depicted by vertical error bars).

Feature	Pre-Bicuculline Value
Overall spike rate	42.51 \pm 55.36
Burst frequency	0.24 \pm 0.24
Inter-burst interval spike frequency	8.14 \pm 8.21
Burst duration	1.07 \pm 2.23
Spike rate within a burst	166.27 \pm 76.46
Number of channels in a burst	16.24 \pm 14.11

Table 2.1. Mean and standard deviation of all spiking activity features that were analyzed for culture preparations. All features are reported in Hz, except for burst duration (seconds) and the number of channels.

Burst frequency/IBI spike rate

Since most spikes occurred within bursts, we also assessed burst frequency. Previously, it was found that burst frequency increased following bicuculline application, although it did not reach significance¹⁸⁸. Here, we show burst frequency tracked across individual cultures over a 24 hr period and found that burst frequency showed an apparent homeostatic nature if one only looked at the average values following bicuculline treatment (thick black line – Figure 2.2B). However, once again, this view was a simplistic one as the dramatic variability to this perturbation complicated such an interpretation. Unlike overall spike rate, most cultures reduced burst frequency after GABAergic blockade (Figure 2.2B, Figure 2.3B). On the other hand, three of the cultures showed very large increases in burst frequency, which did appear to be in the process of recovering back toward control levels, although they did not fully recover by 24 hours. The cultures that expressed reduced burst frequency following bicuculline either returned to control levels or were maintained at lower

levels. Ultimately, we found that cultures demonstrated high variability, and not all demonstrated a homeostatic recovery of burst frequency. Very similar results were observed when looking at the spike rate across channels in the inter-burst interval (most decreased, some increased, no obvious homeostatic response, Figure 2.2C, Figure 2.3C).

Burst duration

We also analyzed burst duration (the period of synchronous spiking across channels) and found dramatic variability in burst duration following GABA_A receptor blockade (Figure 2.2D, Figure 2.3D). Some cultures increased burst duration, some were unchanged, and some were profoundly decreased. However, whether there was an increase, decrease, or no change in burst duration, the post-bicuculline value was largely maintained for the 24-hour treatment. The majority of cultures did not demonstrate homeostasis of burst duration and responded to bicuculline in a highly variable manner.

Spike rate within a burst

We analyzed the SRWB, or the total number of spikes across all channels within a burst divided by the total duration of the bursts (Figure 2.4). Within the first 30 minutes of disinhibition, there was a significant and dramatic increase in the SRWB for all cultures, and this effect persisted to some extent until approximately the 6th hour after bicuculline application, when the values homeostatically returned to levels seen before bicuculline was added and to levels seen in the untreated cultures at the corresponding time points. The first three hours of bicuculline-treated cortical cultures demonstrate a significant increase in SRWB, while the 6-hour and 24-hour time points were no different than control cultures (Figure 2.4C). This result was remarkable, and so we further analyzed this interesting finding. We examined individual SRWBs for each burst in an individual culture and plotted the average value and standard deviation of this parameter, and did so without normalization. It was clear that following bicuculline, SRWB was increased and homeostatically

recovered within several hours of drug application in every single culture (Figure 2.5). Finally, bicuculline has been reported to modulate potassium channel conductances¹⁸⁹, so we also tested a weaker but more specific GABA receptor antagonist gabazine (5 μ M) in 3 additional cultures. The results were no different than those using bicuculline (Figure 2.6). These striking results suggested that the blockade of GABAergic transmission triggered a uniform increase in SRWB that was then homeostatically brought back down to control levels.

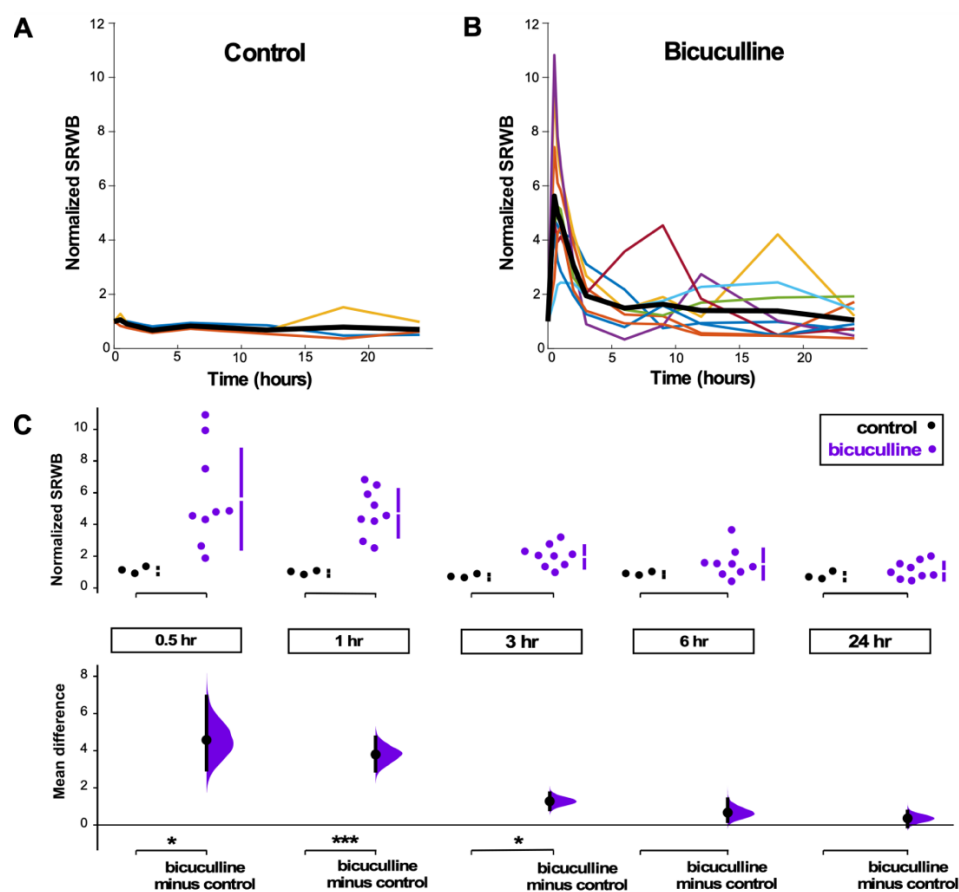


Figure 2.4. Spike rate within a burst (SRWB) following GABA blockade is consistently homeostatically recovered in cortical cultures. **A and B)** SRWB displayed over a 24-hour period for **(A)** control (untreated) and **(B)** bicuculline-treated cultures. Values at each time point are normalized to baseline (pre-drug) condition. Each color line represents a single culture, with the thick black line representing the mean of all cultures. **C)** SRWB is compared for control and bicuculline-treated cultures at 0.5hr, 1hr, 3hrs, 6hrs, and 24hrs after addition of bicuculline. The mean differences at different time points are compared to control and displayed in Cumming estimation plots. Significant differences denoted by * $p < 0.05$, *** $p < 0.001$. Upper panel shows raw data from single culture recordings (filled circles), where the mean value is represented by the gap in the vertical bars and the SD is represented by the vertical bars. Lower panel shows mean differences between control and treated groups as a bootstrap sampling distribution (mean difference is represented by filled circle and the 95% CIs are depicted by vertical error bars).

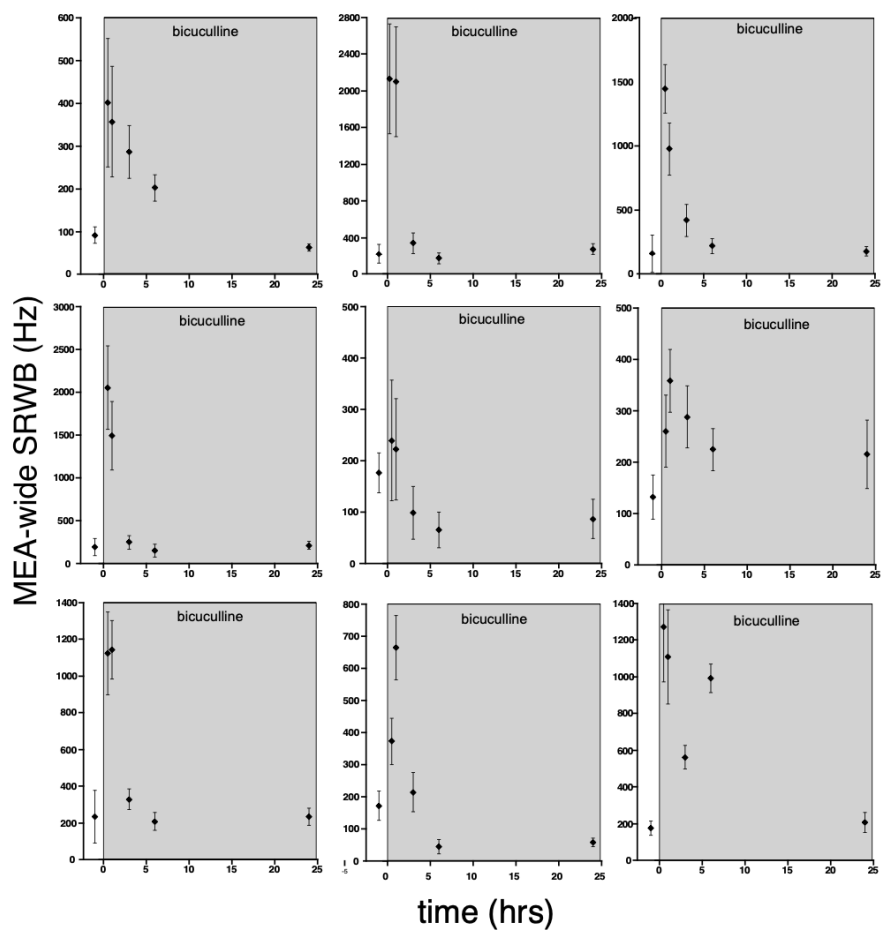


Figure 2.5. Nine different cortical cultures show that addition of bicuculline triggers an increase in SRWB, which then is homeostatically returned to baseline levels. SRWB is calculated as the average SRWB across individual bursts and standard deviation of SRWB is shown as error bars. Data is not normalized so represents the MEA-wide spike of each culture before and after bicuculline.

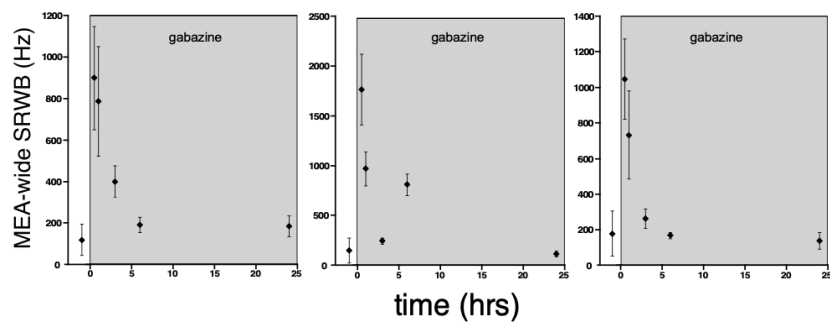


Figure 2.6. Three different cortical cultures show that addition of gabazine triggers an increase in SRWB, which then is homeostatically returned to baseline levels. SRWB is calculated as the average SRWB across individual bursts and standard deviation of SRWB is shown as error bars. Data is not normalized so represents the MEA-wide spike of each culture before and after gabazine.

Homeostatic index of spiking features

To better analyze and compare the homeostatic nature of each firing rate property, we assessed a homeostatic index (Figure 2.7). We calculated this index to provide a percentage recovery of the perturbed state. This was calculated as the most extreme normalized value in the first hour after bicuculline minus the normalized value 24 hours after bicuculline (actual recovery); this value was then divided by the most extreme normalized value in the first hour after bicuculline minus the normalized value in control cultures at 24 hours (full recovery). For example, if the parameter increased to 5 times the initial value within the first hour and then returned to twice the 24-hr control value, then the index would show a 75% recovery ($(5-2) / (5-1)$). In this way, values that don't recover at all are 0%, those that recover completely are at 100%, those above 100% recover but then continue past baseline control values, and those that are negative have continued to move in the direction of the first hour. We found that there was high variability in terms of homeostatic recovery for most of the firing rate properties we measured. However, for each one of the individual cultures SRWB was the one property that most consistently returned to control levels (100%) and was associated with the smallest variability (coefficient of variation or CV) (Figure 2.7, Table 2.2). These studies demonstrate a critical importance of this firing rate property that only occurs when the network is synaptically active.

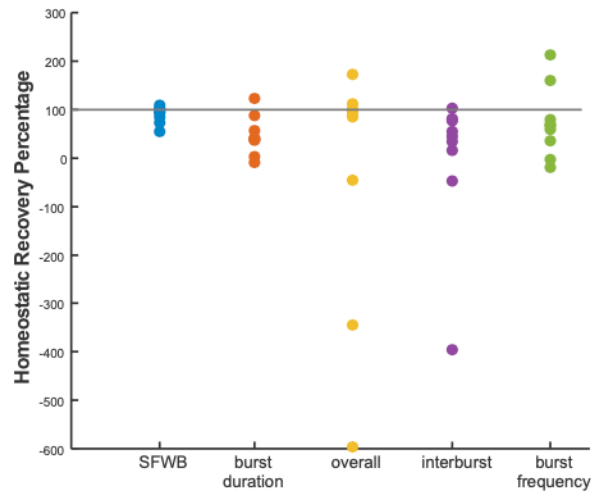


Figure 2.7. Homeostatic recovery percentage for firing rate properties. The homeostatic index for each bicuculline-treated culture was calculated by subtracting the 24-hr bicuculline time point from the greatest bicuculline-induced change in the first hour divided by the immediate bicuculline-induced change minus the 24-hr control time point. For example, if the parameter increased 5 times within the first hour and then returned to twice the 24-hr control value, then the index would be 75% ($(5-2) / (5-1)$). Horizontal line represents 100% recovery. Spike frequency within a burst is the firing rate property that most consistently demonstrates near 100% homeostatic recovery.

Feature	CV	Mean
SRWB	0.19	90.32
Burst duration	0.86	46.65
Overall spike rate	-7.12	-36.56
Inter-burst interval spike rate	-46.22	-3.32
Burst frequency	0.99	73.75

Table 2.2. Coefficient of variation (CV) and mean of all spiking activity features that were analyzed for culture preparations. All features are reported in Hz, except for burst duration and episode duration (seconds).

SRWB is homeostatically regulated at both the population and single cell levels

It is possible that individual cells regulated their spike rate within a burst and/or that the number of recruited neurons that contributed to a burst was regulated. Therefore, we looked at the number of channels contributing to a burst. Following GABAergic blockade, we found that a higher proportion of the channels contributed to each burst in all but one culture (Figure 2.8B). Before bicuculline treatment different subsets of channels contributed to any given burst, but after GABAergic

blockade, the majority of the active channels contributed to most bursts. After 18 hours of bicuculline treatment the number of channels per burst recovered to pre-drug values (Figure 2.8B). We then looked to identify the SRWB for single units. Different waveforms were identified on individual channels at the time the recordings were obtained based on principal component analysis of the waveform in the TDT acquisition program (Figure 2.8C1-2). We then examined channels that only contained one waveform (Figure 2.8C1). We only accepted these individual waveforms if less than 1% of the inter-spike intervals were less than 2ms (refractory period for the spike). This eliminated certain cultures entirely and the vast majority of the channels across cultures, while leaving us with 12 single unit recordings that we could follow across conditions. We found that most of the individual units (11/12) increased to some extent following disinhibition and then returned to lower levels over the next 24 hrs (Figure 2.8C). However, SRWB for individual units did not respond uniformly, consistent with the idea that there is heterogeneity in the population of recorded cells – some increased dramatically, some less so, one remained largely unchanged through the perturbation, and some (2 of 12) increased slightly but then went below 50% of their original levels. Together, these results suggested that the increase and homeostatic recovery of SRWB was occurring both at the level of individual cells and the population.

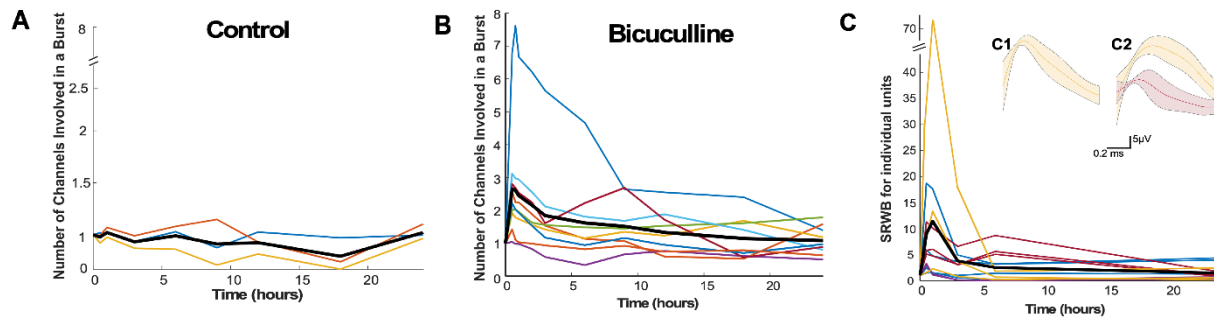


Figure 2.8. Spike rate within a burst (SRWB) following GABAR blockade was homeostatically recovered at both the population and single unit level. **A)** In control cultures, the number of MEA channels contributing to a burst remained stable. **B)** Following bicuculline, the number of MEA channels contributing to a burst increased and was then homeostatically restored over a 24-hour period. Values at each time point were normalized to the baseline (pre-drug) condition. Each color line represents a single culture, with the thick black line representing the mean of all cultures. **C)** Following bicuculline, SRWB for most individual sorted units increased and were homeostatically restored over a 24-hour period. Values at each time point were normalized to the baseline (pre-drug) condition. Each line represents a single unit from one of four cultures (units from same cultures are of the same color), with the thick black line representing the mean of all units. Inset - one (**C1**) or two (**C2**) waveforms were identified on two different channels (SD shown in shaded area).

2.3.2 SRWB is homeostatically restored following GABAergic blockade in the isolated chick embryo spinal cord

The unexpected finding that SRWB was the parameter that was best homeostatically maintained in cortical cultures was clear and interesting. However, cultured cortical networks are a somewhat artificial circuit predisposed to variability due to many aspects of this system – density of plating, glial or inhibitory neuron content, brain regions that contribute to a particular culture (somatosensory vs visual). Therefore, it was important to see if similar results might be observed in a defined class of neurons in a more intact circuit. Thus, we chose the embryonic chick spinal cord preparation, which has been shown to express several homeostatic mechanisms following both *in vivo* and *in vitro* blockade of GABAergic transmission^{27, 190}. An important difference from cortical cultures is that GABA is depolarizing and excitatory in the embryonic spinal cord¹⁹¹. As a result, the spinal cord is highly active and recruits the majority of neurons in network-wide bursts of activity called episodes, which last for several seconds, and *in vivo*, drive embryonic movements by recruiting motoneurons^{28, 29}. These episodes are also referred to as spontaneous network activity or SNA and

occur every 5-10 minutes; each episode is composed of several depolarizing bursts (Figure 2.9)^{28, 192}. We isolated lumbosacral spinal cords with intact ventral roots as described previously (See methods)^{6, 40}. We then drove a 32-channel NeuroNexus probe into the spinal cord (Figure 2.9A). Antidromic stimulation of the ventral root identified which channels on the probe corresponded to motoneurons (Figure 2.10).

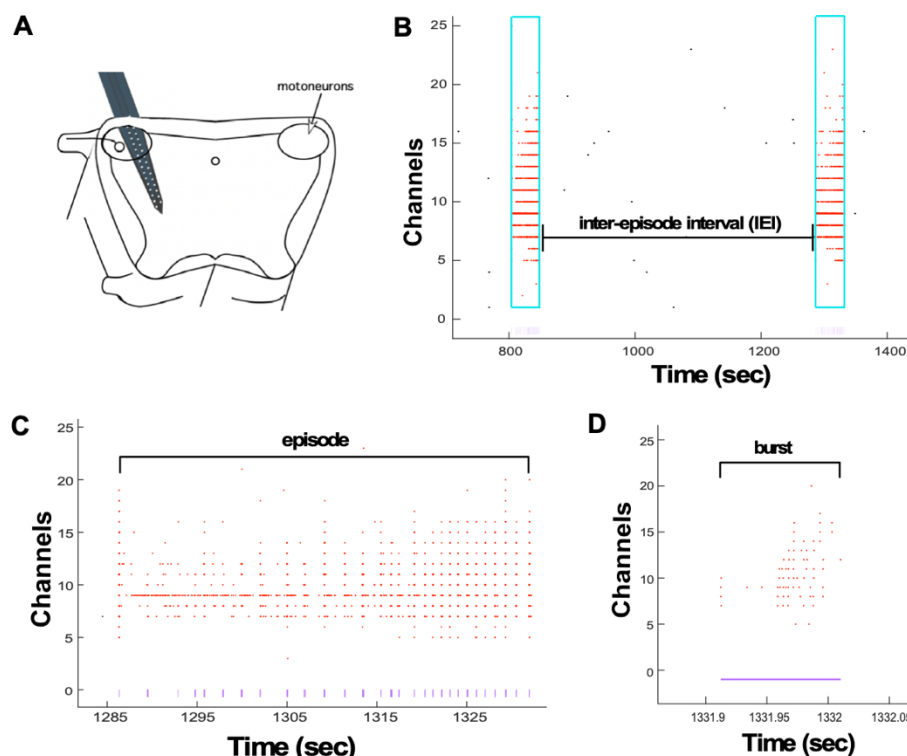


Figure 2.9. Firing rate characteristics analyzed in the isolated embryonic chick spinal cord. **A)** Schematic of 32-channel NeuroNexus probe inserted into the spinal cord, specifically penetrating the motor column. **B)** Raster plot of network burst and episode activity across channels on the NeuroNexus probe. Episodes caught by the custom-written Matlab program are highlighted in blue, with spikes caught in the episodes as red dots. Purple lines below the episodes represent where bursts occurred within the episode. Black dots are spikes that occurred outside of the episode. Thus, the inter-episode interval spike rate is calculated by taking the spike rate outside of the episodes. **C)** The raster is zoomed into the last episode from (A). The red dots again represent the spikes within the episode and the purple lines denote the bursts. From this data, we can calculate the episode spike rate, which includes all spikes within the episode, regardless of whether or not the spikes were part of a burst. **D)** The raster is zoomed into the last burst from (B). We calculated the burst duration and spike rate within the burst within episodes from this data.

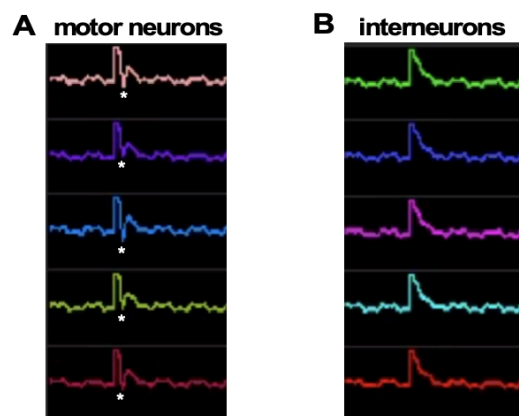


Figure 2.10. Antidromic stimulation to identify embryonic chick spinal cord motor neurons. **A)** Asterisks mark the component that identifies motor neurons in the raw trace. **B)** No motor neuron component is present in the interneurons.

Recordings were made for approximately 3-4 hours, where the first 30 minutes of the recording provided the baseline activity. Then, excitatory GABAergic transmission was blocked with 10 μ M gabazine or no antagonist was added (control). In order to better quantify spiking activity, we divided the length of the recording into 30-minute time bins, and if multiple episodes were observed, the episode activity was averaged for that time bin. We analyzed overall spike rate, episode spike rate, episode duration, inter-episode interval spike rate (spike rate between episodes), burst duration, and SRWB within an episode to determine which firing properties were homeostatically maintained.

Overall spike rate/episode frequency

First, we analyzed overall spike rate (Figure 2.11A), and noticed a significant decrease in spike rate compared to the control cords within the first 30 minutes of gabazine addition, and this decrease persisted throughout the length of the recording (Figure 2.12A). Pre-gabazine values for all parameters (not normalized) are shown in Table 2.3. This result for the overall spike rate was not surprising as previous work has shown that most spikes occur within episodes and that blockade of a depolarizing GABAergic transmission reduced the frequency of these episodes²⁸. We therefore analyzed episode frequency in these cords and found that indeed, all cords decreased the frequency

of episodes following GABAergic blockade, and we did not observe signs of homeostatic recovery in the following hours (Figure 2.13). Since neither the overall spike rate nor the episode frequency recovered, it is clear that these features were not homeostatically maintained within the three hours of the recording. Thus, we moved on to examine other firing rate properties to see if they were homeostatically regulated.

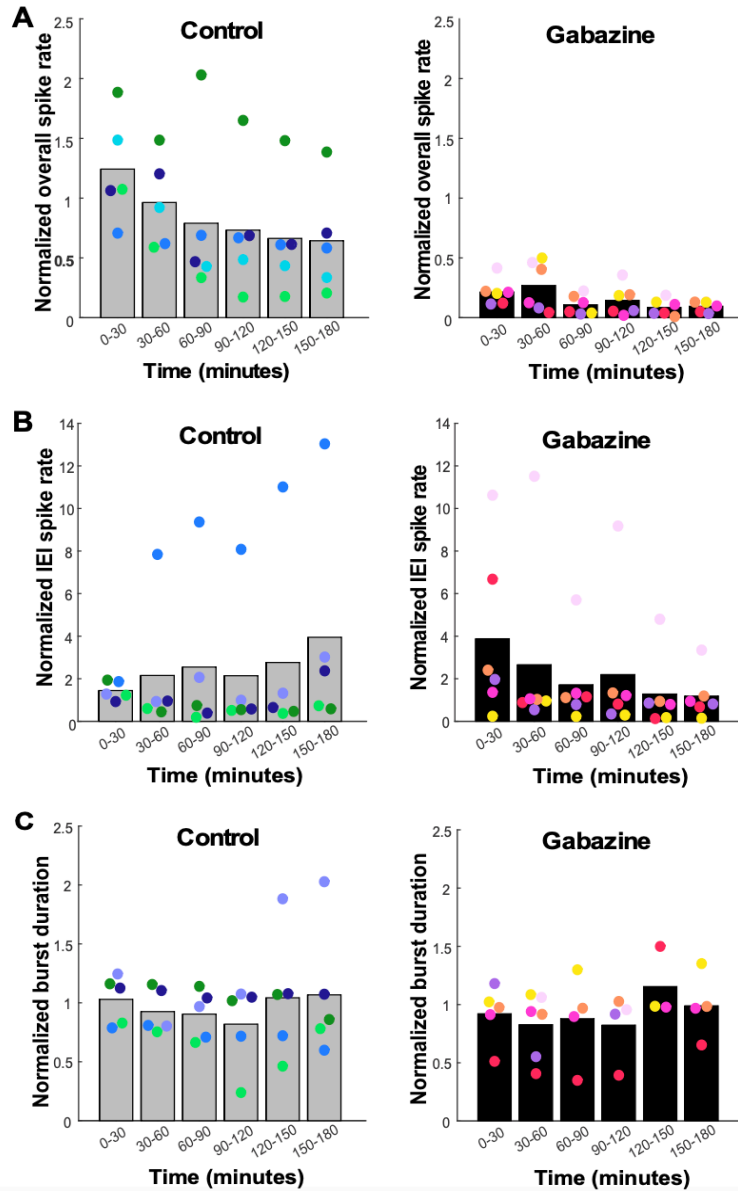


Figure 2.11. Spiking parameters measured following gabazine-blockade in embryonic chick spinal cords. **A)** Normalized overall spike rate **B)** Normalized inter-episode interval (IEI) spike rate and **C)** Normalized burst duration displayed over a 3-hour period for control (untreated) and gabazine-treated cords. Each color dot represents a single cord, with the height of the bar representing the mean of all cords.

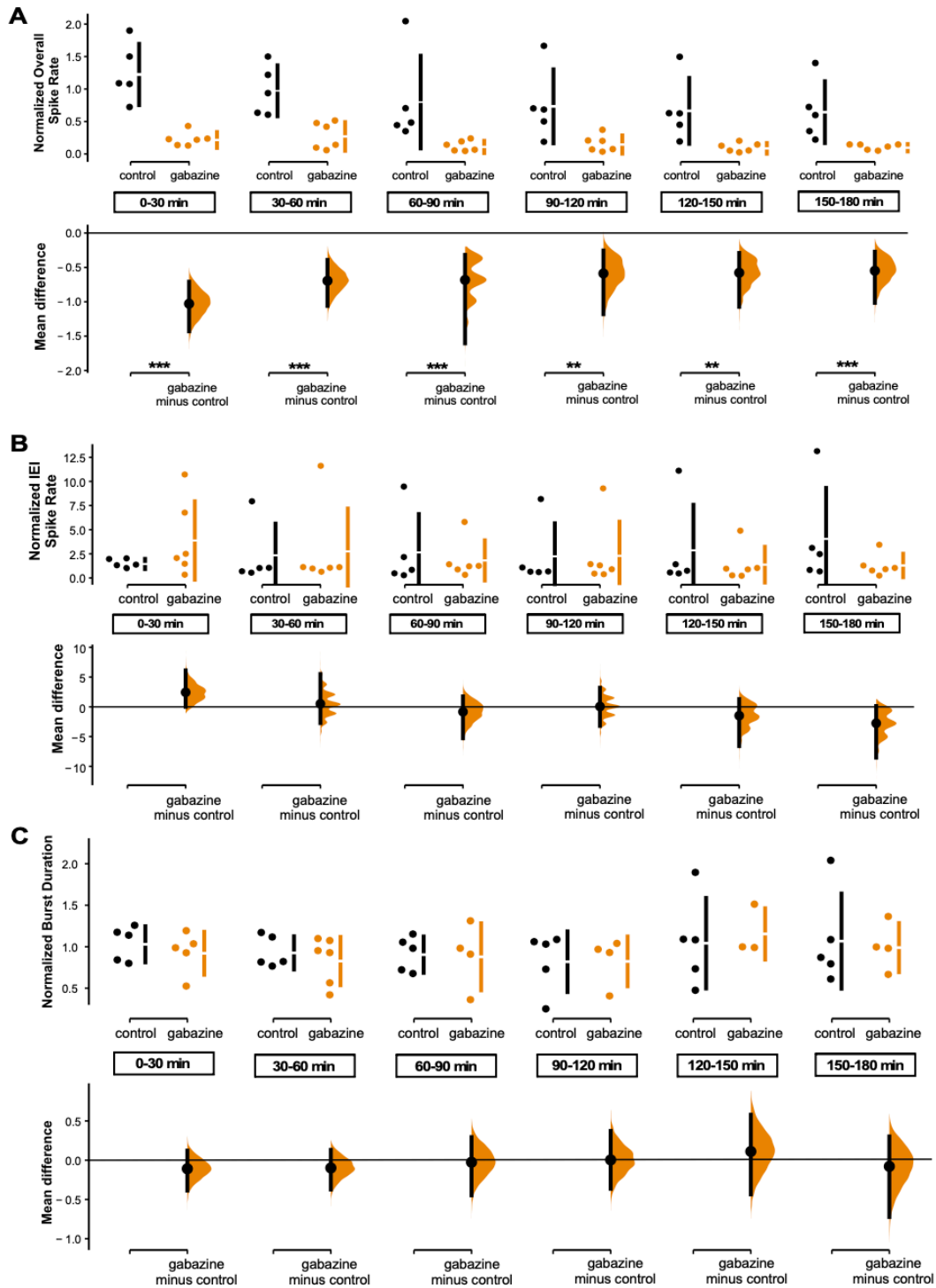


Figure 2.12. Estimation statistics of firing dynamics parameters from gabazine-treated spinal cords for **A**) overall spike rate **B**) inter-episode interval (IEI) spike rate and **C**) burst duration. The mean differences at each time point are compared to control and displayed in Cumming estimation plots. Significant differences denoted by ** $p < 0.01$, *** $p < 0.001$. Upper panel shows raw data from single spinal cord recordings (filled circles), where the mean value is represented by the gap in the vertical bars and the SD is represented by the vertical bars. Lower panel shows mean differences

mean differences between control and treated groups as a bootstrap sampling distribution (mean difference is represented by filled circle and the 95% CIs are depicted by vertical error bars).

Feature	Pre-Gabazine Value
Overall spike rate	0.19 ± 0.06
Inter-episode interval spike frequency	0.01 ± 0.01
Burst duration	0.09 ± 0.02
Episode spike rate	0.13 ± 0.04
Episode duration	42.74 ± 8.16
Spike rate within a burst	1.72 ± 0.71

Table 2.3. Mean and standard deviation of all spiking activity features that were analyzed for spinal cord preparations. All features are reported in Hz, except for burst duration and episode duration (seconds).

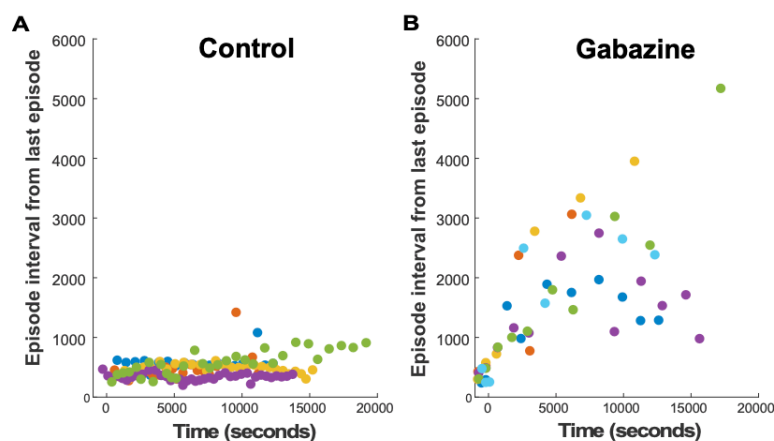


Figure 2.13. Episode frequency following GABA blockade in the isolated spinal cord is not homeostatically recovered. Occurance of episodes in spinal cords is displayed as the time interval from the last episode. Each color dot represents a single spinal cord. Gabazine was added at time point 0 seconds. **A)** Episode frequency of control cords. **B)** Episode frequency of gabazine-treated cords.

Inter-episode interval spike rate

Next, we analyzed spiking within the inter-episode interval, or the spike rate outside of episodes (Figure 2.11B). We observed variability in both the control and gabazine-treated spinal cords, such that no significant differences were observed at any of the time points and therefore there was no homeostatic recovery of inter-episode interval spike rate (Figure 2.12B).

Episode duration and spike rate

We next computed firing properties associated with the episode. We calculated the episode spike rate and episode duration (Figure 2.14). Both of these firing properties were variable in control and gabazine-treated cords, though both were clearly more variable after gabazine treatment. On average, neither property showed any significant changes following gabazine treatment. Further, any changes in individual cords that occurred following gabazine appeared to be maintained. Therefore, neither episode spike rate nor episode duration showed homeostatic regulation. These results showed that GABAergic blockade reduced the frequency of episodes, but when they occurred, the average duration and spike frequency within the episode were unaltered. However, it was clear that gabazine altered these parameters in very different ways in each individual cord (increasing in some, decreasing in others).

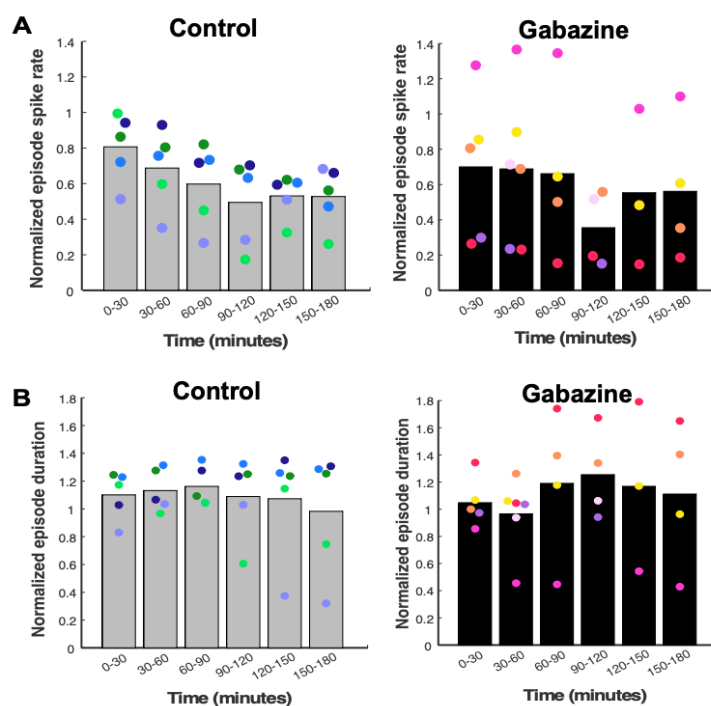


Figure 2.14. Episode spike rate and episode duration following GABA blockade are variable in both control and gabazine- treated spinal cords. **A)** Episode spike rate displayed over a 3-hour period for control (untreated) and gabazine-treated cords. Values in each 30-minute bin are normalized to baseline condition. Each color dot represents a single spinal cord, with the height of the bar representing the mean of all cords. **B)** Episode duration displayed over a 3-hour period for control (untreated) and gabazine-treated cords. Values in each 30-minute bin are normalized to baseline condition. Each color dot represents a single spinal cord, with the height of the bar representing the mean of all cords.

Burst duration

We also examined the duration of the bursts within the episode (Figure 2.11C). Again, we observed no difference in the average values between gabazine-treated and control cords (Figure 2.12C). Yet, once again burst duration was highly variable in the first 90 minutes of GABAergic blockade. Homeostatic control of burst duration was not observed.

Spike rate within a burst

Finally, we examined SRWB, in this case, in bursts within an episode (Figure 2.15A-B). We found that although the SRWB was highly variable in the first 30 minutes following gabazine addition, there was a significant increase in this firing property compared to the control (Figure 2.15C). Moreover, the SRWB after the first 30 minutes then decreased and was similar to control cords that were not treated with gabazine. These bursts in the spinal cord drive the kicking behavior that we have observed *in ovo*, suggesting that the behavioral output of the system was being maintained at a specific set point. In this case, changes in SRWB likely would manifest as changes in movement amplitude or speed. Regardless, these changes in SRWB are the same as those observed in the disinhibited cortical cultures. This demonstrated that the SRWB was one of the more important firing properties because it was homeostatically regulated (see Discussion).

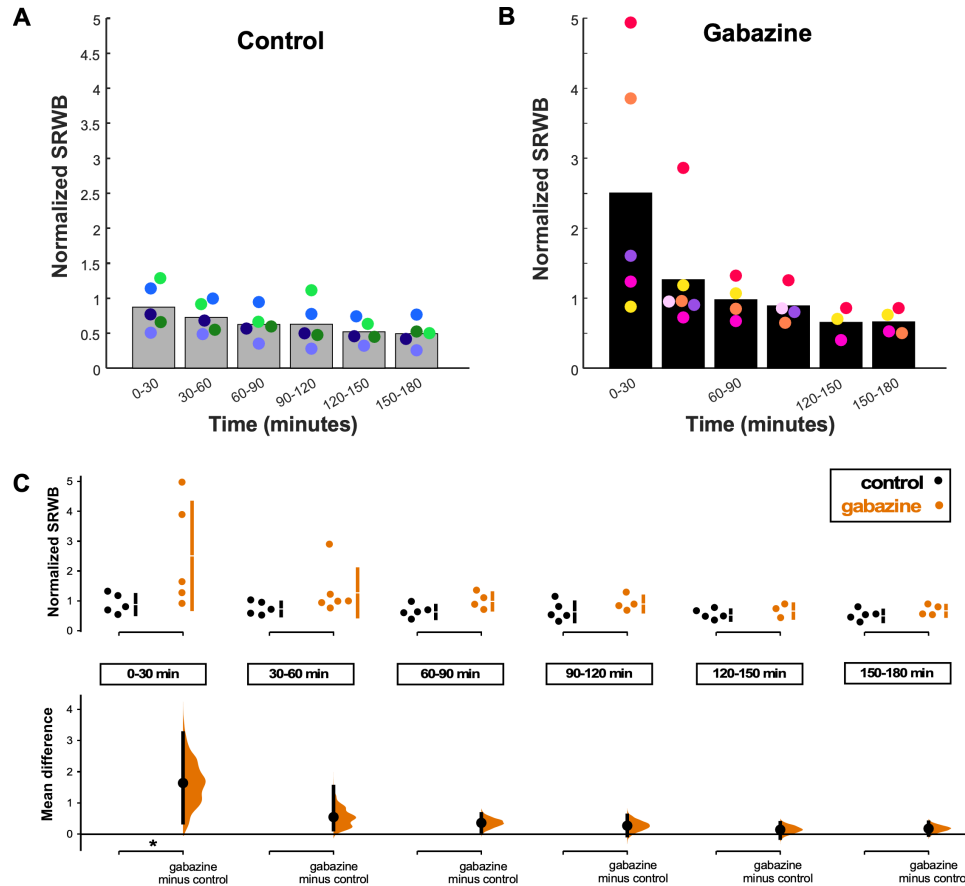


Figure 2.15. Spike rate within a burst (SRWB) within episodes following GABA blockade in the isolated spinal cord is consistently homeostatically recovered. **A and B)** SRWB displayed over a 3-hour period for **(A)** control (untreated) and **(B)** gabazine-treated cords. Values in each 30-minute bin are normalized to baseline (pre-drug) condition. Each color dot represents a single spinal cord, with the height of the bar representing the mean of all cords. **C)** SRWB is compared for control and gabazine-treated cords at 30-minute intervals during the 3-hour recording period. The mean differences at each time point are compared to control and displayed in Cumming estimation plots. Significant differences denoted by * $p < 0.05$. Upper panel shows raw data from single spinal cord recordings (filled circles), where the mean value is represented by the gap in the vertical bars and the SD is represented by the vertical bars. Lower panel shows mean differences between control and treated groups as a bootstrap sampling distribution (mean difference is represented by filled circle and the 95% CIs are depicted by vertical error bars).

If SRWB was increased and homeostatically recovered in individual motoneurons, then we would expect to see increases in calcium entry, which are correlated with spike frequency, in individual cells. Therefore, we decided to do optical calcium imaging of individual motoneurons labeled with a calcium indicator (Figure 2.16A). We retrogradely labeled motoneurons overnight with calcium indicator Calcium Green-1 dextran (see methods). We then imaged the calcium transients from 10

motoneurons per cord, in three different cords (30 motoneurons total). We triggered episodes and recorded the calcium transients (% change in fluorescence) before and during 2+ hours of gabazine exposure. As expected, we found that within 30 minutes of blocking GABAergic transmission, the calcium transient associated with an episode increased and then more slowly was reduced toward baseline values over the next 2 hours (Figure 2.16B). The result was consistent with the idea that following GABAergic blockade, individual motoneurons increased their spike rate within a burst and then homeostatically regulated this feature.

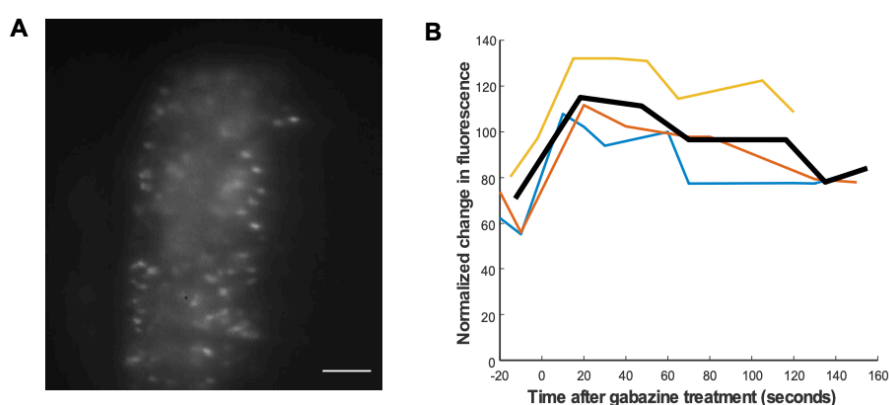


Figure 2.16. Calcium imaging of gabazine-treated embryonic chick spinal cords. **A)** Motor neurons were labeled with Calcium Green Dextran overnight. Scale bar = 100 μm. **B)** Results demonstrate an initial increase in calcium fluorescence transients associated with episodes followed by a recovery to baseline levels. Episodes were stimulated and calcium transients were recorded for three spinal cords (black line = average).

3.4 Discussion

In this study, we found that SRWB was the spiking property that was most consistently homeostatically recovered following GABAergic blockade. We found that additional firing properties were highly variable following GABAR block, consistent with degeneracy. Further, homeostatic recovery of these other features was either weak or only occurred in some of the preparations. The homeostatic control of SRWB is logical for a circuit that must execute a specific action when the network is driven to fire during synaptic bursts.

3.4.1 Variability in firing properties following GABAergic blockade

Following GABAR block, variability was seen across many spiking features. Individual cultures demonstrated dramatic variability in overall spike rate after bicuculline application. We might have expected an initial increase in overall spike rate since the system was disinhibited. On average, there was a slight increase in the first hours (although it did not reach significance, Figure 2.3A). This result was largely consistent with similar studies in culture^{187, 193}. However, when assessing individual cultures, we saw dramatic variability in the response to disinhibition as some increased 3-4 fold, while others nearly stopped firing. Why would disinhibition cause a reduction in overall spiking? One possibility is that it led to a depolarizing block, inactivating voltage-gated sodium channels¹⁹⁴. While the overall spike rate in cultures was highly variable following GABAergic blockade, this feature was consistently lower than control levels in the isolated spinal cord. This was due to the fact that such a perturbation reduced episode frequency, where most spikes occur. In the embryonic chick spinal cord, this makes sense because gabazine blocks a depolarizing excitatory current that is important in episode generation³⁴.

Overall spike rate was highly variable even though SRWB consistently increased and then homeostatically recovered. One might have expected that overall spike rate would be impacted by SRWB, but this did not appear to be the case, as some cultures decreased overall spike rate at the same time SRWB increased, and in all spinal cord preparations overall spike rate decreased dramatically at the same time SRWB increased. This occurred because overall spike rate was influenced by SRWB, burst frequency, burst duration, and inter-burst interval spiking. For instance, in the spinal cord, overall spike rate decreased due to a reduction in the episode frequency, and therefore burst frequency. Interestingly, the interaction of SRWB with other activity features was itself variable. The interaction of these features can be seen by comparing different cultures. For example, SRWB in the red culture goes up for 9 hrs and then recovers, which is similar to overall spike frequency, but different than burst frequency (goes down and stays there) or burst duration

(goes up and stays there). On the other hand, the purple culture has a typical increase and recovery of SRWB within ~ 3 hrs, which is different than overall spike rate or burst duration (goes down and stays there) or burst frequency (largely unchanged).

Why does such variability exist? This is consistent with the initial hypothesis that there is significant variability in synaptic strengths and voltage-gated conductances within neurons in circuits expressing similar activity patterns (degeneracy)^{17, 178-180, 195}. This variability is thought to be driven by homeostatic plasticity goals (e.g. achieving proper activity patterns), but different preparations use different strategies to accomplish this. In the context of development, these results are particularly profound because the many challenges during development are even more consequential and will therefore strongly shape the strategies used to accomplish homeostasis. Thus, the response to a perturbation will depend on the strategies chosen by that particular network. Therefore, it may not be surprising that networks with similar behaviors respond so differently to distinct perturbations. For instance, a network that developed using a strategy more strongly dependent on GABAergic synaptic strength would likely be more affected by GABAergic blockade. The observations that different constellations of ionic conductances and synaptic strengths can produce similar activity patterns and that perturbations can uncover such variability have been well documented in invertebrate systems^{17, 179}. However, similar experiments have been carried out far less in vertebrate preparations, and our results appear to support the concepts initially recognized in invertebrates. Finally, this variability is obvious, but the recognition of this is often lost when simply looking at average values, as suggested several years ago¹⁹⁶.

3.4.2 Homeostasis of SRWB in both preparations

In both the isolated spinal cord and cortical cultures, GABAergic blockade induced an increase in SRWB that displayed far less variability than other activity features – all cultures and 4 of 5 spinal preparations increased SRWB, which then recovered. The increase and homeostatic recovery of

SRWB appear to be due to changes that are occurring at the individual cellular level as these changes were observed in single unit recordings in culture and through calcium imaging of individual motoneurons in the spinal cord (Figure 2.8 & 2.16). Such changes are likely to be driven, at least in part, by a shift in the driving force for synaptic currents underlying bursts. In control spinal cords, the currents associated with SNA are predominantly glutamatergic and GABAergic. Previous work has demonstrated that the reversal potential for SNA in E10 chick spinal neurons was around -20 mV (GABAergic and glutamatergic), close to the GABA reversal potential of -30mV, and this then shifted to ~ 0 mV after the addition of bicuculline (now only glutamatergic)³⁴. The GABA reversal potential is close to the membrane potential during a burst and so it can actually shunt action potentials. Moreover, when GABA receptors are blocked, fewer chloride channels would be open, thus increasing the input resistance. In the chick embryo, it has been shown that puffing a GABAR antagonist onto the cord during SNA can increase burst discharge acutely, presumably by shutting off what can be a shunting conductance¹⁹⁷. In cultured cortical neurons, we would expect a similar mechanism underlying the increased SRWB following GABA receptor blockade, as input resistance should also increase and we are removing a synaptic current that is hyperpolarizing. The increase in SRWB following GABAergic blockade appears to be similar to that reported previously^{186, 187, 198}. The consistency across preparations of increased SRWB is likely due to the twofold nature of a stronger inward current in a tighter cell (lower input resistance). Such a mechanism could also underlie the recruitment of more neurons into each burst as more of the population is brought to threshold.

Since we saw the recovery of SRWB while GABAR blockade was still in effect, there must be a mechanism to bring this firing rate back to control levels that is independent of GABAR activation. We hypothesize that this effect could be due, in part, to a depolarization of the resting membrane potential³⁸. Previous work from our lab has shown that the resting membrane potential

was depolarized about 10mV in motoneurons 1-2 hours after GABAergic blockade. While this could suggest the cells are more excitable and could increase firing rate, it is possible that in combination with a more depolarized reversal potential for SNA, the cells could enter depolarizing block, thus inactivating voltage-gated sodium channels³⁴. In addition, or alternatively, it is possible that rapid activity-dependent changes in intrinsic cellular excitability, such as K⁺ channel current densities, mediate the recovery. Following reductions in voltage-gated Na⁺ channel conductances, acutely dissociated Purkinje cells maintained spikes within a burst through rapid reductions in K⁺ channel currents¹⁹⁹. In the stomatogastric ganglia, it was shown that depolarization of an all-inhibitory synaptic network reduced spikes within a burst, which then began to recover within the first hour by hyperpolarizing the action potential threshold, potentially through reduced K⁺ channel conductance²⁰⁰.

It remains unclear how the increase in SRWB is sensed and then triggers whatever homeostatic mechanism that restores this feature. One possibility is that the increased firing rate leads to an increased calcium transient (Figure 2.16), that could trigger calcium signaling cascades that lead to the appropriate homeostatic mechanisms that restore SRWB, thus avoiding cellular hyperexcitability that could be deleterious for the cell. Regardless of the mechanism, homeostatic control suggests an elevated importance of this feature as it requires a sensor of the feature and the metabolic cost to regulate it. Further supporting the importance of the finding is the fact that we see this homeostatic regulation of SRWB in 2 very different systems - 2 different cell types, species, temperatures, GABAR antagonists, and developmental stages.

Previous work has often been ambiguous about the exact variable that is homeostatically regulated, but in general, studies have focused on the recovery of overall spike rate after a perturbation. However, our current study suggests that SRWB is one important variable that is tightly homeostatically controlled in both the *in vitro* cortical cultures and *ex vivo* embryonic spinal

cords. Although we didn't see evidence of a full recovery in the overall spike rate in the embryonic chick spinal preparation, embryonic movements *in ovo* did recover after 12 hours³⁷. Thus, some homeostatic mechanisms must exist in the fully intact living embryo for this recovery. This may be due to the fact that we only looked at the first 3+ hours of recovery or there may be compensations in the periphery, descending input, or neuromodulators that are not recapitulated in the isolated *ex vivo* cord. Regardless, SRWB initially increases, then robustly returns to baseline levels in these preparations. Therefore, SRWB represents a critical firing rate property that is homeostatically maintained in a reliable manner, but is rarely considered in homeostatic studies. The bursts in culture are representative of activity that the network generates, while the bursts in the spinal cord drive kicking behavior that we have previously observed *in ovo*. In both preparations, the bursts are the synaptic outcome of the system, and the spike rate within these bursts is the feature that is consistently homeostatically regulated following this perturbation.

2.5 Experimental Procedures

2.5.1 Cell culture

Brain cortices were obtained from C57BL/6J embryonic day 17 mice from BrainBits (unknown sex). Neurons were obtained after cortical tissue was enzymatically dissociated with papain. Cell suspension was diluted to 2,500 live cells per μL and 35,000 cells were plated on planar multielectrode arrays (MEAs) coated with poly-D-lysine (Sigma, P-3143) and laminin. The cultures were maintained in Neurobasal medium supplemented with 2% B27 and 2mM GlutaMax. No antibiotics or antimycotics were used. Medium was changed completely after one day *in vitro* (1 DIV) and half of the volume was then changed every 7 days. Spiking activity was monitored starting \sim 10 DIV to determine if a bursting phenotype was expressed and continuous recordings were made between 14-20 DIV. Cultures were discarded after 20 DIV. All protocols followed the National

Research Council's Guide on regulations for the Care and Use of Laboratory Animals and from the Animal Use and Care Committee.

2.5.2 *Spinal cord dissection*

Experiments were performed on White Leghorn chicken embryos (Hyline North America, unknown sex) at embryonic day 11 (E11 or Stage 37²⁴). The spinal cords were isolated at E11, with ventral roots attached, in cooled (14°C) and oxygenated (95% O₂/5% CO₂) Tyrode's solution containing the following (in mM): 139 NaCl, 12 D-glucose, 17 NaHCO₃, 3 KCl, 1 MgCl₂, and 3 CaCl₂⁶. After dissection, the cord was left overnight to recover in Tyrode's solution at 18°C. The cord was then transferred to a recording chamber and continuously oxygenated in Tyrode's solution that was warmed up to 27 ± 1°C and contained 5 mM KCl rather than the 3 mM used in the dissecting Tyrode's solution, which produced more consistent episodes of spontaneous network activity (SNA).

2.5.3 *Electrophysiology recordings*

Culture. Extracellular spiking was recorded from cultures plated on a planar 64-channel MEA (Multichannel Systems) recorded between 14-20 DIV. MEAs were placed in the MZ60 headstage (Tucker-Davis Technologies - TDT), which was housed in a 5% CO₂ incubator at 37°C. Drugs were added separately in a sterile hood and then returned to the MEA recording system. Recordings were band-pass filtered between 200 and 3000 Hz and acquired at 25 kHz sampling rate. For bicuculline-treated cultures, 20 μM bicuculline was added to the culture following 2-3 hours of baseline activity recordings.

Spinal cord. Ventral roots were drawn into suction electrodes and motoneurons were identified by antidromically stimulating the ventral root at 30 μA with an ISO-Flex stimulator isolator.

Extracellular recordings were made using silicon probes (A1x32-Poly2-5mm-50s-177, NeuroNexus, USA) with 32 recording sites covering 775 μm in depth. The probe was inserted at a 30° angle

(lateral to medial) into the upper lumbar region of the isolated spinal cord from the ventral side. Recordings were band-pass filtered between 300 and 2000 Hz and acquired at 25 kHz. For gabazine-treated cords, 10 μ M gabazine was added to the bath after recording baseline activity for approximately one hour. Synapse software (Tucker-Davis Technologies / TDT) was used to monitor activity on a TDT electrophysiological platform consisting of the PZ2 pre-amplifier and the RZ2 BioAmp Processor for both preparations.

2.5.4 Calcium imaging

Calcium indicator Calcium Green-1 dextran (10,000MW) was used to retrogradely label motoneurons overnight as described previously²⁰¹. After isolation of the embryonic chick spinal cord (see above), lumbosacral spinal nerves were drawn into a suction electrode. Saline was then withdrawn from the suction electrode and replaced by a concentrated solution of Calcium Green (1mg in 10 μ l of H₂O). The indicator then retrogradely labeled motoneuron somata overnight. The next morning, the pia was removed in the area of the labeled motoneurons and the preparation was moved to a chamber and placed ventral side-down on a coverslip. Images were continuously acquired of labeled motoneurons through the ventral white matter using an inverted microscope (Olympus IX 70) via an intensified charge-coupled detector video camera (Stanford Photonics). The tissue was illuminated using a 75-W xenon arc lamp with an excitation filter of 450–490 nm, dichroic of 510 nm, and a barrier filter of 520 nm. Various ND filters were used to reduce photodynamic damage. During the experiment, video data (7-15 frames per second) were acquired and stored using Simple PCI. Images were then processed and analyzed using Fiji software (WS Rasband, ImageJ, National Institutes of Health, Bethesda, MD, <http://rsb.info.nih.gov/ij/>, 1997–2006). To record calcium transients during episodes of SNA, spinal nerves were stimulated. Video recordings were ~2 minutes in length. During episodes of network activity, virtually all labeled neurons showed changes in fluorescence or became optically active (O'Donovan et al., 1994). An average image was then

made in order to draw regions of interest (ROIs) over individually labeled motoneurons. The change in fluorescence was monitored by measuring average pixel intensity for 10 ROIs per spinal cord in three different cords. To assess the change in fluorescence as a percentage of the baseline fluorescence of a motoneuron, we measured fluorescence by taking the ROI value of each frame and subtracting the average value of 30 frames before the episode of SNA. We then took the change in fluorescence of each ROI and divided it by the average before the episode minus an ROI in a non-labeled region (autofluorescence) $((ROI - ROI \text{ average before episode}) / (ROI \text{ average before episode} - \text{autofluorescence}))$.

2.5.5 Data analysis

Spiking activity from cortical cultures and isolated spinal cords was analyzed offline with a custom-written Matlab program¹⁸⁸. The recordings (acquired in TDT) were subsequently converted using the function TDTbin2mat to Matlab files (Mathworks). A custom written Matlab program identified bursts of network spikes using an inter-spike interval-threshold detection algorithm as described previously, where “A burst was identified if N spikes occurred in less than T ms, where the threshold T was automatically determined from observing the probability distribution of inter-spike-intervals” – The number of spikes comprising the smallest burst was considered N ²⁰². The program plotted the probability distribution for the periods between 10 consecutive spikes. The longest duration minima were chosen as the threshold duration (T – Figure 2.17A) to find a user defined number of spikes (N) within a burst as described previously²⁰². Spiking activity was labeled as a network burst when it met a user-defined minimum number of spikes across all channels (culture: 10; cord: 4-8) occurring across a user-defined minimum number of channels (culture: 5-10; cord: 3-5). We removed channels that did not contribute to bursts or were constantly active (potential noise). For example, in Figure 2.17A we plotted the interval between the first and tenth consecutive spike and saw the largest minima (dip in the probability distribution) was around 200ms. We then

used this value to search for periods where 10 spikes occurred within 200ms and then repeat this process after advancing one spike at a time (e.g. spike 1-10 occur within 200ms and then determine if spike 2-11 is still within 200ms – if so, the identified burst is lengthened). We then visually assessed the bursts identified by the program (Figure 2.17B, the duration of the identified bursts is shown as a red line below the burst and spike times can be seen within the burst (red) and outside the burst (black). The program also automatically computed network burst metrics including burst frequency, overall spike rate, and other characteristics. An additional feature of the program is its ability to identify and calculate characteristics of spontaneous network activity (SNA) in the isolated spinal cord. SNA presents as a series of bursts within 30-60 seconds (called an episode), followed by a 5-10 minute quiescent period. Spiking activity was labeled as an episode when it met user-defined criteria. This included episode duration (typically 20-100 seconds). The episodes were then visually inspected to ensure that the chosen parameters accurately identified episodes and the bursts within the episodes. The program also computed episode metrics, such as the number of spikes, duration, and channels involved.

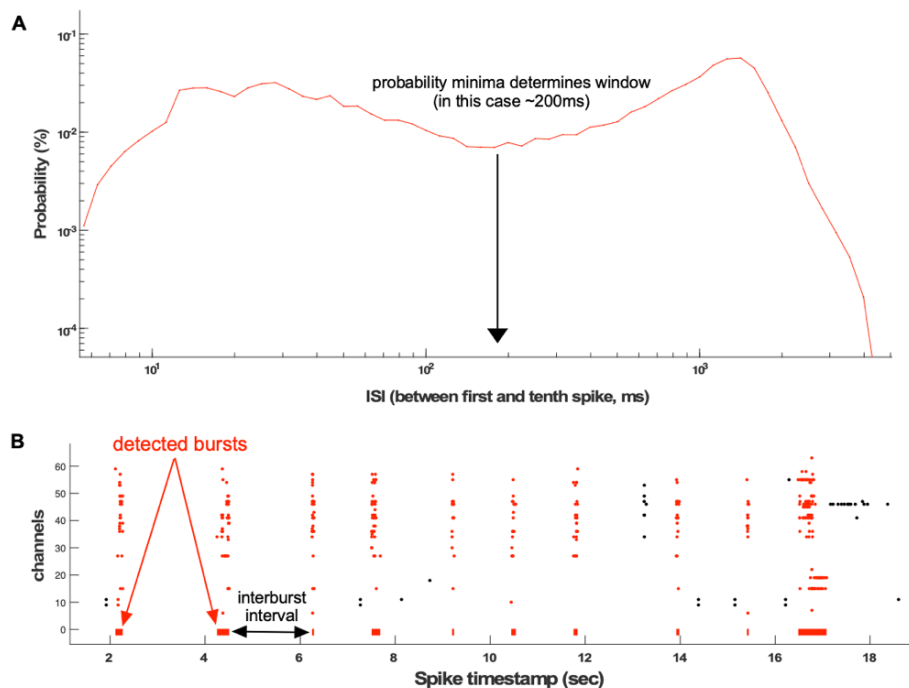


Figure 2.17. Program that detects and analyzes bursts. **A)** Probability distribution of ISI durations between 10 consecutive spikes (n to $n + 9$) largest dip in the distribution (200ms) is used to detect bursts in the burst detection subroutine of the program. **B)** Burst detection program identifying bursts that contain at least 10 spikes in 200ms. Burst duration is shown in red line below raster plot. Burst spikes are red and spikes in the inter-burst interval are black.

Culture. Each time point (0, 0.5, 1, 3, 6, 9, 12, 18, 24 hrs) indicated in the figures represents recordings acquired in a 15-minute interval (900 seconds), where multiple features of spiking were calculated. Overall spike rate was defined as the total number of spikes across all channels divided by the duration of that recording period (total # spikes / 900 sec). The burst frequency was calculated as the number of bursts identified in a recording session divided by the total duration of that recording session (total # bursts / 900 sec). Inter-burst interval (IBI) spike rate was calculated as the number of spikes that occur outside of bursts divided by the total inter-burst interval (combined durations of all inter-burst periods) in the 900 sec recording session. Average burst duration was the average duration of all bursts in a recording session. SRWB was calculated in 2 different ways – line graphs in main figures show the total number of spikes within all bursts divided by the sum of the burst durations, or in extended data, line graphs are calculated by averaging all SRWBs calculated for each burst thus providing standard deviation for each time point within a culture. Due to the mentioned variability between cultures, the line graphs of the main figures show the data normalized to baseline. Additionally, in the line graphs of extended data, we show raw data (not normalized). Homeostatic recovery of spiking features (homeostatic index) was computed by first calculating the recovery in bicuculline-treated cultures (maximum normalized value within the first hour in bicuculline minus the normalized value at the 24-hour time point in bicuculline). This number was then divided by the maximum normalized value within the first hour in bicuculline minus the normalized value in control cultures at 24 hours (typically near 1). The homeostatic index was calculated and is displayed for each culture separately (individual dots in Figure 2.7).

Spinal cord. Spiking activity was divided into 30-minute bins, and only spiking in motoneuron channels, as determined by antidromic ventral root stimulation, was included in the analyses. Within each time bin, the following characteristics were calculated: episode duration, episode spike rate, burst duration, SRWB, inter-episode interval spike rate, and overall spike rate. Episode duration was calculated as the time between the onset of the first burst and the end of the last burst. Episode spike rate is the number of spikes in motoneuron channels divided by the episode duration. Burst duration is the average burst period within the episodes. SRWB is the total number of spikes across motoneuron channels that occur during bursts within the episode divided by the total duration of the bursts (spikes that occurred in the episode but outside of the bursts were not included). If more than one episode occurred during the 30-minute bin, the metrics were averaged so that only one value for each spinal cord is displayed. In addition, in each 30-minute window, the overall spike rate (as described above) and the inter-episode interval spike rate (number of spikes outside of episodes divided by the inter-episode time window) were calculated. Since each isolated spinal cord had different baseline values, all data shown are normalized to baseline (30 minutes of recording before drugs).

2.5.6 Statistical analysis

Estimation statistics have been used throughout the manuscript. 5000 bootstrap samples were taken; the confidence interval is bias-corrected and accelerated. The p values reported are the likelihoods of observing the effect sizes, if the null hypothesis of zero difference is true. For each permutation p value, 5000 reshuffles of the control and test labels were performed (Moving beyond P values: data analysis with estimation graphics²⁰³).

Chapter 3: Homeostatic capacity of L5/6 neurons in *Fmr1* KO mice following unilateral whisker deprivation

3.1 Abstract

Mouse models of Fragile X Syndrome (FXS) have demonstrated impairments in excitatory and inhibitory sensory-evoked neuronal firing. Homeostatic plasticity, which encompasses a set of mechanisms to stabilize baseline activity levels, does not compensate for these changes in activity. Previous work has shown that impairments in homeostatic plasticity are observed in FXS, including deficits in synaptic scaling and intrinsic excitability. Here, we aimed to examine how homeostatic plasticity is altered *in vivo* in an *Fmr1* KO mouse model following unilateral whisker deprivation (WD). We show that WD in the wild type leads to an increase in the proportion of L5/6 somatosensory neurons that are recruited, but this does not occur in the KO. In addition, we observed a change in the threshold of excitatory neurons at a later developmental stage in the KO. Compromised homeostatic plasticity in development could influence sensory processing and long-term cortical organization.

3.2 Introduction

Fragile X Syndrome (FXS) is a neurodevelopmental disorder that is the most common monogenetic form of intellectual disability, with up to 50% of FXS male patients receiving a co-diagnosis of autism spectrum disorder (ASD)²⁰⁴. In addition to cognitive impairments, patients with FXS can have seizures, circadian rhythm disruptions, and sensory and auditory hypersensitivity^{205,206}. FXS is caused by a trinucleotide repeat expansion that inactivates the *Fmr1* gene on the X-chromosome, resulting in the absence of fragile X messenger ribonucleoprotein (FMRP)²⁰⁷. FMRP is an mRNA translational repressor that plays an important role in synaptic function and plasticity^{73,206}. For

instance, the mGluR (metabotropic glutamate receptors) theory of FXS states that the loss of FMRP increases long-term depression (LTD), a protein-synthesis dependent form of plasticity^{106,120}.

The *Fmr1* KO mouse cortex exhibits weaker whisker-evoked activity compared to the wild type (WT)¹³⁵. For instance, layer 2/3 (L2/3) excitatory and inhibitory neurons in the somatosensory cortex (S1) fire less frequently following whisker stimulation compared to WT neurons.

Homeostatic plasticity encompasses a set of mechanisms thought to maintain activity levels within appropriate boundaries^{208,209}. When perturbations to cellular or network activity occur, compensatory changes in synaptic strength (homeostatic synaptic plasticity) and/or intrinsic membrane excitability (homeostatic intrinsic plasticity) are engaged to stabilize neural function. It is unclear why homeostatic plasticity does not compensate for the reduced whisker-evoked cortical activity in FXS mice. However, previous studies have suggested that both homeostatic synaptic plasticity^{62,138,210}, and homeostatic intrinsic plasticity can be impaired in *Fmr1* KO mice⁶³. Since this work has been largely performed in cultures or slices, we aimed to test the homeostatic capacity of FXS mice in an intact, *in vivo* system.

We chose to examine the barrel cortex for several reasons. The somatosensory cortex (S1) somatotopically represents the whiskers on the snout of a rodent; each individual whisker is represented in the contralateral cortex by a distinct region called the barrel^{141,147}. The whisker system is crucial for a mouse's sensory experience, helping them navigate and interact with the environment. Individual whiskers can be stimulated to examine the responsiveness of cortical neurons in the corresponding barrel to a relevant sensory input, as the previous study showing weakened responses in the *Fmr1* KO had exploited¹³⁵. Unilateral whisker deprivation, removing all whiskers on one side of the snout, has been shown to trigger a homeostatic increase in the responsiveness of S1 cortical neurons to whisker stimulation¹⁷⁴. Finally, impairments in whisker-evoked processing are prevalent in different models of ASD in developing rodents^{134,135,160,161,163,211}.

Thus, in order to investigate the homeostatic capacity of the *Fmr1* somatosensory cortex, we performed unilateral whisker deprivation during a critical developmental window (P14-P21, at the onset of whisking) to test homeostatic plasticity in the output layer of S1 (L5/6). We found reduced recruitment of L5/6 neurons during whisker stimulation in the KO at P16, but not P21. Further, we found that recruitment of this L5/6 cortical population was significantly increased following both 2- and 7-day whisker deprivation in the WT cortex, but not in the KO cortex. Our results show that while the KO L5/6 mouse cortex has some homeostatic capacity, it fails to compensate for reduced sensory input by recruiting a larger portion of the L5/6 population.

3.3 Results

3.3.1 *P16 WT RS neurons respond to whisker stimulation more than KO RS neurons*

In order to compare excitability in the WT and *Fmr1* KO S1 cortex, we examined the regular spiking (RS, presumed excitatory) L5/6 neurons, as these layers provide the output of the cortical column, projecting to the secondary somatosensory cortex, motor cortex, subcortical structures, and the corticothalamic pathway^{141,212}. Since FXS and autism are neurodevelopmental disorders, we examined evoked responses during an early developmental stage where homeostatic plasticity mechanisms are most robustly expressed^{160,209,213}. Mice were lightly anesthetized at postnatal day 16 (P16), and a 64-channel probe was inserted into the barrel cortex to record spiking activity. We stimulated 9 individual whiskers at varying velocities to generate a velocity response curve (VRC) that measured the responsiveness of cortical L5/6 RS neurons, and curated units with Kilosort 2.5 (see methods, Figure 3.1).

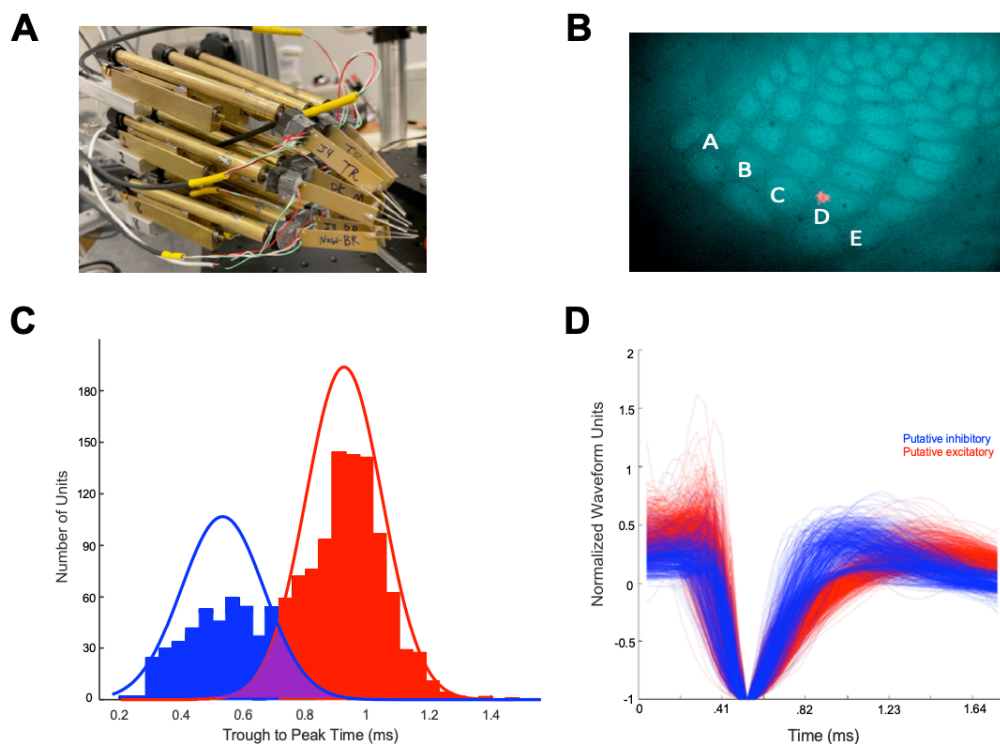


Figure 3.1. Classification of single units. A) Nine whiskers were inserted into a 3x3 piezoelectric stimulator array, ideally inserting the whisker that elicited the strongest response across all 64 channels in the middle of the array. B) Example histology section of the barrel cortex. Red fluorescence indicates the location of the probe (in this case, D1). C) The bimodal distribution of waveforms from extracellular recordings using the trough to peak time. A Gaussian Mixture Model was fit to this distribution. The point at which the two curves intersect was used as the boundary between putative inhibitory and excitatory units. Overlap area is approximately 10%. D) Mean waveform of all units used in the analyses. Blue waveforms represent putative inhibitory neurons, and red waveforms represent putative excitatory neurons.

We first tested whether there were any differences in spontaneous activity in WT and KO L5/6 excitatory neurons at baseline (no whisker stimulation), and observed that the spontaneous firing rate of individual neurons was no different (Figure 3.2A). We then calculated the whisker-evoked VRC of the columnar whisker (CW, also referred to as the principal whisker), histologically identified following the experiment (Figure 3.1B, see methods). The average CW VRC of KO L5/6 neurons was reduced compared to the WT, demonstrating that these neurons were less responsive to whisker stimulation (Figure 3.2B). These VRCs will be referred to as overall VRCs as they include all L5/6 RS neurons, whether they were responsive to the CW stimulation or not. Therefore, this population response could be due to decreased sensitivity at the single neuron level, decreased

proportion of responsive neurons, or both. We found that there was no difference between WT and KO VRCs if we only included neurons that significantly respond to CW stimulation (CW-responsive neurons; Figure 3.2C), suggesting that there was a reduction in the proportion of CW-responsive L5/6 neurons. Indeed, we found a reduced proportion of neurons that were CW-responsive in the KO, albeit this did not reach significance (Figure 3.2D). In fact, when we compared the proportions of all whisker-responsive L5/6 neurons in WT and KO mice (proportion of neurons responsive to any of the 9 whiskers stimulated compared to total number of neurons – whisker responsive or not), we found that there was a significant decrease in the KO (Figure 3.3A).

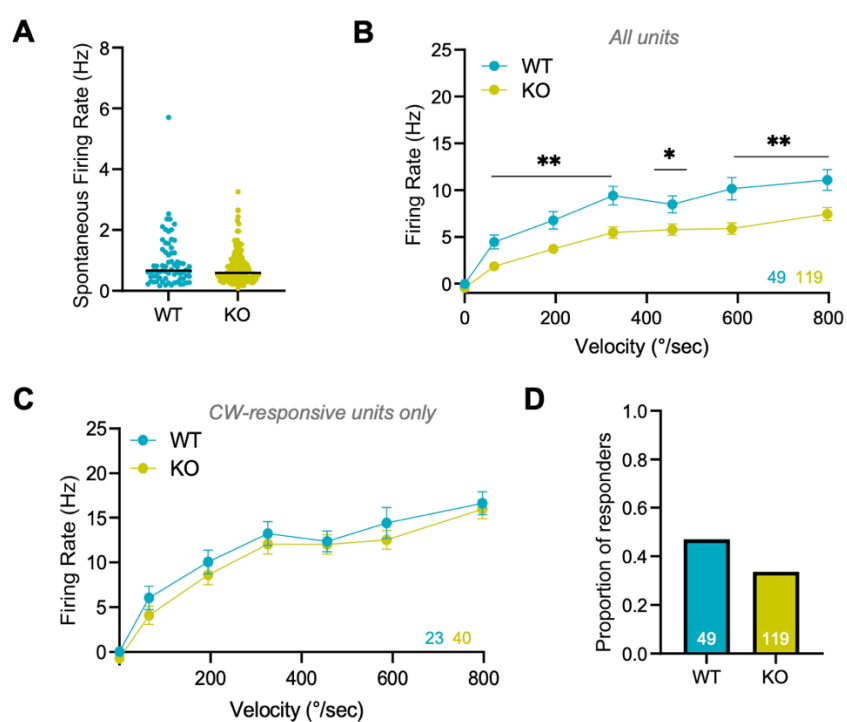


Figure 3.2. Baseline WT and *Fmr1* KO whisker-responsiveness at P16. A) Spontaneous firing rates of WT and *Fmr1* KO neurons. B) Overall velocity response curve (VRC) of all neurons following columnar whisker (CW) stimulation at varying velocities. Number of units for each condition is color-coded and shown at the bottom-right. C) VRC of CW-responsive neurons only. D) The proportion of neurons that significantly respond to CW stimulation. * $p < 0.05$, ** $p < 0.01$.

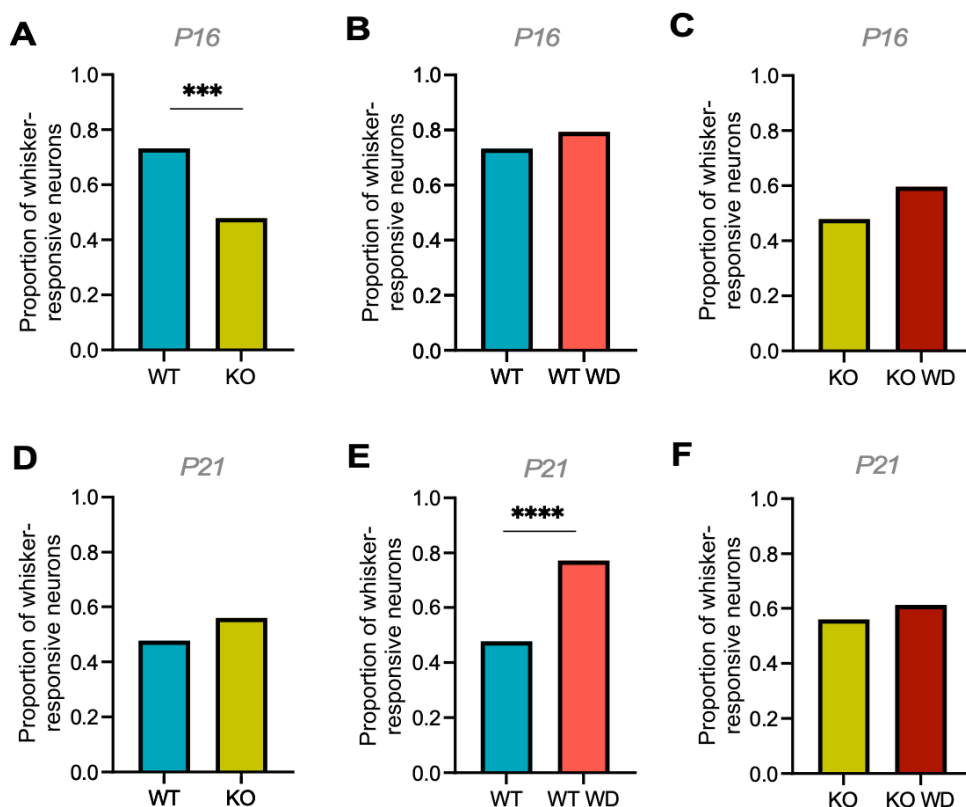


Figure 3.3. The proportion of whisker-responsive neurons in all experimental conditions, at baseline and following whisker deprivation. A) P16 WT vs KO. B) P16 WT vs WT WD. C) P16 KO vs KO WD. D) P21 WT vs KO. E) P21 WT vs WT WD. F) P21 KO vs KO WD. *** $p < 0.001$, **** $p < 0.0001$.

We were also interested in evaluating the VRC for the best whisker (BW) of the neuron, which is the whisker that elicited the strongest response for that neuron, regardless of the anatomical location of the cell (including neurons in barrels and septa). Like the VRC for CW-responsive neurons, the average BW VRC was nearly identical in WT and *Fmr1* KO L5/6 RS neurons (Figure 3.4A). These results suggested that at baseline, there were no differences in the excitability of whisker-responsive (CW or BW) neurons in WT and KO neurons. Thus, while the proportion of neurons recruited in a column was reduced in the KO, the whisker-responsive neurons were similar. Since the VRCs produced by stimulating the CW or BW were similar, for clarity we will discuss CW VRCs in all further comparisons, but show BW VRCs in Figure 3.4.

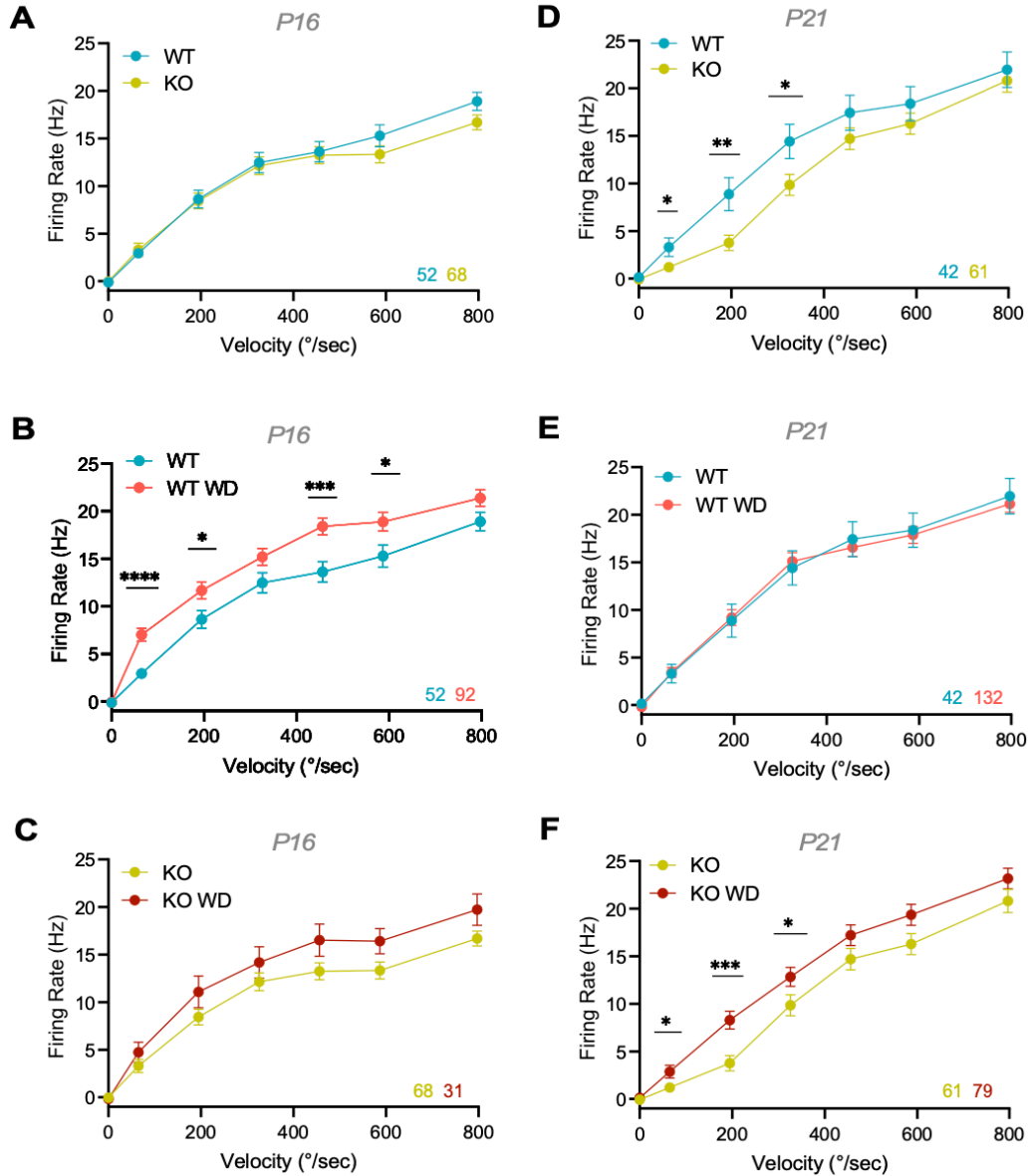


Figure 3.4. Best whisker (BW) velocity response curves (VRCs) of all experimental conditions. A) P16 WT vs KO. B) P16 WT vs WT WD. C) P16 KO vs KO WD. D) P21 WT vs KO. E) P21 WT vs WT WD. F) P21 KO vs KO WD. Numbers at the bottom right are neurons per condition. Number of units for each condition is color-coded and shown at the bottom-right. * $p < 0.05$, ** $p < 0.01$, *** $p < 0.001$, **** $p < 0.0001$.

3.3.2 P16 2-day whisker-deprived WT and KO neurons increased their responsiveness, but only WT neurons increased neuronal recruitment

In order to test the homeostatic capacity of RS neurons, we unilaterally trimmed whiskers to 2mm at P14, and recorded activity from the barrel cortex at P16 (2 days of whisker deprivation – WD). We found that following WD, there was an increase in overall VRCs from CW stimulation across all

velocities (Figure 3.5B). We also found a slight increase in the VRC of CW-responsive neurons (Figure 3.5C). In this case, the main increase in the VRC was due to an increased proportion of neurons within a barrel that significantly responded to the CW deflection (Figure 3.5D, ~45% to 80% after WD). Therefore, following sensory deprivation, more of the WT S1 L5/6 RS neurons were recruited in a homeostatic manner, and of those that responded, there was a slight increase in the evoked output.

We had hypothesized that KO neurons would demonstrate some impairment in homeostatic plasticity. CW stimulation shifted the overall VRC significantly upward following 2-day sensory deprivation in the KO, for all neurons and for CW-responsive neurons alone (Figure 3.5F and 3.5G). However, the proportion of neurons that responded to CW stimulation in the KO did not increase significantly with WD (34% to 49% after WD, Figure 3.5H). The findings suggest that while *Fmr1* KO L5/6 neurons at P16 demonstrate some homeostatic capacity following WD, there is an impairment in increasing the population recruited by CW stimulation, which is considerably reduced compared to the WT WD neurons (49% vs 80%). Interestingly, the spontaneous firing rate following WD in both the WT and KO conditions decreased compared to their respective baseline values (Figures 3.5A and 3.5E).

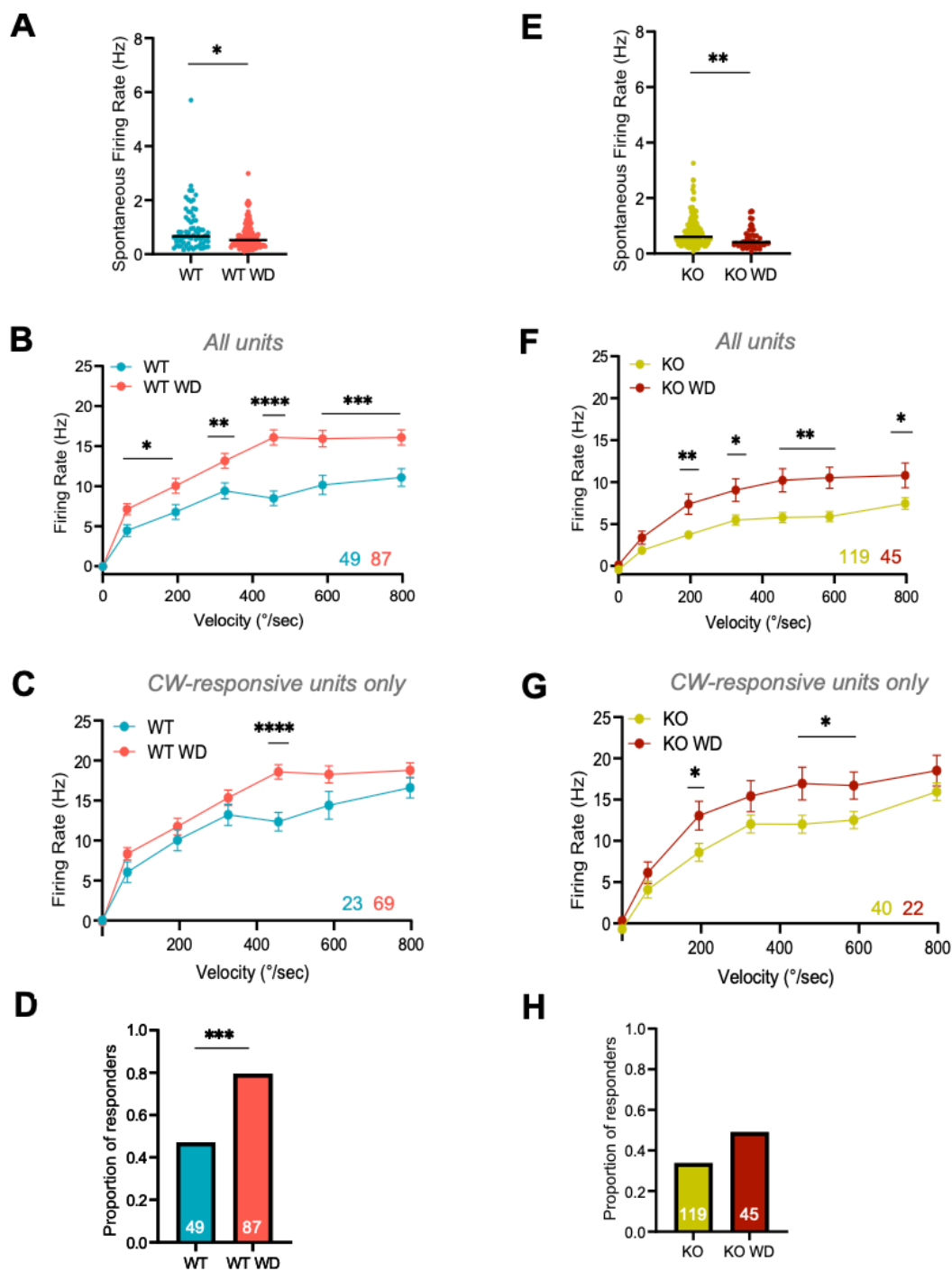


Figure 3.5. WT and *Fmr1* KO whisker-responsiveness following whisker deprivation at P16. A) Spontaneous firing rates of WT and WT whisker-deprived (WT WD) neurons. B) Overall velocity response curve (VRC) of all WT and WT WD neurons following columnar whisker (CW) stimulation at varying velocities. Number of units for each condition is color-coded and shown at the bottom-right. C) VRC of CW-responsive neurons only for WT and WT WD. D) The proportion of neurons that significantly respond to CW stimulation. E) Spontaneous firing rates of KO and KO whisker-deprived (KO WD) neurons. F) Overall velocity response curve (VRC) of all KO and KO WD neurons following CW stimulation at varying velocities. G) VRC of CW-responsive neurons only for KO and KO WD. H) The proportion of neurons that significantly respond to CW stimulation. * $p < 0.05$, ** $p < 0.01$, *** $p < 0.001$, **** $p < 0.0001$.

3.3.3 P21 KO RS neurons exhibit an increased threshold to whisker stimulation compared to WT neurons

We extended these studies to P21 with a 7-day whisker deprivation, but will first compare the P21 WT and KO at baseline (without whisker deprivation). We first tested whether there were any changes in spontaneous activity between the WT and KO L5/6 RS neurons. We found that, like P16, the spontaneous firing rate of single neurons was the same in both genotypes (Figure 3.6A). We then examined the overall VRCs from CW stimulation, and interestingly, discovered that the KO VRC exhibited a shift in the shape of the curve compared to the WT VRC (Figure 3.6B). This trend was even more apparent when we analyzed the VRC using CW-responsive neurons, where the lowest velocity whisker deflection to elicit a response was higher in the KO than in the WT (Figure 3.6C). These results suggested a potential change in the sensitivity or threshold of the KO L5/6 RS neurons. Indeed, when we calculated the minimum whisker stimulation velocity that neurons required to elicit a significant whisker-evoked response, we found that this velocity was greater in the KO condition (Table 3.1). However, at the faster whisker stimulations, we observed no difference in the firing rate of KO neurons, indicating that the decrease in spiking activity only occurred at slower velocities. Moreover, there was no significant difference in the proportion of neurons that responded to CW stimulation at the fastest velocity (Figure 3.6D). These results demonstrate an increase in the threshold to activate KO L5/6 RS neurons at P21, but no change in the number of cells recruited. Interestingly, this decreased sensitivity is unique to P21 neurons, and this change occurred in the responsiveness of KO L5/6 RS neurons in just five days.

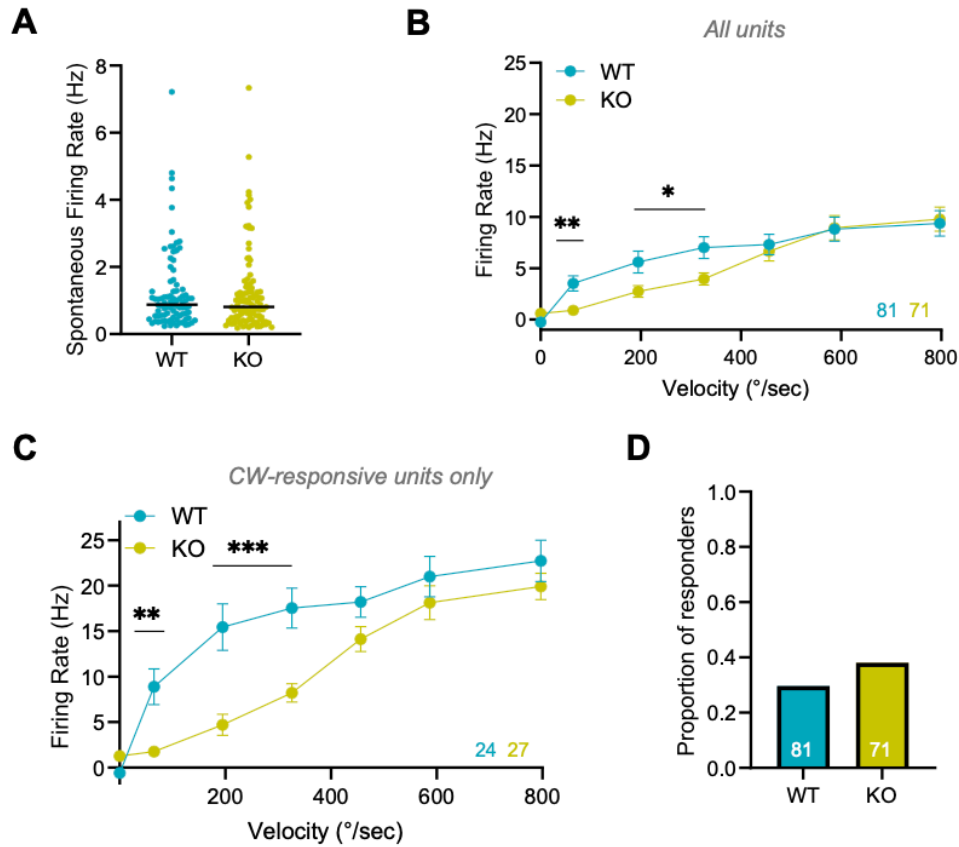


Figure 3.6. Baseline WT and *Fmr1* KO whisker-responsiveness at P21. A) Spontaneous firing rates of WT and *Fmr1* KO neurons. B) Overall velocity response curve (VRC) of all neurons following columnar whisker (CW) stimulation at varying velocities. Number of units for each condition is color-coded and shown at the bottom-right. C) VRC of CW-responsive neurons only. D) The proportion of neurons that significantly respond to CW stimulation. * $p < 0.05$, ** $p < 0.01$, *** $p < 0.001$.

Experimental Condition	Velocity Threshold
P16 WT	332.2 ± 236.8
P16 KO	373.5 ± 251.8
P16 WT WD	232.4 ± 163.9
P16 KO WD	315.8 ± 240.8
P21 WT	302.6 ± 226.3
P21 KO	452.2 ± 188.8
P21 WT WD	309.3 ± 213.6
P21 KO WD	351.5 ± 194.5

[] *
 [] ***
 [] **

Table 3.1. Velocity threshold for each condition, calculated using only CW-responsive neurons. All values are mean + standard deviation. * $p < 0.05$, ** $p < 0.01$, *** $p < 0.001$.

3.3.4 P21 7-day whisker-deprived WT and KO neurons increased their responsiveness, but only WT neurons increased neuronal recruitment

Next, we examined the effect of a longer (7-day) sensory deprivation period on WT L5/6 RS neurons. Whiskers were unilaterally trimmed to 2mm at P14 and then trimmed every other day until the day of recording, P21. We found that following whisker deprivation, there was a slight increase in the overall VRC in response to CW stimulation (Figure 3.7B). VRCs of CW-responsive neurons were no different in WT and whisker-deprived WT mice (Figure 3.7C). Instead, the increase in the overall CW VRC was a direct result of a strong increase in the proportion of responsive neurons (30% to 57% after WD, Figure 3.7D). Thus, a 7-day whisker deprivation in WT mice did not alter the responsiveness of L5/6 RS neurons that responded, but the network was able to compensate by recruiting twice as many neurons.

Since the spiking activity of KO L5/6 RS neurons was already different than the WT neurons at baseline across the lower whisker stimulation velocities, we were curious to see how whisker deprivation would affect responsiveness and recruitment. The overall CW VRC of KO neurons following sensory deprivation was higher than the control, demonstrating that these neurons homeostatically became more responsive to whisker stimulation (Figure 3.7F). We discovered the same result when examining only the VRCs of CW-responsive neurons (Figure 3.7G). Interestingly, as in P16 KO neurons, the proportion of CW-responsive neurons was not significantly different following deprivation in the KO at P21 (Figure 3.7H). Thus, the increased VRC was directly due to an increase in the responsiveness of individual neurons that were CW-responsive. Therefore, although the spiking activity increased in both WT and KO neurons after a sensory perturbation, the recruitment of neurons in the cortical column was different: only in the WT did the proportion of recruited cells significantly increase. Further, although WD increased the overall VRC in the KO, these mice were still less responsive than the WT at the lowest frequencies.

Finally, following 7-day whisker deprivation, the spontaneous firing rate of WD neurons in the WT significantly decreased, but remained unchanged in the KO at P21 (Figure 3.7A and 3.7E).

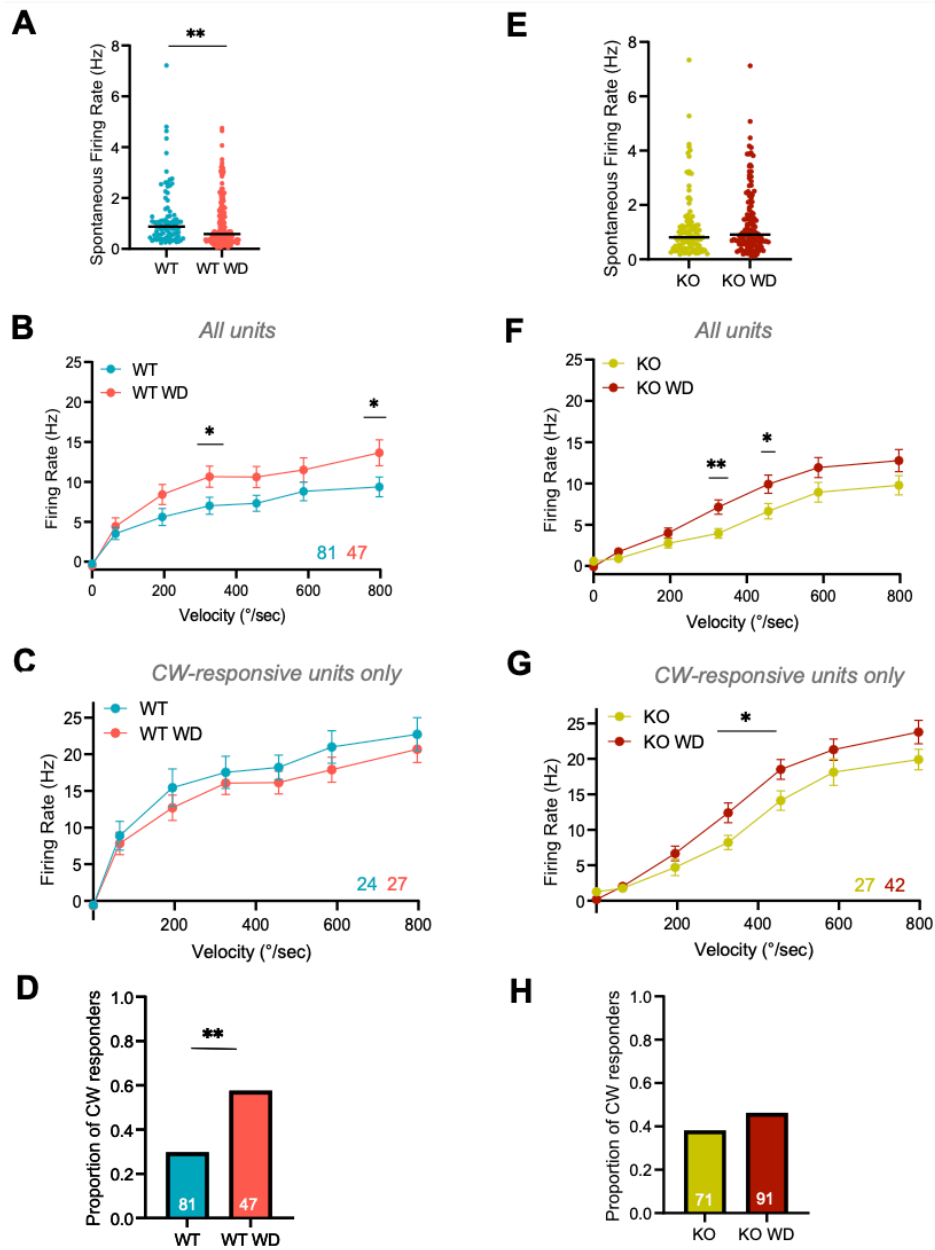


Figure 3.7. WT and *Fmr1* KO whisker-responsiveness following whisker deprivation at P21.

A) Spontaneous firing rates of WT and WT whisker-deprived (WT WD) neurons. B) Overall velocity response curve (VRC) of all WT and WT WD neurons following columnar whisker (CW) stimulation at varying velocities. Number of units for each condition is color-coded and shown at the bottom-right. C) VRC of CW-responsive neurons only for WT and WT WD. D) The proportion of neurons that significantly respond to CW stimulation. E) Spontaneous firing rates of KO and KO whisker-deprived (KO WD) neurons. F) Overall velocity response curve (VRC) of all KO and KO WD neurons following CW stimulation at varying velocities. G) VRC of CW-responsive neurons only for KO and KO WD. H) The proportion of neurons that significantly respond to CW stimulation. * $p < 0.05$, ** $p < 0.01$.

3.3.5 *WT and KO FS neurons respond similarly to RS neurons at P16*

Finally, we wanted to test whether there were changes in fast-spiking (FS) putative inhibitory neurons for each condition and how they might impact what we observed in the RS neurons. Unfortunately, we were not able to record from a sufficient number of FS units at P21 or in CW-responsive neurons at P16, but here, we present overall VRCs and proportions of responders for FS neurons at P16. At baseline, without whisker deprivation, we observed a weakening in the overall CW VRC of KO FS neurons compared to WT FS neurons (Figure 3.8A). This was, at least in part, due to a slight decrease in the proportion of FS neurons that were recruited following CW stimulation (Figure 3.8B). Following a 2-day whisker deprivation in WT mice, we observed an increase in the overall VRC, and this was due to an increase in the proportion of neurons recruited in WT mice (Figure 3.8C and 3.8D). In the KO mice, we observed an increase in the overall CW VRC after WD, but observed no change in the proportion of CW-responsive neurons (Figure 3.8E and 3.8F). These results are very similar to what we observed for L5/6 RS neurons at P16, suggesting that both excitatory and inhibitory neurons might respond similarly to whisker deprivation.

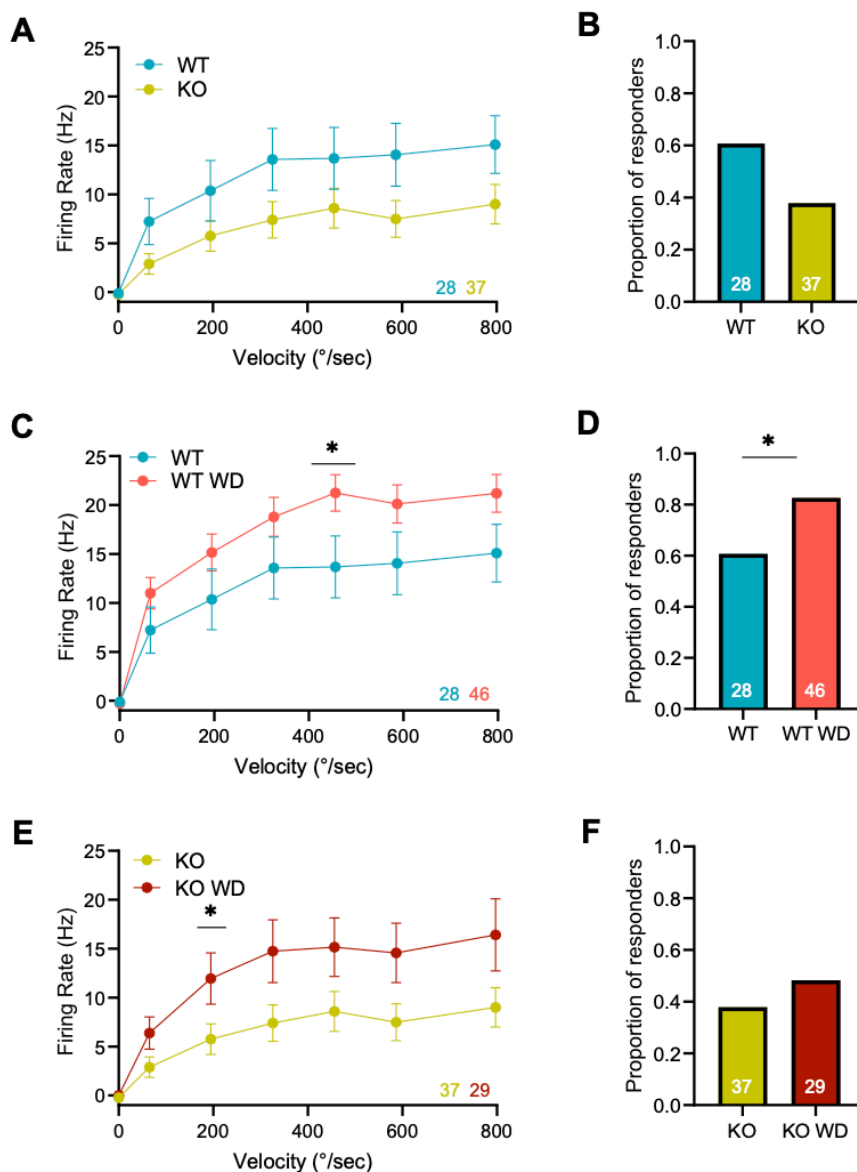


Figure 3.8. WT and *Fmr1* KO FS whisker responsiveness at baseline and following whisker deprivation at P16. A) Overall velocity response curve (VRC) of all neurons following columnar whisker (CW) stimulation at varying velocities for WT and KO mice at baseline. Numbers of units for each condition is color-coded and shown at the bottom-right. B) The proportion of neurons that significantly respond to CW stimulation. C and D) Similar to A and B except for WT and WT WD (whisker-deprived) neurons. E and F) Similar to A and B except for KO and KO WD (whisker-deprived) neurons. Number of units for each condition is color-coded and shown at the bottom-right. * $p < 0.05$.

3.4 Discussion

In this study, we have asked about the homeostatic capacity of WT and *Fmr1* KO L5/6 neurons, as this represents the output of the cortical column in the barrel cortex and therefore, the drive to

downstream brain regions in the sensory circuit. We observe homeostatic increases in whisker-evoked responses in this part of the barrel cortex in WT mice following whisker deprivation. Further, we show that the KO can express homeostatic plasticity in some ways, but fails in other ways. The overall L5/6 whisker-evoked response exhibited a compensatory increase following WD in both the WT and KO mice. However, unlike WT littermates, following WD, the KO failed to recruit larger proportions of the L5/6 population with whisker stimulation. In addition, at baseline, overall whisker-evoked responses were weaker in the KO compared to WT, although this occurred through different mechanisms at the two developmental stages. These results suggest that the output of the S1 cortex is altered in FXS mice at baseline and in their homeostatic capacity.

3.4.1 *Baseline differences in WT and KO neurons*

Changes in the overall VRCs can occur because of changes in the proportion of neurons that are recruited by the evoked synaptic activity (proportion of responsive neurons) and/or changes in the responsiveness of neurons that already respond to whisker stimulation. At P16, we observed that overall VRCs were reduced for L5/6 KO RS neurons (Figure 3.2B). A prior study had shown that KO L2/3 RS neurons demonstrated a decrease in the whisker-evoked overall VRC, in anesthetized adult and juvenile *Fmr1* KO mice, as well as awake adult mice¹³⁵. We further examined what may have caused such a reduction in the overall VRC in our study, and found that it was due to a reduction in the proportion of L5/6 excitatory neurons that were recruited following CW stimulation in the KO mice compared to the WT mice (Figure 3.2D). Similar to these results, previous work had demonstrated that fewer L2/3 RS neurons responded to whisker stimulation in juvenile *Fmr1* KO mice¹⁶³. On the other hand, the CW-responsive VRCs were no different in the WT and KO mice (Figure 3.2C). Therefore, although fewer L5/6 RS neurons were recruited by whisker stimulation in the KO, the ones that were recruited responded to the same extent as the WT. The similarity of the VRCs of the whisker-responsive units in the WT and KO could be due to

a compensatory increase in intrinsic excitability; increased membrane excitability has been observed repeatedly in *Fmr1* KO mice in layers 2/3, 4, and 5^{65, 134, 135, 214}.

We observed that L5/6 FS neurons had a reduced overall VRC to CW stimulation, albeit not significant (Figure 3.8A). Similar to the L5/6 RS neuronal changes, this reduced VRC appears to be mediated by a reduction in the proportion of FS neurons that were recruited. Previous work has suggested that L2/3 parvalbumin (PV) neurons are less responsive to sensory stimulation in the KO^{135, 215, 216}. This result is plausible given the significant connectivity between RS and FS neurons; thus, if fewer excitatory neurons are recruited, fewer inhibitory neurons may also be recruited. Further investigation of changes in the GABAergic circuitry and therapeutic strategies to rescue inhibitory neuron deficits may prove to be useful in combating FXS circuit deficits²¹⁷.

Later in development, at P21, we also observed a reduction in the overall VRC of the KO compared to the WT, but not in the same way. First, the proportion of CW-responsive neurons was no different in the KO, so whisker stimulation was capable of recruiting the same number of L5/6 RS neurons (Figures 3.6D). This was consistent with a previous study that found no change in the proportion of whisker-responsive L2/3 neurons in the adult *Fmr1* KO mouse¹³⁵. However, while the CW-responsive L5/6 RS neurons demonstrated weaker whisker-evoked activity in the KO, this only existed in the lower half of the whisker stimulation velocities (Figure 3.6C). This would mean that the neurons would need a stronger signal from incoming connections to ensure a full neuronal response. Intriguingly, even though KO L5/6 RS neurons initially require a faster whisker stimulation to elicit a whisker-evoked response, the VRCs were similar in the WT and KO neurons at the three fastest whisker stimulation velocities. Thus, despite the altered sensitivity, once the KO neurons were sufficiently stimulated, they responded normally, possibly through homeostatic mechanisms. These alterations in response threshold could impact learning abilities, which are an important clinical phenotype in FXS patients.

Our results showing differences in the recruitment of neurons at P16 but not at P21 could imply that there are developmental changes that occur in the KO mouse model. There may be homeostatic compensatory mechanisms at play that allow for the recovery of some cortical function by P21. This result is consistent with previous findings demonstrating that early developmental deficits in cortical circuitry are eventually resolved, suggesting developmental delays in FXS mice. Examples of developmental delay in the *Fmr1* KO model include the synaptic strength of the L4 to L3 connection, the window for long-term potentiation, and the transition of GABA from depolarizing to hyperpolarizing currents^{160, 161, 218}.

3.4.2 *Plasticity in WT neurons*

In WT mice, we observed that both 2- and 7-day unilateral whisker deprivation led to an increase in the overall VRC of L5/6 RS neurons (increase in whisker-evoked spiking). This is consistent with a previous study using unilateral whisker deprivation that showed increased spiking in L4 and L2/3 RS neurons following CW stimulation by 7-day WD¹⁷⁴. Several previous studies have found that removing one row of whiskers (typically the D-row) for 5-10 days leads to a weakening of the deprived CW-evoked spiking in excitatory neurons²¹⁹⁻²²¹. However, D-row deprivation represents a competitive condition where the CW is deprived but adjacent whiskers can compete for cortical space and therefore can trigger Hebbian sorts of plasticity. On the other hand, unilateral whisker deprivation appears to trigger a homeostatic increase in RS spiking, as competing whiskers have been removed. Therefore, it is likely that selective whisker deprivation may favor Hebbian plasticity, while unilateral or complete whisker deprivation triggers a more homeostatic response. The increase in the overall VRC that we observed following both 2- and 7-day whisker deprivation in WT mice was due to a significant increase in the proportion of CW-responsive neurons (Figure 3.5D & 3.7D). How does this homeostatic increase in the recruitment of L5/6 RS neurons occur? Previous work has shown that unilateral whisker deprivation can produce alterations in the synaptic circuitry in

L2/3 and L5 RS neurons^{172,173}. However, several other studies have demonstrated that such a deprivation leads to weakening of synaptic strength onto L2/3 and L5 RS neurons, which would appear to be anti-homeostatic^{174,219,222}. A likely mechanism underlying the increased responsiveness to whisker stimulation is an increase in the excitability of the membrane (intrinsic excitability), which has been reported in both L2/3 and L5 RS neurons following unilateral WD^{223,224}. Increases in intrinsic excitability can explain the stronger sensory-evoked responses, but is surprising in terms of the observation that spontaneous activity of RS neurons is reduced after 2- and 7- day WD (Figure 3.5A & 3.7A). Reductions in spontaneous activity have also been described following complete visual deprivation in the monocular visual cortex²²⁵.

Finally, we examined changes in L5/6 FS inhibitory neurons at P16 as well, and found increases in the overall VRCs following 2-day WD (Figure 3.8E). This occurred, at least in part, through increases in the proportion of recruited FS neurons (Figure 3.8F). Therefore, the increase in excitatory L5/6 neurons after 2-day WD was not due to reduced activity in inhibitory FS neurons. It will be important to identify the homeostatic mechanisms exhibited by FS neurons following unilateral whisker deprivation. These findings suggest that RS and FS neurons may share some features of plasticity following WD at this age.

3.4.3 Plasticity in KO neurons

The homeostatic capacity of *Fmr1* KO L5/6 neurons was markedly different than what was observed in WT neurons. Following 2-day WD, the overall VRC for L5/6 excitatory neurons did increase, but not to the same extent as WT neurons (Figure 3.5B vs 3.5F). This increase appears to occur largely through an increase in the CW-responsive VRC (Figure 3.5G). The inability of the KO WD VRC to achieve levels similar to the WT WD VRC is due to the fact that the proportion of recruited neurons does not increase following WD in the KO (Figure 3.5D & 3.5H). Therefore, 2-day WD in the KO leads to a compensatory increase in the response of CW-responsive neurons, but

cannot recruit larger proportions of these neurons and therefore, the overall increase in the output of the cortical column is muted. Similar to our results for the L5/6 RS neurons, L5/6 FS neurons show the same deficits in the KO after WD (increase in the overall VRC but not in the proportion of CW-responsive neurons – Figure 3.8E & 3.8F).

Following 7-day WD (P21) in the KO, the overall VRC for L5/6 excitatory neurons did increase, but again, was not as effective as in the WT (Figure 3.7B vs 3.7F). While 7-day WD in the WT led to a significant increase in the proportion of CW-responsive neurons, again, this did not happen in the KO (Figure 3.7H). The increase that was observed in the overall VRC following 7-day WD in the KO appears to occur largely through an increase in the CW-responsive VRC (Figure 3.7G). Thus, as occurred following 2-day WD in the KO, the compensation continued to manifest predominantly as an increase in responsiveness among the neurons that were already responsive to whisker stimulation. If one of the mechanisms for increased responsiveness following unilateral WD is an increase in the intrinsic excitability, then our results could suggest that some neurons can increase excitability (CW-responsive), while others do not. This possibility is very similar to what we have previously observed in WT and KO cortical cultures exposed to a homeostatic perturbation, where some cells increased their ability to fire action potentials while other cells did not⁶³. Another clear difference between 7-day whisker-deprived WT and KO L5/6 neurons was the shape of the VRC. As observed at baseline (without WD), the KO VRC after WD was clearly weaker at lower, but not higher velocities (Figure 3.7). Therefore, WD did not resolve this feature.

Our results show a deficit in the ability to increase neuronal recruitment in a compensatory fashion. In addition to perturbations in homeostatic intrinsic plasticity, it seems likely that impairments in synaptic plasticity contribute. *Fmr1* KO cortical neurons show impairments in activity-dependent spine dynamics^{206, 226}. In fact, one particularly relevant study showed that WT L5 S1 cortical neurons alter the rate of synapse elimination following unilateral WD, but this plasticity is

absent in the *Fmr1* KO¹⁵⁹. Regardless of the mechanism, reduced recruitment of KO L5/6 neurons could result in inappropriate sensory processing and output, as L5/6 neurons are critical for sending output to other cortical and subcortical regions. For instance, reduced signaling could adversely affect the precision and accuracy of processing tactile information from whiskers, potentially impairing the mouse's ability to detect, discriminate, and respond to sensory stimuli¹⁴⁴. These sensory impairments are observed in both FXS animal models and patients.

Few studies have investigated homeostatic plasticity in the FXS model, but deficits have been reported. In hippocampal cultures, previous work has demonstrated an exaggerated homeostatic intrinsic plasticity⁶⁴ and a failure of homeostatic synaptic scaling⁶². Our lab previously demonstrated that homeostatic intrinsic plasticity is impaired in *Fmr1* KO cortical cultures⁶³. Our current findings of impaired homeostatic recruitment in the *Fmr1* KO cortex following a physiologically realistic sensory deprivation suggest homeostatic plasticity deficits in the intact system, and could explain some of the phenotypes associated with this neurodevelopmental disorder. A deeper understanding of these changes could offer insights into how early developmental abnormalities may influence long-term cortical organization and sensory processing impairments in neurodevelopmental disorders such as FXS and ASDs.

3.5 Experimental Procedures

3.5.1 Mice

Heterozygous female *Fmr1* mice (X-linked gene; The Jackson Laboratory, Strain #003025, backcrossed on C57BL/6J background) were crossed with wild type (WT) C57BL/6J males (Jackson Laboratory) to generate litters of pups with mixed genotypes (*Fmr1* KO, *Fmr1* heterozygous, and WT mice). Genotyping was outsourced using Transnetyx, an automated genotyping PCR service, after validation with in-house PCR. For all experiments, *Fmr1* KO male pups were compared to WT male littermate controls. The mice were housed in a 12-hour light/dark

cycle and the animal protocol was approved by the Institutional Animal Care and Use Committee at Emory University.

3.5.2 Whisker deprivation

Mice were lightly anesthetized with isoflurane, and all the whiskers on the right side of the vibrissal pad were trimmed to approximately 2 mm at postnatal day 14 (P14). For experiments conducted at the 2-day time point (~P16), this initial deprivation was the only occurrence. For experiments conducted following a 7-day WD (~P21), whiskers on the right were trimmed every 48 hours, allowing for 48-72 hours to pass after the last trimming session in order to ensure whiskers have regrown sufficiently for whisker stimulation at P21 or P22. Mice that did not undergo whisker deprivation were still anesthetized with isoflurane on corresponding days, and had all the whiskers on the right side of the vibrissal pad acutely trimmed immediately before whisker stimulation on the day of the experiment. Left whiskers were never trimmed.

3.5.3 Electrophysiology recordings

Male mice (P16-P22) were anesthetized with isoflurane and chlorprothixene (0.02 mg dissolved in 10 mL saline, 1 mL injected intraperitoneally). Mice were transferred to a heating pad (37 °C), and the snout was inserted into a nose cone for consistent oxygen and isoflurane. Depth of anesthesia was monitored by breathing rate. A head plate was dental cemented onto the skull, and a small craniotomy was made over the barrel cortex – 3 mm lateral and 1.5 mm caudal to bregma. Anesthesia was then reduced (0.6-1% isoflurane) to maintain a respiratory rate of 1 breath/sec or slightly faster to obtain electrophysiology recordings.

Extracellular recordings were made using silicon probes (H3, Cambridge NeuroTech, United Kingdom) with 64 recording sites covering 1275 μm in depth. The probe was first coated in DiI stain in order to determine penetration location post-recording. The probe was then inserted at a 30° angle with respect to the vertical such that the probe was perpendicular to the surface of the barrel

cortex in the left hemisphere. Recordings were acquired at 25 kHz and band-pass filtered above 300 Hz. Synapse software (TDT) was used to monitor activity on a TDT electrophysiological platform consisting of the PZ2 pre-amplifier and the RZ2 BioAmp Processor. All recordings were made while blind to genotype.

3.5.4 Whisker stimulation

Nine whiskers were inserted into piezoelectric stimulators, generally by inserting the whisker that elicited the strongest response across all 64 channels in the middle of the array (Figure 3.1A)^{135,227}. A custom TDT program stimulated whiskers at different velocities. Each piezoelectric deflection was a ramp-hold-return (4 ms – 100 ms – 4 ms). To obtain a velocity response curve (VRC), whiskers were stimulated at 0, 65, 195, 326, 456, 587, 797 degrees per second, with varying amplitude and velocity throughout the recording period. 25 repetitions of each stimulation combination were recorded at 2-second interstimulus intervals, interleaving the deflections of whiskers and velocities. Spontaneous firing rate (no whisker stimulation) was measured in the 1 second before whisker deflection.

3.5.5 Histology

Mice were euthanized with high dose isoflurane and cervical dislocation. The brain was isolated, cut at an approximately 30° angle, and sectioned on a vibratome with 225 μm sections. Sections were mounted and viewed under a Keyence microscope to determine probe penetration location (Figure 3.1B).

3.5.6 Analysis

Spike sorting. A spike sorting algorithm was used to automatically sort waveforms, and units were then manually curated (both visually and with specific criteria) to identify single neurons.

Recording files in TDT format were converted to a binary file using the TDTbin2mat function in Matlab (MathWorks). Data was then run through Kilosort 2.5 (spike sorting algorithm) on

Ontologic's platform (<https://www.ontologic.ly/>). The following changes were made to the preset parameters: threshold = [7 2], spike threshold = -5, sigma mask = 15, minimum firing rate = 0.1²²⁸. Manual curation of clusters then took place in Phy²²⁹. During this process, clusters were either merged or separated based on waveform shape, cross- and auto- correlogram distributions, and template feature view. Noise waveforms (waveforms that did not have the characteristic shape of a neuron) were also discarded. All remaining clusters were then analyzed by downstream analysis (see below).

Single unit criteria. In order to ensure that clusters were truly single units, they had to pass certain criteria, based on past literature^{135, 230, 231}. We calculated the inter-spike interval (ISI) to determine the refractory period violation, which had to be < 1.5% in the 1 ms bin of the auto-correlogram. A mean firing rate was calculated throughout the length of the recording to ensure that units did not suddenly come into or out of the recording – less than 10% of the recording could be below 20% of the mean firing rate. In addition, < 20% of the missed spikes based on a Gaussian fit of the data was acceptable for a single unit. Finally, < 3% of the spike amplitude distribution could be below 11 μ V. In order to differentiate putative excitatory and inhibitory neurons, we first graphed the trough to peak times for all units. We then fit a Gaussian Mixture Model to this distribution, which predicted an approximately 10% overlap between the two distributions (Figure 3.1C). For this study, we identified putative excitatory neurons as neurons with a half-width of more than 0.72 ms (Figure 1D). In addition, we re-ran all analyses after removing all units that have a half-width between 0.63 ms and .80 ms (the overlapping area), and found that the results remained similar, suggesting that the overlapping area contained mostly putative excitatory neurons.

Current source density (CSD). CSD analysis was performed to elucidate the laminar position of electrodes on the silicon probe. First, the average local field potential (LFP) from stimulation-evoked responses of the best whisker (BW) was calculated. Then, the delta source method of inverse

CSD (iCSD) was utilized to locate current sinks and sources²³². The boundary between L4 and L5a was identified by the sharp change between current sink (L4) and current source (L5a). We assumed a width of 170 μm for L4 and 700 μm for L5/6^{135, 233, 234}.

Analyses conducted. The best whisker (BW) of the neuron was determined by performing a Wilcoxon rank sum test with $p = 0.0056$ ($p = .05/9$), to account for the 9 whiskers that were stimulated. The whisker that elicited the most significant response was deemed the BW for the neuron. The columnar whisker (CW) was defined as the whisker that corresponded to the barrel in which the probe was inserted. Probe penetrations that resulted in septal recordings were not included in the CW analysis, but were included for BW analysis. Velocity response curves (VRCs) were generated using both the BW and CW stimulation for the neurons. The spontaneous firing rate for each neuron was subtracted from the evoked firing rate at each velocity, and a graph was produced to demonstrate how the firing rates changed over increasing velocities. The proportion of neurons that significantly respond to a CW stimulation at the highest velocity was also quantified using a one-sided Wilcoxon rank sum test. Separate VRCs were generated for these neurons to determine if the CW-responsive neurons alter their response to whisker stimulation. The minimum stimulation velocity needed to elicit a significant whisker-evoked response from a neuron was determined by using a one-sided Wilcoxon rank sum test at each stimulation velocity. This analysis was performed for all neurons that significantly responded to CW stimulation.

Statistical analysis. A Two-Way ANOVA (mixed model) was used to determine if VRCs were significantly different when comparing two experimental conditions. Tukey's HSD was then used to determine if there was a statistically significant difference at each velocity. In order to determine if there was a significant difference in the proportion of neurons that respond to CW stimulation, a z-score test was used. Finally, the Mann Whitney U test was utilized to compare the spontaneous firing rates.

3.5.7 Code and Data Availability

All Matlab code (original and previously published) is available on Github

(<https://github.com/lakhanialishah/WhiskerAnalysis>). Data for this paper will be available on The

DANDI Archive (<https://dandiarchive.org/dandiset/001171>).

Chapter 4: General Discussion and Future Directions

4.1 General discussion and future directions for Chapter 2 (cortical cultures and embryonic chick spinal cord)

4.1.1 *Variability and degeneracy of firing properties*

The concepts of variability and degeneracy were central to this project. Variability refers to the differences in firing patterns and properties of individual neurons or networks, while degeneracy refers to the ability of different networks or mechanisms to achieve similar functional outputs.

Together, these two ideas reveal the complexity and flexibility of nervous system.

We observed variability in many of the firing properties, such as burst duration, overall spike rate, and inter-burst interval, in both the cortical cultures and the embryonic chick spinal cord. This variability can arise from several different sources. One explanation is that a neuron may rely more on certain modulatory neurotransmitters or plasticity mechanisms than others. In some thalamocortical neurons, for example, noradrenergic and serotonergic inputs heavily influence spiking patterns via voltage-gated ion channels²³⁵. Thus, removing these inputs or altering their strength will more significantly impact these neurons compared to other neurons that do not rely on this neuromodulatory input. Furthermore, each neuron has a different constellation of ion channels and receives input from a different combination of synapses. With all the various possible arrangements or combinations of ion channels and synaptic strengths, each neuron will differentially receive and respond to incoming signals¹⁹. This could also account for the variability in firing properties. Regardless of how this variability arises, neurons and networks are typically maintained within a parameter space, or a solution space, that is optimal for their final output, which leads us to the idea of degeneracy.

In the context of firing properties, degeneracy highlights the redundancy that is present in neurons and networks so that the end goal of the system remains consistent. For example, different constellations of ion channels have the ability to produce the same firing pattern. Thus, even if some channels are not functioning properly, neurons have other channels that can be altered to maintain a constant output. Additionally, the different homeostatic plasticity mechanisms represent perhaps the most significant way by which degeneracy is achieved. Neurons can alter synaptic strength, presynaptic vesicle release, or intrinsic excitability to ensure that stable firing properties are maintained²³⁶. Each network develops its own feedback mechanisms that could vary from one culture or cord to the next, suggesting that one system could respond to a perturbation differently than another system. This redundancy in homeostatic processes is crucial because it maintains the functional output, whether that be a network that is involved in information processing, motor behavior, or something else.

Altogether, variability provides a system with the ability to respond to a wide range of inputs and perturbations, and encode information in multiple ways. This variability could explain why people respond so differently to specific drugs or treatments, and why it is important to include a broad range of people in clinical trials²³⁷⁻²³⁹. On the other hand, degeneracy ensures that the functional output of the network can be achieved, even if it is through different mechanisms. Degeneracy is thought to play an important role in humans through the evolution of complex adaptive systems and natural selection²⁴⁰⁻²⁴². These concepts provide systems with the ability to be adaptable and robust, both at the level of the individual cell and the human population.

4.1.2 Significance of SRWB homeostasis

In both the embryonic chick spinal cord and the cortical cultures, we discovered that GABAergic blockade induced a consistent increase in SRWB that then recovered to baseline control levels over the span of a few hours. In neuronal cultures, bursts of activity represent the collective behavior of

the network. These bursts are a fundamental aspect of how neurons encode and transmit information and how they respond to stimuli. Thus, homeostatic mechanisms in culture may work to ensure that bursting properties remain within a specific range, even when the network experiences pharmacological perturbations. This stability is crucial for maintaining consistent neural coding and for the proper execution of network functions in a more intact system. Some computational models have suggested that the number of spikes in a burst can convey important information about the stimulus^{243, 244}. However, the importance of SRWB in particular has not been previously established as far as we know, so it would be important to further investigate this firing property.

Similarly, in the embryonic chick spinal cord, SRWB could play an important role in driving behavior, specifically the kicking movements observed *in ovo*. The spinal cord generates and coordinates motor output, and it appears to rely on homeostatic mechanisms to maintain consistent burst patterns and spike rates during these movements. When spontaneous activity is not appropriately maintained, it causes disruptions in dorsal-ventral as well as anterior-posterior motoneuronal axonal pathfinding²⁴⁵. This spontaneous activity is also crucial for muscle and joint development^{25, 26, 246, 247}. During development, the nervous system faces numerous challenges to activity, such as changes in cell growth, differentiation, and connectivity. The homeostatic strategies employed by cells or networks during this critical period are likely to have a profound impact on embryonic development. Therefore, the influence of these homeostatic mechanisms is likely more impactful during early development compared to later stages, when homeostatic mechanisms become more restricted and less adaptable. Thus, it is possible that changes in SRWB may lead to abnormal motor circuitry or behavioral deficits that could impact the development of the embryo. Furthermore, bursting dynamics *in vivo* has been shown to impact attention, perception, information processing, and learning²⁴⁸. Therefore, it would be critical to examine how SRWB influences these processes in more experimental and computational models.

When we found that SRWB was the main firing property under tight regulation, we observed that it was maintained at the network level, but also at the individual neuron level, in cortical cultures. This was an interesting finding because previous studies have presented data showing either that firing rate was maintained at the network level or at the individual cell level, not necessarily both. For example, Slomovitz et al. blocked GABA receptors in hippocampal cultures and found that this triggered synaptic and intrinsic compensatory changes, but that these changes resulted in firing rate homeostasis at the population level, and that homeostasis at the single neuron level was not achieved²⁴⁹. Furthermore, they observed that burst duration and number of spikes per burst changed after a perturbation, and then returned to baseline levels, suggesting that the burst pattern of the population is maintained even though individual neurons do not maintain this. On the other hand, Hengen et al. investigated firing rate homeostasis in an intact model by performing monocular deprivation in rats and then recording from V1. They found that even though average firing rates of pyramidal neurons could differ by a large magnitude, the firing rate for each neuron was maintained around its individual set point and returned to this set point after it was perturbed by sensory deprivation⁴³. Our results could bridge these two theories by showing that SRWB homeostasis can be maintained across both levels simultaneously, suggesting a more integrated mechanism of this firing property, and can perhaps point to other properties that are similarly maintained. Although this is one possibility, it does not have to be the case, as homeostasis at the single neuron level could occur independently of network-wide changes.

4.1.3 Future directions

This study guides us toward several possible avenues for future research. One such path would be to investigate the mechanisms behind SRWB homeostasis. Although we observed that SRWB was a firing property that was maintained in two different systems, we do not yet understand how SRWB was maintained. Using techniques like patch-clamp electrophysiology, we can examine how changes

in voltage-gated ion channel conductances and/or other channels (ex: synaptic) influence SRWB. These channels play an important role in shaping firing properties, some of which will be mentioned here. Since previous work has suggested that the increase in SRWB is most likely occurring through an increase in input resistance and a depolarization of the driving force for currents underlying spontaneous network activity, I will mention a channel that might be involved in the restoration of SRWB to baseline levels. Changes in the persistent sodium current (I_{NaP}) can influence the spike rate. In this case, if I_{NaP} were reduced, the resting membrane potential would become more hyperpolarized, and the neuron would likely become less excitable, which could contribute towards the decrease in SRWB. By systematically manipulating channels and observing how SRWB recovers following a perturbation, we can gain deeper insights into the underlying mechanisms of firing rate homeostasis.

In my current study, I found that the amplitude of calcium transients of motoneurons in the embryonic chick spinal cord increased following GABAR blockade, and that the amplitude of these transients were slowly beginning to return to baseline levels within a few hours after adding the blocker. Thus, it would be important to explore how calcium signaling pathways, which are important for many processes, are impacted during the regulation of SRWB. Previous literature has shown that the mitochondrial calcium uniporter complex (MCUc) acts as a calcium sensor that triggers a homeostatic response. The insulin-like growth factor-1 receptor (IGF-1R) in mitochondria couples spiking activity with downstream mitochondrial calcium via the MCUc²⁵⁰. This mechanism of action was shown to be critical for mean firing rate homeostasis, not necessarily SRWB homeostasis. However, it is possible that either these specific mitochondrial molecules or others in the mitochondria can detect changes in the calcium level and trigger a downstream signaling cascade to return SRWB back to baseline levels. Our lab is currently looking into the possibility of mitochondrial matrix calcium as a trigger for homeostasis and have preliminary evidence suggesting

that MCUC activity is important in triggering synaptic scaling in the embryonic chick spinal cord (Pekala et al., in preparation).

After understanding the mechanisms and calcium signaling pathways underlying SRWB homeostasis, it would also be important to investigate if there are developmental trajectories that play a role in SRWB homeostasis. It is possible that SRWB regulation is crucial at certain time points in development, but at other time points, it may be that another firing property is maintained following perturbations. By exploring these developmental trajectories, future work could identify critical periods when SRWB is most vital and how different firing properties may compensate or interact with SRWB regulation during various developmental phases. These insights could deepen our understanding of how disruptions in SRWB and other firing properties could contribute to developmental disorders and aid in the creation of age-specific therapeutic strategies.

Previous studies have highlighted the importance of computational modeling in homeostatic plasticity research^{17,18}. Developing these models to now simulate SRWB homeostasis and variability of firing properties could possibly prove to be incredibly useful. Models could identify key parameters that influence SRWB dynamics and predict how changes in these parameters affect network behavior. There have already been studies conducted to analyze how bursting dynamics, such as synchronization, impact learning^{251,252}. In addition, there have been significant advances in technology that could be beneficial in further investigation. For example, combining multi-electrode array (MEA) recordings with closed loop stimulation could potentially allow researchers to change SRWB in culture, and record other firing properties, or vice versa – change other firing properties and observe what happens to SRWB. This could involve the utilization of halorhodopsin, an optically activated protein that transfers chloride ions into the cytoplasm to hyperpolarize the cell. In an experiment, for instance, if a burst occurs in the embryonic chick spinal cord or cortical culture, light stimulation could activate the halorhodopsin, which would result in a decrease in spiking and

prevent an increase in the SRWB. On the other hand, using a channelrhodopsin, a protein that depolarizes the cell by opening channels permeable to cations, to artificially increase SRWB could help confirm that SRWB is the firing property that is homeostatically maintained. These studies would allow us to better characterize the interactions between these different spiking characteristics and observe changes in SRWB in a bidirectional manner. Ultimately, integrating novel methods with computational modeling will allow researchers to better manipulate SRWB homeostasis and understand how it impacts neural function.

As previously discussed in Section 4.1.2, earlier studies investigating firing rate homeostasis came to different conclusions, and this might have to do with the fact that some of these studies were performed in culture, whereas others were performed in the intact animal model. Extending these findings of SRWB homeostasis and variability to *in vivo* animal models would allow us to better understand how homeostatic plasticity operates in a more complex, physiologically intact, model. By analyzing SRWB in the context of intact neural circuits, researchers can investigate how fluctuations in SRWB affect network dynamics, sensory processing, and cognitive functions. Moreover, examining these dynamics *in vivo* could potentially reveal how disruptions in SRWB homeostasis could contribute to neurological disorders. We know that homeostatic plasticity is impaired in both neurodevelopmental and neurodegenerative disorders^{62, 253, 254}. Thus, studying SRWB in these contexts and determining if there are changes in this firing property in disease can potentially guide the development of targeted interventions. For instance, if a disease is found to alter neuronal firing properties that result in certain phenotypes, correcting the changes with pharmacological treatments or neurostimulation or inhibition could potentially alleviate some symptoms.

In summary, this project in my dissertation work provided important information about the regulation of SRWB and the variability of other firing properties in two different systems. The consistent change in SRWB and its recovery demonstrates the importance of this firing property as a

target for homeostatic plasticity mechanisms. The variability in firing properties further underscores the significance of degeneracy and the idea that neural circuits can employ different mechanisms to reach the same output, which in this case, would be the maintenance of SRWB. Future research should focus on elucidating the mechanisms associated with sensing and carrying out SRWB homeostasis and the relevance of SRWB homeostasis in *in vivo* models at different developmental time points.

4.2 General discussion and future directions for Chapter 3 (barrel cortex in the *Fmr1* KO mouse model)

4.2.1 Developmental changes in sensory processing in the *Fmr1* KO model

One of the main differences that we observed between the WT and *Fmr1* KO mouse model was the change in baseline responsiveness of neurons at the later developmental time point. At P21, KO whisker-responsive neurons demonstrated a shift in their responsiveness to whisker stimulation, becoming less sensitive at lower velocities but similarly responsive at the higher velocities. This suggests that KO L5/6 excitatory neurons might initially need a stronger signal from incoming connections, but once they are sufficiently driven, they spike normally. This observed shift occurred in just five days, over a critical developmental period during which the brain undergoes significant changes in synaptic connectivity and maturation²⁵⁵. As mentioned earlier, the nervous system encounters many challenges during development, and the homeostatic strategies that are used by cells during these critical periods impact the formation of the network. However, with the absence of FMRP, many of these homeostatic mechanisms (both synaptic and intrinsic plasticity) are impaired^{62,63}. Thus, as the *Fmr1* KO mice develop and begin processing sensory input (active whisking begins at P14), it may not process this information in the same way as WT mice due to the differences in the strategies chosen during this altered development.

We know that most KO barrel cortex excitatory neurons (L2-L5) are intrinsically more excitable than their WT counterparts, but how does this translate to the shift that we observed^{65, 134, 135, 256}? One possible theory is that the increased intrinsic excitability of KO neurons could be compensating for a broader network-level deficiency in sensory processing. The reduced sensitivity at lower velocities might reflect an imbalance in the network's ability to process weaker changes in sensory input, potentially due to altered synaptic scaling or excitatory-inhibitory balance. The normal responsiveness at higher velocities might indicate that the KO neurons homeostatically adjusted so they are able to respond normally, as long as the neurons have enough drive. This discrepancy between the WT and KO cortex could highlight a compensatory mechanism where the neurons become more reliant on higher-intensity stimuli to achieve a normal response, which may be a result of disrupted or weakened homeostatic plasticity. Another interpretation for the decreased responsiveness that we observed could be that the *Fmr1* KO cortex strategically shifts its sensory processing abilities. In this diseased state, the cortex could prioritize responding to these stronger inputs rather than precisely detecting and responding to subtle inputs. This would result in decreased sensory discrimination, which has been previously reported in the visual and auditory system in FXS models^{257, 258}.

Ultimately, the absence of FMRP could disrupt the fine-tuning of sensory processing during critical developmental windows. These sensory processing abnormalities are not only important for understanding FXS pathology, but they are also crucial for developing targeting therapies to alleviate sensory-related symptomology.

4.2.2 Impaired recruitment of neurons at baseline and following perturbations in the *Fmr1* KO

We discovered that the *Fmr1* KO mice can express homeostatic plasticity in some ways, but that it fails in other ways, specifically in terms of a larger recruitment of the neuronal population. At P16, we observed that at baseline, there was a slight decrease in the proportion of CW-responsive

neurons in the KO compared to the WT cortex, albeit not significant. Additionally, after both 2 and 7 days of whisker deprivation, WT mice demonstrated an increase in the proportion of CW-responsive neurons, but KO mice did not exhibit a similar increase. These results highlight the significant impairment in recruiting neurons following whisker stimulation.

The reduced recruitment of the population at baseline at P16 in the *Fmr1* KO cortex could potentially lead to problems, even though recruitment at P21 was very similar between the WT and KO. For instance, sensory processing deficits at this developmentally young age could translate to problems later in life. A prior study in a rat model of FXS discovered that the visual cortex demonstrated hypoexcitability at an early time point, but by the third and fourth week of development, neurons were actually hyperexcitable²⁵⁹. Although this is different than our finding in terms of how recruitment of the population changes (reduced initially, and then the same), it points to a potential way in which early developmental changes in cortical excitability could influence later sensory processing. A weakened response during the critical period, as we found at P16, could trigger changes in other parts of the brain. For example, homeostatic plasticity mechanisms could try to compensate for this reduced recruitment further downstream in the processing of sensory information, but instead, the compensations could overshoot the target and result in a hyperresponsive state elsewhere, for instance in S2. This could account for the hypersensitive phenotypes observed later in life in children with the *Fmr1* premutation^{260,261}. It would be interesting to perform my experiments again at an even later time point, say P28, to investigate whether there might be further changes and to observe neural activity downstream of L5/6. If this shift from hypoexcitability early in life to hyperexcitability later in life is discovered, then it would be important to target therapeutic interventions that can prevent this maladaptive shift, or address both these components.

The decrease in neuronal recruitment following whisker deprivation in the *Fmr1* KO mouse could suggest several potential changes occurring in the barrel cortex. One potential change could be impaired sensory processing. Since WT mice almost doubled the neurons recruited following whisker deprivation but KO mice did not demonstrate this significant increase, the sensory perturbation could not trigger the same level of neural plasticity or compensatory responses in the KO mice as it did in the WT mice. This would suggest that the underlying mechanisms that detect and respond to sensory changes, or the mechanisms for homeostasis, are impaired. Previous literature supports this theory, as the *Fmr1* KO model demonstrates a lack of homeostatic plasticity in different contexts^{62, 63, 206, 262}. If the KO model is unable to adjust to changes in sensory input, then it also likely struggles to accurately process incoming information. Sensory adaptation probably requires the recruitment of additional neurons, or the modulation of neurons already recruited. Thus, if a population cannot change the recruitment of neurons, as is the case of the KO cortex, it would fail to adjust to a new sensory environment. This reduced sensory adaptation has been previously observed in the KO mouse model, in which repetitive whisker stimulation did not result in neuronal adaptation¹⁶³.

Another possible change that may occur in the *Fmr1* KO barrel cortex following whisker deprivation is a change in dendrite morphology, which can result in a change in neuronal recruitment. Dendrites are crucial for receiving and integrating sensory inputs, and their structure can influence neuronal responsiveness and plasticity. One study found that a brief increase in activity, which trigger morphological changes in WT dendritic spines, did not result in any changes in *Fmr1* KO hippocampal neurons, suggesting that activity-dependent plasticity is impaired²²⁶. Another more relevant study observed that KO L5 pyramidal neurons in the barrel cortex demonstrated an increase in dendritic spine formation and elimination at baseline, and that these spines were not as responsive to unilateral whisker deprivation as the WT spines¹⁵⁹. Thus, the KO

barrel cortex could exhibit altered dendritic properties that could lead to the differences we observed in terms of recruitment and plasticity. If dendritic spines are less responsive to sensory deprivation, this could impair the ability of these neurons to synaptically adapt to changes in sensory input. Consequently, this may result in the above-mentioned impaired plasticity and sensory processing deficits.

Finally, it would be important to therapeutically target these lower levels of neuronal recruitment. One possible pharmacological strategy is utilizing NMDA receptor (NMDAR) modulators. NMDARs play a crucial role in synaptic plasticity and processing incoming information, and are a major target for FMRP^{263,264}. It is possible that in the *Fmr1* KO barrel cortex, NMDA receptors are hypoactive, as has been previously discovered in the hippocampus, and therefore pharmacologically increasing NMDAR activity could potentially rescue some deficits²⁶⁵⁻²⁶⁷.

To conclude, *Fmr1* KO L5/6 neurons exhibit impairments in recruitment at baseline and following whisker deprivation, which demonstrate fundamental disruptions in sensory processing and adaptation. These findings emphasize the importance of further investigating the dynamic changes in neural recruitment, both at later developmental stages and at the molecular level, to guide therapeutic strategies.

4.2.2 Future Directions

Since we observed that the *Fmr1* KO mouse has some homeostatic capacity, but it is different from that of the WT mice, it would be interesting to next investigate what specific mechanisms of homeostatic plasticity are impaired. For instance, changes in intrinsic excitability are one mechanism by which cells adapt. Previous studies have established that the L2-5 neurons in the *Fmr1* KO model have increased intrinsic excitability at baseline^{65, 134, 135, 211, 256}. However, it is difficult to determine how sensory perturbations affect intrinsic excitability, as different perturbations trigger different changes. A prior study reported that just one day of D-row whisker deprivation caused a reduction

in the intrinsic excitability of L2/3 parvalbumin (PV) inhibitory neurons by upregulating voltage-gated potassium channels¹⁷⁶. Another study reported that the intrinsic excitability of L5 neurons increased after unilateral whisker deprivation, but the sensory deprivation began very early in development (P3) or after the critical period (P20)²⁶⁸. Thus, it would be important to investigate the differences in membrane excitability and conductances to determine how the sensory perturbation of unilateral whisker deprivation, which specifically triggers homeostatic changes, affects WT and *Fmr1* KO neurons during a critical period in development. Alternatively, compensatory changes in synaptic strength represent another potential failed homeostatic mechanism. Many papers suggest that synaptic scaling and connectivity is impaired in the *Fmr1* KO model^{62,160}. We also know that D-row whisker deprivation weakens the L4 to L2/3 synapse and inhibitory synapses in L4^{269,270}. However, there are only a few studies that examine changes in L5 of the barrel cortex, even though it is the important output of the cortical column. Understanding how these homeostatic plasticity mechanisms are altered in L5/6 of the barrel cortex in the *Fmr1* KO, both at baseline and following sensory deprivation, could provide insight into how *Fmr1* KO mice adapt, or fail to adapt, to changes in sensory input, and lead the way in potential therapeutic approaches. If certain molecules or signaling pathways are impaired, then developing drugs that enhance or mimic these underlying mechanisms might resolve some of the sensory phenotypes.

Along with studying changes in homeostatic plasticity mechanisms, it would also be interesting to investigate the excitation-inhibition (E-I) balance and circuitry. Many studies suggest that there is an imbalance in FXS and autism in general^{56,134,271}. Examining how the recruitment and activity of excitatory and inhibitory neurons in the overall network change following a sensory perturbation could shed light on more widespread network dysfunction.

After gaining a better understanding of L5/6 homeostatic mechanisms and E-I balance, it would be beneficial to analyze other cortical layers to determine whether the deficits we observed

are consistent across all layers or specific to L5/6. A prior study has shown that the decrease in whisker-evoked responses and recruitment we observed at baseline in the *Fmr1* KO also occur in L2/3, so it is possible that these changes in the overall responsiveness of excitatory and inhibitory neurons take place throughout the cortical layers¹³⁵. This could suggest a more global disruption in cortical processing. On the other hand, if the changes we observed are layer-specific, it could suggest that there are differentially regulated processes and localized circuit dysfunction. It could also suggest that each layer compensates for any changes in layer before it in the cortical pathway. Additionally, it would be interesting to compare the homeostatic processes and neuronal recruitment in the barrel cortex with other sensory cortices (ex: visual cortex or auditory cortex) to determine if other sensory modality deprivations also demonstrate similar deficits. Previous literature has shown that there are differences in how sensory experience affects network development in other sensory cortices^{272,273}. Thus, it would be important to compare our results to other brain regions to determine if there are any overarching similarities, though this comparison would need to be performed carefully as different deprivations might affect cortical neurons differently.

Another important result we observed was the difference in baseline recruitment of the neuronal population and the sensitivity of neurons from P16 to P21. Thus, it would be important to conduct longitudinal studies to explore these developmental changes in more detail. Since we observed these changes over just five days, conducting the same experiments in *Fmr1* KO mice at earlier developmental stages (ex: before active whisking begins) and later developmental stages (ex: after the closure of the critical period) could be helpful in assessing how homeostatic plasticity and sensory processing abilities evolve over time. This could help identify critical periods when interventions might be the most effective, initially in mice, and perhaps later in clinical trials.

Finally, analyzing neuronal recruitment and whisker-evoked responses in awake, behaving mice would provide a more comprehensive understanding of how sensory processing works.

Previous studies demonstrate that the *Fmr1* KO mouse model has behavioral deficits when it performs paradigms that require information from whiskers^{162,164}. However, there are no studies that examine how these mice respond to perturbations such as whisker deprivation. It would be interesting to observe what homeostasis might look like in mice that are performing tasks or exploring the environment. This could reveal how the deficits in neuronal activity we observed in an anesthetized animal translate into behavioral impairments, and how sensory integration and cognitive functions are affected.

In conclusion, there are many future avenues of research from this work. Investigating intrinsic excitability, synaptic strength, and E-I imbalance in all cortical layers and different brain regions would help us determine the extent of the impairments we observed. Longitudinal studies, as well as studies in awake mice, would provide a timeline of the impairments and homeostatic processes and how sensory processing is disrupted. These potential future directions for this project in my dissertation aim to deepen the understanding of the mechanisms underlying altered homeostatic plasticity in *Fmr1* KO mice and explore potential avenues for therapeutic intervention and translational research.

4.3 What aspect of neuronal activity is homeostatically maintained

An important question to ask is what exactly is homeostatically maintained after a cell or network encounters a perturbation. In my dissertation, I've found that in three different systems, the most crucial aspect that the system adjusts to is the evoked response. In cortical cultures, after the pharmacological blockade of GABA receptors, the spike rate within the burst (SRWB) increased and then returned to baseline levels. These bursts represent the final output of the neuronal network in culture, as close to a naturally evoked response as possible in this system. In the embryonic chick spinal cord, we found that SRWB again was the firing property that returned to baseline levels following GABA receptor blockade. The bursts in the spinal cord are representative of the kicks that

occur in the embryonic chick. Both the bursts in culture and the bursts in the spinal cord are synaptically driven events. Finally, in the barrel cortex, we observed that whisker deprivation triggers an increase in the responsiveness of cortical neurons (an increase in the velocity response curve, VRC). This increased excitability appears to be a compensation of the sensory pathway in order to remain sensitive to the lost input from the whiskers, suggesting that the evoked firing rate is important to this system as well. In conclusion, these findings highlight the importance of homeostatically maintaining the evoked response. Future studies should focus on understanding the mechanisms through which the evoked response is maintained, and how it might be altered in disease states.

Chapter 5: References

1. Turrigiano G, Abbott LF, Marder E. Activity-dependent changes in the intrinsic properties of cultured neurons. *Science*. 1994;264(5161):974-7. Epub 1994/05/13. doi: 10.1126/science.8178157. PubMed PMID: 8178157.
2. Turrigiano G, LeMasson G, Marder E. Selective regulation of current densities underlies spontaneous changes in the activity of cultured neurons. *The Journal of Neuroscience*. 1995;15(5):3640-52. doi: 10.1523/jneurosci.15-05-03640.1995.
3. Turrigiano G. Homeostatic synaptic plasticity: local and global mechanisms for stabilizing neuronal function. *Cold Spring Harb Perspect Biol*. 2012;4(1):a005736-a. doi: 10.1101/cshperspect.a005736. PubMed PMID: 22086977.
4. Turrigiano GG, Leslie KR, Desai NS, Rutherford LC, Nelson SB. Activity-dependent scaling of quantal amplitude in neocortical neurons. *Nature*. 1998;391(6670):892-6. Epub 1998/03/12. doi: 10.1038/36103. PubMed PMID: 9495341.
5. Kilman V, van Rossum MCW, Turrigiano GG. Activity Deprivation Reduces Miniature IPSC Amplitude by Decreasing the Number of Postsynaptic GABA_A Receptors Clustered at Neocortical Synapses. *The Journal of Neuroscience*. 2002;22(4):1328. doi: 10.1523/JNEUROSCI.22-04-01328.2002.
6. Pekala D, Wenner P. The Uniform and Nonuniform Nature of Slow and Rapid Scaling in Embryonic Motoneurons. *J Neurosci*. 2022;42(7):1224-34. Epub 2021/12/31. doi: 10.1523/jneurosci.0899-21.2021. PubMed PMID: 34965976; PMCID: PMC8883842.
7. Hanes AL, Koesters AG, Fong MF, Altimimi HF, Stellwagen D, Wenner P, Engisch KL. Divergent Synaptic Scaling of Miniature EPSCs following Activity Blockade in Dissociated Neuronal Cultures. *J Neurosci*. 2020;40(21):4090-102. Epub 2020/04/22. doi: 10.1523/jneurosci.1393-19.2020. PubMed PMID: 32312887; PMCID: PMC7244191.
8. Wang G, Zhong J, Guttieres D, Man HY. Non-scaling regulation of AMPA receptors in homeostatic synaptic plasticity. *Neuropharmacology*. 2019;158:107700. Epub 20190705. doi: 10.1016/j.neuropharm.2019.107700. PubMed PMID: 31283924; PMCID: PMC6745258.
9. Davis GW. Homeostatic control of neural activity: from phenomenology to molecular design. *Annu Rev Neurosci*. 2006;29:307-23. Epub 2006/06/17. doi: 10.1146/annurev.neuro.28.061604.135751. PubMed PMID: 16776588.
10. Turrigiano GG, Nelson SB. Homeostatic plasticity in the developing nervous system. *Nat Rev Neurosci*. 2004;5(2):97-107. Epub 2004/01/22. doi: 10.1038/nrn1327. PubMed PMID: 14735113.
11. Desai NS, Rutherford LC, Turrigiano GG. Plasticity in the intrinsic excitability of cortical pyramidal neurons. *Nat Neurosci*. 1999;2(6):515-20. Epub 1999/08/17. doi: 10.1038/9165. PubMed PMID: 10448215.

12. O'Leary T, Williams AH, Caplan JS, Marder E. Correlations in ion channel expression emerge from homeostatic tuning rules. *Proceedings of the National Academy of Sciences*. 2013;110(28):E2645-E54. doi: 10.1073/pnas.1309966110.
13. Schulz DJ, Goaillard JM, Marder E. Variable channel expression in identified single and electrically coupled neurons in different animals. *Nat Neurosci*. 2006;9(3):356-62. Epub 2006/01/31. doi: 10.1038/nn1639. PubMed PMID: 16444270.
14. MacLean JN, Zhang Y, Johnson BR, Harris-Warrick RM. Activity-independent homeostasis in rhythmically active neurons. *Neuron*. 2003;37(1):109-20. Epub 2003/01/16. doi: 10.1016/s0896-6273(02)01104-2. PubMed PMID: 12526777.
15. Marder E, Prinz AA. Current compensation in neuronal homeostasis. *Neuron*. 2003;37(1):2-4. Epub 2003/01/16. doi: 10.1016/s0896-6273(02)01173-x. PubMed PMID: 12526765.
16. Cannon J, Miller P. Stable Control of Firing Rate Mean and Variance by Dual Homeostatic Mechanisms. *J Math Neurosci*. 2017;7(1):1. Epub 2017/01/18. doi: 10.1186/s13408-017-0043-7. PubMed PMID: 28097513; PMCID: PMC5264207.
17. Prinz AA, Bucher D, Marder E. Similar network activity from disparate circuit parameters. *Nat Neurosci*. 2004;7(12):1345-52. Epub 2004/11/24. doi: 10.1038/nn1352. PubMed PMID: 15558066.
18. Marder E, Prinz AA. Modeling stability in neuron and network function: the role of activity in homeostasis. *Bioessays*. 2002;24(12):1145-54. Epub 2002/11/26. doi: 10.1002/bies.10185. PubMed PMID: 12447979.
19. Marder E, Goaillard JM. Variability, compensation and homeostasis in neuron and network function. *Nat Rev Neurosci*. 2006;7(7):563-74. Epub 2006/06/23. doi: 10.1038/nrn1949. PubMed PMID: 16791145.
20. Bucher D, Prinz AA, Marder E. Animal-to-animal variability in motor pattern production in adults and during growth. *J Neurosci*. 2005;25(7):1611-9. Epub 2005/02/18. doi: 10.1523/jneurosci.3679-04.2005. PubMed PMID: 15716396; PMCID: PMC6725924.
21. Olsen O, Nadim F, Hill AA, Edwards DH. Uniform growth and neuronal integration. *J Neurophysiol*. 1996;76(3):1850-7. Epub 1996/09/01. doi: 10.1152/jn.1996.76.3.1850. PubMed PMID: 8890297.
22. Hochner B, Spira ME. Preservation of motoneuron electrotonic characteristics during postembryonic growth. *J Neurosci*. 1987;7(1):261-70. Epub 1987/01/01. doi: 10.1523/jneurosci.07-01-00261.1987. PubMed PMID: 3806197; PMCID: PMC6568842.
23. Tien N-W, Kerschensteiner D. Homeostatic plasticity in neural development. *Neural Dev*. 2018;13(1):9-. doi: 10.1186/s13064-018-0105-x. PubMed PMID: 29855353.
24. Hamburger V, Hamilton HL. A series of normal stages in the development of the chick embryo. *J Morphol*. 1951;88(1):49-92. Epub 1951/01/01. PubMed PMID: 24539719.

25. Hanson MG, Landmesser LT. Normal patterns of spontaneous activity are required for correct motor axon guidance and the expression of specific guidance molecules. *Neuron*. 2004;43(5):687-701. Epub 2004/09/02. doi: 10.1016/j.neuron.2004.08.018. PubMed PMID: 15339650.
26. Kastanenka KV, Landmesser LT. In vivo activation of channelrhodopsin-2 reveals that normal patterns of spontaneous activity are required for motoneuron guidance and maintenance of guidance molecules. *J Neurosci*. 2010;30(31):10575-85. Epub 2010/08/06. doi: 10.1523/jneurosci.2773-10.2010. PubMed PMID: 20686000; PMCID: PMC2934783.
27. Wenner P. Development of the locomotor system—Chick embryo. In: Patrick Whelan, Sharples S, editors. *The Neural Control of Movement*: Academic Press; 2020. p. 221-36.
28. O'Donovan MJ. The origin of spontaneous activity in developing networks of the vertebrate nervous system. *Curr Opin Neurobiol*. 1999;9(1):94-104.
29. O'Donovan MJ, Chub N, Wenner P. Mechanisms of spontaneous activity in developing spinal networks. *J Neurobiol*. 1998;37(1):131-45. Epub 1998/10/20. doi: 10.1002/(sici)1097-4695(199810)37:1<131::aid-neu10>3.0.co;2-h. PubMed PMID: 9777737.
30. O'Donovan MJ, Landmesser L. The development of hindlimb motor activity studied in the isolated spinal cord of the chick embryo. *J Neurosci*. 1987;7(10):3256-64. doi: 10.1523/jneurosci.07-10-03256.1987. PubMed PMID: 3668626; PMCID: PMC6569173.
31. Ben-Ari Y. Excitatory actions of gaba during development: the nature of the nurture. *Nat Rev Neurosci*. 2002;3(9):728-39. Epub 2002/09/05. doi: 10.1038/nrn920. PubMed PMID: 12209121.
32. Blanco W, Bertram R, Tabak J. The Effects of GABAergic Polarity Changes on Episodic Neural Network Activity in Developing Neural Systems. *Front Comput Neurosci*. 2017;11:88. Epub 2017/11/01. doi: 10.3389/fncom.2017.00088. PubMed PMID: 29085291; PMCID: PMC5649201.
33. Chub N, O'Donovan MJ. Post-episode depression of GABAergic transmission in spinal neurons of the chick embryo. *J Neurophysiol*. 2001;85(5):2166-76. Epub 2001/05/16. doi: 10.1152/jn.2001.85.5.2166. PubMed PMID: 11353031.
34. Chub N, O'Donovan MJ. Blockade and recovery of spontaneous rhythmic activity after application of neurotransmitter antagonists to spinal networks of the chick embryo. *J Neurosci*. 1998;18(1):294-306. Epub 1998/01/24. doi: 10.1523/jneurosci.18-01-00294.1998. PubMed PMID: 9412508; PMCID: PMC6793395.
35. Wilhelm JC, Wenner P. GABAA transmission is a critical step in the process of triggering homeostatic increases in quantal amplitude. *Proc Natl Acad Sci U S A*. 2008;105(32):11412-7. Epub 2008/08/06. doi: 10.1073/pnas.0806037105. PubMed PMID: 18678897; PMCID: PMC2516260.
36. Gonzalez-Islas C, Wenner P. Spontaneous network activity in the embryonic spinal cord regulates AMPAergic and GABAergic synaptic strength. *Neuron*. 2006;49(4):563-75. Epub 2006/02/16. doi: 10.1016/j.neuron.2006.01.017. PubMed PMID: 16476665.
37. Wilhelm JC, Rich MM, Wenner P. Compensatory changes in cellular excitability, not synaptic scaling, contribute to homeostatic recovery of embryonic network activity. *Proc Natl Acad Sci U S*

A. 2009;106(16):6760-5. Epub 2009/04/03. doi: 10.1073/pnas.0813058106. PubMed PMID: 19346492.

38. Gonzalez-Islas C, Garcia-Bereguian MA, Wenner P. Homeostatic Recovery of Embryonic Spinal Activity Initiated by Compensatory Changes in Resting Membrane Potential. *eNeuro*. 2020;7(4). Epub 2020/06/17. doi: 10.1523/eneuro.0526-19.2020. PubMed PMID: 32540879; PMCID: PMC7340840.

39. Garcia-Bereguian MA, Gonzalez-Islas C, Lindsly C, Butler E, Hill AW, Wenner P. In vivo synaptic scaling is mediated by GluA2-lacking AMPA receptors in the embryonic spinal cord. *J Neurosci*. 2013;33(16):6791-9. Epub 2013/04/19. doi: 10.1523/jneurosci.4025-12.2013. PubMed PMID: 23595738; PMCID: PMC3661002.

40. Gonzalez-Islas C, Chub N, Garcia-Bereguian MA, Wenner P. GABAergic synaptic scaling in embryonic motoneurons is mediated by a shift in the chloride reversal potential. *J Neurosci*. 2010;30(39):13016-20. Epub 2010/10/01. doi: 10.1523/jneurosci.1659-10.2010. PubMed PMID: 20881119; PMCID: PMC2950003.

41. Lindsly C, Gonzalez-Islas C, Wenner P. Activity blockade and GABAA receptor blockade produce synaptic scaling through chloride accumulation in embryonic spinal motoneurons and interneurons. *PLoS One*. 2014;9(4):e94559. Epub 2014/04/16. doi: 10.1371/journal.pone.0094559. PubMed PMID: 24733046; PMCID: PMC3986094 not alter the authors' adherence to all the PLOS ONE policies on sharing data and materials.

42. Hengen KB, Lambo ME, Van Hooser SD, Katz DB, Turrigiano GG. Firing rate homeostasis in visual cortex of freely behaving rodents. *Neuron*. 2013;80(2):335-42. doi: 10.1016/j.neuron.2013.08.038. PubMed PMID: 24139038.

43. Hengen KB, Torrado Pacheco A, McGregor JN, Van Hooser SD, Turrigiano GG. Neuronal Firing Rate Homeostasis Is Inhibited by Sleep and Promoted by Wake. *Cell*. 2016;165(1):180-91. Epub 2016/03/17. doi: 10.1016/j.cell.2016.01.046. PubMed PMID: 26997481.

44. Kuhlman SJ, Olivas ND, Tring E, Ikrar T, Xu X, Trachtenberg JT. A disinhibitory microcircuit initiates critical-period plasticity in the visual cortex. *Nature*. 2013;501(7468):543-6. Epub 2013/08/27. doi: 10.1038/nature12485. PubMed PMID: 23975100; PMCID: PMC3962838.

45. Slomowitz E, Styr B, Vertkin I, Milshtein-Parush H, Nelken I, Slutsky M, Slutsky I. Interplay between population firing stability and single neuron dynamics in hippocampal networks. *Elife*. 2015;4. Epub 2015/01/06. doi: 10.7554/eLife.04378. PubMed PMID: 25556699; PMCID: PMC4311497.

46. Ma Z, Turrigiano GG, Wessel R, Hengen KB. Cortical Circuit Dynamics Are Homeostatically Tuned to Criticality In Vivo. *Neuron*. 2019;104(4):655-64 e4. Epub 2019/10/12. doi: 10.1016/j.neuron.2019.08.031. PubMed PMID: 31601510; PMCID: PMC6934140.

47. Rich MM, Wenner P. Sensing and expressing homeostatic synaptic plasticity. *Trends Neurosci*. 2007;30(3):119-25. Epub 2007/01/30. doi: 10.1016/j.tins.2007.01.004. PubMed PMID: 17267052.

48. Turrigiano GG. The self-tuning neuron: synaptic scaling of excitatory synapses. *Cell*. 2008;135(3):422-35. Epub 2008/11/06. doi: 10.1016/j.cell.2008.10.008. PubMed PMID: 18984155; PMCID: PMC2834419.
49. Thiagarajan TC, Piedras-Renteria ES, Tsien RW. alpha- and betaCaMKII. Inverse regulation by neuronal activity and opposing effects on synaptic strength. *Neuron*. 2002;36(6):1103-14. Epub 2002/12/24. doi: 10.1016/s0896-6273(02)01049-8. PubMed PMID: 12495625.
50. Joseph A, Turrigiano GG. All for One But Not One for All: Excitatory Synaptic Scaling and Intrinsic Excitability Are Coregulated by CaMKIV, Whereas Inhibitory Synaptic Scaling Is Under Independent Control. *The Journal of neuroscience : the official journal of the Society for Neuroscience*. 2017;37(28):6778-85. Epub 2017/06/07. doi: 10.1523/JNEUROSCI.0618-17.2017. PubMed PMID: 28592691.
51. Ibata K, Sun Q, Turrigiano GG. Rapid synaptic scaling induced by changes in postsynaptic firing. *Neuron*. 2008;57(6):819-26. Epub 2008/03/28. doi: 10.1016/j.neuron.2008.02.031. PubMed PMID: 18367083.
52. Rutherford LC, Nelson SB, Turrigiano GG. BDNF has opposite effects on the quantal amplitude of pyramidal neuron and interneuron excitatory synapses. *Neuron*. 1998;21(3):521-30. Epub 1998/10/13. doi: 10.1016/s0896-6273(00)80563-2. PubMed PMID: 9768839.
53. Luther JA, Robie AA, Yarotsky J, Reina C, Marder E, Golowasch J. Episodic bouts of activity accompany recovery of rhythmic output by a neuromodulator- and activity-deprived adult neural network. *J Neurophysiol*. 2003;90(4):2720-30. Epub 2003/07/04. doi: 10.1152/jn.00370.2003. PubMed PMID: 12840081; PMCID: PMC3557508.
54. MacLean JN, Zhang Y, Goeritz ML, Casey R, Oliva R, Guckenheimer J, Harris-Warrick RM. Activity-independent coregulation of IA and Ih in rhythmically active neurons. *J Neurophysiol*. 2005;94(5):3601-17. Epub 2005/07/29. doi: 10.1152/jn.00281.2005. PubMed PMID: 16049145.
55. Ransdell JL, Nair SS, Schulz DJ. Rapid homeostatic plasticity of intrinsic excitability in a central pattern generator network stabilizes functional neural network output. *J Neurosci*. 2012;32(28):9649-58. Epub 2012/07/13. doi: 10.1523/jneurosci.1945-12.2012. PubMed PMID: 22787050; PMCID: PMC6622259.
56. Sohal VS, Rubenstein JLR. Excitation-inhibition balance as a framework for investigating mechanisms in neuropsychiatric disorders. *Mol Psychiatry*. 2019;24(9):1248-57. Epub 2019/05/16. doi: 10.1038/s41380-019-0426-0. PubMed PMID: 31089192; PMCID: PMC6742424.
57. Nelson SB, Valakh V. Excitatory/Inhibitory Balance and Circuit Homeostasis in Autism Spectrum Disorders. *Neuron*. 2015;87(4):684-98. doi: 10.1016/j.neuron.2015.07.033. PubMed PMID: 26291155.
58. Chen K, Aradi I, Thon N, Eghbal-Ahmadi M, Baram TZ, Soltesz I. Persistently modified h-channels after complex febrile seizures convert the seizure-induced enhancement of inhibition to hyperexcitability. *Nat Med*. 2001;7(3):331-7. Epub 2001/03/07. doi: 10.1038/85480. PubMed PMID: 11231632; PMCID: PMC3382967.

59. Petriti U, Dudman DC, Scosyrev E, Lopez-Leon S. Global prevalence of Rett syndrome: systematic review and meta-analysis. *Syst Rev*. 2023;12(1):5. Epub 2023/01/16. doi: 10.1186/s13643-023-02169-6. PubMed PMID: 36642718; PMCID: PMC9841621.
60. Qiu Z, Sylwestrak EL, Lieberman DN, Zhang Y, Liu XY, Ghosh A. The Rett syndrome protein MeCP2 regulates synaptic scaling. *J Neurosci*. 2012;32(3):989-94. Epub 2012/01/21. doi: 10.1523/jneurosci.0175-11.2012. PubMed PMID: 22262897; PMCID: PMC3711796.
61. Klein ME, Liroy DT, Ma L, Impey S, Mandel G, Goodman RH. Homeostatic regulation of MeCP2 expression by a CREB-induced microRNA. *Nat Neurosci*. 2007;10(12):1513-4. Epub 2007/11/13. doi: 10.1038/nn2010. PubMed PMID: 17994015.
62. Soden ME, Chen L. Fragile X protein FMRP is required for homeostatic plasticity and regulation of synaptic strength by retinoic acid. *J Neurosci*. 2010;30(50):16910-21. Epub 2010/12/17. doi: 10.1523/jneurosci.3660-10.2010. PubMed PMID: 21159962; PMCID: PMC3073636.
63. Bulow P, Murphy TJ, Bassell GJ, Wenner P. Homeostatic Intrinsic Plasticity Is Functionally Altered in Fmr1 KO Cortical Neurons. *Cell Rep*. 2019;26(6):1378-88.e3. Epub 2019/02/07. doi: 10.1016/j.celrep.2019.01.035. PubMed PMID: 30726724; PMCID: PMC6443253.
64. Booker SA, Simões de Oliveira L, Anstey NJ, Kozic Z, Dando OR, Jackson AD, Baxter PS, Isom LL, Sherman DL, Hardingham GE, Brophy PJ, Wyllie DJA, Kind PC. Input-Output Relationship of CA1 Pyramidal Neurons Reveals Intact Homeostatic Mechanisms in a Mouse Model of Fragile X Syndrome. *Cell Reports*. 2020;32(6):107988. doi: <https://doi.org/10.1016/j.celrep.2020.107988>.
65. Domanski APF, Booker SA, Wyllie DJA, Isaac JTR, Kind PC. Cellular and synaptic phenotypes lead to disrupted information processing in Fmr1-KO mouse layer 4 barrel cortex. *Nat Commun*. 2019;10(1):4814. Epub 2019/10/28. doi: 10.1038/s41467-019-12736-y. PubMed PMID: 31645553; PMCID: PMC6811545.
66. Tataavarty V, Torrado Pacheco A, Groves Kuhnle C, Lin H, Koundinya P, Miska NJ, Hengen KB, Wagner FF, Van Hooser SD, Turrigiano GG. Autism-Associated Shank3 Is Essential for Homeostatic Compensation in Rodent V1. *Neuron*. 2020;106(5):769-77.e4. Epub 2020/03/22. doi: 10.1016/j.neuron.2020.02.033. PubMed PMID: 32199104; PMCID: PMC7331792.
67. Kavalali ET, Monteggia LM. Targeting Homeostatic Synaptic Plasticity for Treatment of Mood Disorders. *Neuron*. 2020;106(5):715-26. Epub 2020/06/05. doi: 10.1016/j.neuron.2020.05.015. PubMed PMID: 32497508; PMCID: PMC7517590.
68. Martin JP, Bell J. A PEDIGREE OF MENTAL DEFECT SHOWING SEX-LINKAGE. *J Neurol Psychiatry*. 1943;6(3-4):154-7. Epub 1943/07/01. doi: 10.1136/jnnp.6.3-4.154. PubMed PMID: 21611430; PMCID: PMC1090429.
69. Verkerk AJ, Pieretti M, Sutcliffe JS, Fu YH, Kuhl DP, Pizzuti A, Reiner O, Richards S, Victoria MF, Zhang FP, et al. Identification of a gene (FMR-1) containing a CGG repeat coincident with a breakpoint cluster region exhibiting length variation in fragile X syndrome. *Cell*. 1991;65(5):905-14. Epub 1991/05/31. doi: 10.1016/0092-8674(91)90397-h. PubMed PMID: 1710175.

70. Wang LW, Berry-Kravis E, Hagerman RJ. Fragile X: leading the way for targeted treatments in autism. *Neurotherapeutics*. 2010;7(3):264-74. Epub 2010/07/21. doi: 10.1016/j.nurt.2010.05.005. PubMed PMID: 20643379; PMCID: PMC4084556.
71. Tassone F, Protic D, Allen EG, Archibald AD, Baud A, Brown TW, Budimirovic DB, Cohen J, Dufour B, Eiges R, Elvassore N, Gabis LV, Grudzien SJ, Hall DA, Hessel D, Hogan A, Hunter JE, Jin P, Jiraanont P, Klusek J, Kooy RF, Kraan CM, Laterza C, Lee A, Lipworth K, Losh M, Loesch D, Lozano R, Mailick MR, Manolopoulos A, Martinez-Cerdeno V, McLennan Y, Miller RM, Montanaro FAM, Mosconi MW, Potter SN, Raspa M, Rivera SM, Shelly K, Todd PK, Tutak K, Wang JY, Wheeler A, Winarni TI, Zafarullah M, Hagerman RJ. Insight and Recommendations for Fragile X-Pre-mutation-Associated Conditions from the Fifth International Conference on FMR1 Pre-mutation. *Cells*. 2023;12(18). Epub 2023/09/28. doi: 10.3390/cells12182330. PubMed PMID: 37759552; PMCID: PMC10529056.
72. Cao Y, Peng Y, Kong HE, Allen EG, Jin P. Metabolic Alterations in FMR1 Pre-mutation Carriers. *Front Mol Biosci*. 2020;7:571092. Epub 2020/11/17. doi: 10.3389/fmolb.2020.571092. PubMed PMID: 33195417; PMCID: PMC7531624.
73. Bassell GJ, Warren ST. Fragile X syndrome: loss of local mRNA regulation alters synaptic development and function. *Neuron*. 2008;60(2):201-14. Epub 2008/10/30. doi: 10.1016/j.neuron.2008.10.004. PubMed PMID: 18957214; PMCID: PMC3691995.
74. Coffee B, Keith K, Albizua I, Malone T, Mowrey J, Sherman SL, Warren ST. Incidence of fragile X syndrome by newborn screening for methylated FMR1 DNA. *Am J Hum Genet*. 2009;85(4):503-14. Epub 2009/10/07. doi: 10.1016/j.ajhg.2009.09.007. PubMed PMID: 19804849; PMCID: PMC2756550.
75. Hunter J, Rivero-Arias O, Angelov A, Kim E, Fotheringham I, Leal J. Epidemiology of fragile X syndrome: A systematic review and meta-analysis. *American Journal of Medical Genetics Part A*. 2014;164(7):1648-58. doi: <https://doi.org/10.1002/ajmg.a.36511>.
76. Irwin SA, Patel B, Idupulapati M, Harris JB, Crisostomo RA, Larsen BP, Kooy F, Willems PJ, Cras P, Kozlowski PB, Swain RA, Weiler IJ, Greenough WT. Abnormal dendritic spine characteristics in the temporal and visual cortices of patients with fragile-X syndrome: a quantitative examination. *Am J Med Genet*. 2001;98(2):161-7. Epub 2001/02/27. doi: 10.1002/1096-8628(20010115)98:2<161::aid-ajmg1025>3.0.co;2-b. PubMed PMID: 11223852.
77. Swanson MR, Wolff JJ, Shen MD, Styner M, Estes A, Gerig G, McKinstry RC, Botteron KN, Piven J, Hazlett HC, Network ftIBIS. Development of White Matter Circuitry in Infants With Fragile X Syndrome. *JAMA Psychiatry*. 2018;75(5):505-13. doi: 10.1001/jamapsychiatry.2018.0180.
78. Razak KA, Dominick KC, Erickson CA. Developmental studies in fragile X syndrome. *J Neurodev Disord*. 2020;12(1):13. Epub 2020/05/04. doi: 10.1186/s11689-020-09310-9. PubMed PMID: 32359368; PMCID: PMC7196229 National Institute of Neurological Disorders and Stroke (NINDS), American Academy of Child and Adolescent Psychiatry, and Cincinnati Children's Hospital Medical Center. She is a clinical trial site investigator for F. Hoffman-La Roche Ltd. and Ovid Therapeutics. CAE has received current or past funding from Confluence Pharmaceuticals, Novartis, F. Hoffmann-La Roche Ltd., Seaside Therapeutics, Riovant Sciences, Inc., Fulcrum

Therapeutics, Neuren Pharmaceuticals Ltd., Alcobra Pharmaceuticals, Neurotrope, Zynerba Pharmaceuticals, Inc., Lenire Bioscience, and Ovid Therapeutics Inc. to consult on trial design or development strategies and/or conduct clinical trials in FXS or other neurodevelopmental disorders. CAE is additionally the inventor or co-inventor on several patents held by the Cincinnati Children's Hospital Medical Center or Indiana University School of Medicine describing methods of treatment in FXS or other neurodevelopmental disorders.

79. Lachiewicz AM, Dawson DV, Spiridigliozzi GA. Physical characteristics of young boys with fragile X syndrome: reasons for difficulties in making a diagnosis in young males. *Am J Med Genet.* 2000;92(4):229-36. Epub 2000/06/08. doi: 10.1002/(sici)1096-8628(20000605)92:4<229::aid-ajmg1>3.0.co;2-k. PubMed PMID: 10842286.

80. Elhawary NA, AlJahdali IA, Abumansour IS, Azher ZA, Falemban AH, Madani WM, Alosaimi W, Alghamdi G, Sindi IA. Phenotypic variability to medication management: an update on fragile X syndrome. *Human Genomics.* 2023;17(1):60. doi: 10.1186/s40246-023-00507-2.

81. Salcedo-Arellano MJ, Hagerman RJ, Martínez-Cerdeño V. Fragile X syndrome: clinical presentation, pathology and treatment. *Gac Med Mex.* 2020;156(1):60-6. Epub 2020/02/07. doi: 10.24875/gmm.19005275. PubMed PMID: 32026885.

82. Sobesky WE, Taylor AK, Pennington BF, Bennetto L, Porter D, Riddle J, Hagerman RJ. Molecular/clinical correlations in females with fragile X. *Am J Med Genet.* 1996;64(2):340-5. Epub 1996/08/09. doi: 10.1002/(sici)1096-8628(19960809)64:2<340::Aid-ajmg21>3.0.Co;2-e. PubMed PMID: 8844077.

83. Ciaccio C, Fontana L, Milani D, Tabano S, Miozzo M, Esposito S. Fragile X syndrome: a review of clinical and molecular diagnoses. *Ital J Pediatr.* 2017;43(1):39. Epub 2017/04/20. doi: 10.1186/s13052-017-0355-y. PubMed PMID: 28420439; PMCID: PMC5395755.

84. Rajaratnam A, Shergill J, Salcedo-Arellano M, Saldarriaga W, Duan X, Hagerman R. Fragile X syndrome and fragile X-associated disorders. *F1000Res.* 2017;6:2112. Epub 2017/12/21. doi: 10.12688/f1000research.11885.1. PubMed PMID: 29259781; PMCID: PMC5728189.

85. Kim K, Hessel D, Randol JL, Espinal GM, Schneider A, Protic D, Aydin EY, Hagerman RJ, Hagerman PJ. Association between IQ and FMR1 protein (FMRP) across the spectrum of CGG repeat expansions. *PLoS One.* 2019;14(12):e0226811. Epub 2020/01/01. doi: 10.1371/journal.pone.0226811. PubMed PMID: 31891607; PMCID: PMC6938341 PJH has received support for studies from BioMarin and is on the scientific advisory board of NeuCyte. DH has received funding for outcome measure research from Ovid and Zynerba. This does not alter our adherence to PLOS ONE policies on sharing data and materials.

86. Schmitt LM, Will M, Shaffer R, Erickson C. A Paradigm Shifting View of Intellectual Disability: A Near Normal Distribution of IQ in Fragile X Syndrome. *Res Sq.* 2023. Epub 2023/05/19. doi: 10.21203/rs.3.rs-2869313/v1. PubMed PMID: 37205401; PMCID: PMC10187411 to the content of this manuscript. L.M.S. is a current consultant to Confluence and Forge. R.C.S. is a current consultant to Forge. C.A.E is a current consultant to Confluence, Stalica, Impel, Forge, and Scioto Bioscience. C.A.E is the inventor on patents related to the treatment of autism and/or Fragile X Syndrome.

87. Gantois I, Popic J, Khoutorsky A, Sonenberg N. Metformin for Treatment of Fragile X Syndrome and Other Neurological Disorders. *Annu Rev Med.* 2019;70:167-81. Epub 2018/10/27. doi: 10.1146/annurev-med-081117-041238. PubMed PMID: 30365357.
88. Dy ABC, Tassone F, Eldeeb M, Salcedo-Arellano MJ, Tartaglia N, Hagerman R. Metformin as targeted treatment in fragile X syndrome. *Clin Genet.* 2018;93(2):216-22. Epub 2017/04/25. doi: 10.1111/cge.13039. PubMed PMID: 28436599; PMCID: PMC6944702.
89. Biag HMB, Potter LA, Wilkins V, Afzal S, Rosvall A, Salcedo-Arellano MJ, Rajaratnam A, Manzano-Nunez R, Schneider A, Tassone F, Rivera SM, Hagerman RJ. Metformin treatment in young children with fragile X syndrome. *Mol Genet Genomic Med.* 2019;7(11):e956. Epub 2019/09/15. doi: 10.1002/mgg3.956. PubMed PMID: 31520524; PMCID: PMC6825840.
90. Osterweil EK, Chuang SC, Chubykin AA, Sidorov M, Bianchi R, Wong RK, Bear MF. Lovastatin corrects excess protein synthesis and prevents epileptogenesis in a mouse model of fragile X syndrome. *Neuron.* 2013;77(2):243-50. Epub 2013/01/29. doi: 10.1016/j.neuron.2012.01.034. PubMed PMID: 23352161; PMCID: PMC3597444.
91. Çaku A, Pellerin D, Bouvier P, Riou E, Corbin F. Effect of lovastatin on behavior in children and adults with fragile X syndrome: an open-label study. *Am J Med Genet A.* 2014;164a(11):2834-42. Epub 2014/09/27. doi: 10.1002/ajmg.a.36750. PubMed PMID: 25258112.
92. Thurman AJ, Potter LA, Kim K, Tassone F, Banasik A, Potter SN, Bullard L, Nguyen V, McDuffie A, Hagerman R, Abbeduto L. Controlled trial of lovastatin combined with an open-label treatment of a parent-implemented language intervention in youth with fragile X syndrome. *J Neurodev Disord.* 2020;12(1):12. Epub 2020/04/23. doi: 10.1186/s11689-020-09315-4. PubMed PMID: 32316911; PMCID: PMC7175541.
93. Aishworiya R, Valica T, Hagerman R, Restrepo B. An Update on Psychopharmacological Treatment of Autism Spectrum Disorder. *Neurotherapeutics.* 2022;19(1):248-62. Epub 2022/01/15. doi: 10.1007/s13311-022-01183-1. PubMed PMID: 35029811; PMCID: PMC9130393.
94. Gannon CE, Britton TC, Wilkinson EH, Hall SS. Improving social gaze behavior in fragile X syndrome using a behavioral skills training approach: a proof of concept study. *J Neurodev Disord.* 2018;10(1):25. Epub 2018/08/30. doi: 10.1186/s11689-018-9243-z. PubMed PMID: 30153790; PMCID: PMC6114729.
95. Hall SS, Hammond JL, Hirt M, Reiss AL. A 'learning platform' approach to outcome measurement in fragile X syndrome: a preliminary psychometric study. *J Intellect Disabil Res.* 2012;56(10):947-60. Epub 2012/04/27. doi: 10.1111/j.1365-2788.2012.01560.x. PubMed PMID: 22533667; PMCID: PMC3417081.
96. Hall SS, Hustyi KM, Hammond JL, Hirt M, Reiss AL. Using discrete trial training to identify specific learning impairments in boys with fragile X syndrome. *J Autism Dev Disord.* 2014;44(7):1659-70. Epub 2014/01/24. doi: 10.1007/s10803-014-2037-6. PubMed PMID: 24452992; PMCID: PMC5786464.
97. Liu XS, Wu H, Krzisch M, Wu X, Graef J, Muffat J, Hnisz D, Li CH, Yuan B, Xu C, Li Y, Vershkov D, Cacace A, Young RA, Jaenisch R. Rescue of Fragile X Syndrome Neurons by DNA

- Methylation Editing of the FMR1 Gene. *Cell*. 2018;172(5):979-92.e6. Epub 2018/02/20. doi: 10.1016/j.cell.2018.01.012. PubMed PMID: 29456084; PMCID: PMC6375087.
98. Yrigollen CM, Davidson BL. CRISPR to the Rescue: Advances in Gene Editing for the FMR1 Gene. *Brain Sci*. 2019;9(1). Epub 2019/01/24. doi: 10.3390/brainsci9010017. PubMed PMID: 30669625; PMCID: PMC6357057.
99. Richter JD, Zhao X. The molecular biology of FMRP: new insights into fragile X syndrome. *Nature Reviews Neuroscience*. 2021;22(4):209-22. doi: 10.1038/s41583-021-00432-0.
100. Myrick LK, Hashimoto H, Cheng X, Warren ST. Human FMRP contains an integral tandem Agenet (Tudor) and KH motif in the amino terminal domain. *Hum Mol Genet*. 2015;24(6):1733-40. Epub 2014/11/25. doi: 10.1093/hmg/ddu586. PubMed PMID: 25416280; PMCID: PMC4381759.
101. Eberhart DE, Malter HE, Feng Y, Warren ST. The fragile X mental retardation protein is a ribonucleoprotein containing both nuclear localization and nuclear export signals. *Hum Mol Genet*. 1996;5(8):1083-91. Epub 1996/08/01. doi: 10.1093/hmg/5.8.1083. PubMed PMID: 8842725.
102. Darnell JC, Fraser CE, Mostovetsky O, Stefani G, Jones TA, Eddy SR, Darnell RB. Kissing complex RNAs mediate interaction between the Fragile-X mental retardation protein KH2 domain and brain polyribosomes. *Genes Dev*. 2005;19(8):903-18. Epub 2005/04/01. doi: 10.1101/gad.1276805. PubMed PMID: 15805463.
103. Darnell JC, Van Driesche SJ, Zhang C, Hung KY, Mele A, Fraser CE, Stone EF, Chen C, Fak JJ, Chi SW, Licatalosi DD, Richter JD, Darnell RB. FMRP stalls ribosomal translocation on mRNAs linked to synaptic function and autism. *Cell*. 2011;146(2):247-61. Epub 2011/07/26. doi: 10.1016/j.cell.2011.06.013. PubMed PMID: 21784246; PMCID: PMC3232425.
104. Casingal CR, Kikkawa T, Inada H, Sasaki Y, Osumi N. Identification of FMRP target mRNAs in the developmental brain: FMRP might coordinate Ras/MAPK, Wnt/ β -catenin, and mTOR signaling during corticogenesis. *Mol Brain*. 2020;13(1):167. Epub 2020/12/17. doi: 10.1186/s13041-020-00706-1. PubMed PMID: 33323119; PMCID: PMC7739466.
105. Taha MS, Haghighi F, Stefanski A, Nakhaei-Rad S, Kazemineh Jasemi NS, Al Kabbani MA, Görg B, Fujii M, Lang PA, Häussinger D, Piekorz RP, Stühler K, Ahmadian MR. Novel FMRP interaction networks linked to cellular stress. *Febs j*. 2021;288(3):837-60. Epub 2020/06/12. doi: 10.1111/febs.15443. PubMed PMID: 32525608.
106. Huber KM, Gallagher SM, Warren ST, Bear MF. Altered synaptic plasticity in a mouse model of fragile X mental retardation. *Proc Natl Acad Sci U S A*. 2002;99(11):7746-50. Epub 2002/05/29. doi: 10.1073/pnas.122205699. PubMed PMID: 12032354; PMCID: PMC124340.
107. Ceman S, O'Donnell WT, Reed M, Patton S, Pohl J, Warren ST. Phosphorylation influences the translation state of FMRP-associated polyribosomes. *Hum Mol Genet*. 2003;12(24):3295-305. Epub 2003/10/23. doi: 10.1093/hmg/ddg350. PubMed PMID: 14570712.
108. Prieto M, Folci A, Martin S. Post-translational modifications of the Fragile X Mental Retardation Protein in neuronal function and dysfunction. *Mol Psychiatry*. 2020;25(8):1688-703. Epub 2019/12/12. doi: 10.1038/s41380-019-0629-4. PubMed PMID: 31822816.

109. Deng PY, Carlin D, Oh YM, Myrick LK, Warren ST, Cavalli V, Klyachko VA. Voltage-Independent SK-Channel Dysfunction Causes Neuronal Hyperexcitability in the Hippocampus of Fmr1 Knock-Out Mice. *J Neurosci*. 2019;39(1):28-43. Epub 2018/11/06. doi: 10.1523/jneurosci.1593-18.2018. PubMed PMID: 30389838; PMCID: PMC6325266.
110. Brandalise F, Kalmbach BE, Mehta P, Thornton O, Johnston D, Zemelman BV, Brager DH. Fragile X Mental Retardation Protein Bidirectionally Controls Dendritic I(h) in a Cell Type-Specific Manner between Mouse Hippocampus and Prefrontal Cortex. *J Neurosci*. 2020;40(27):5327-40. Epub 2020/05/30. doi: 10.1523/jneurosci.1670-19.2020. PubMed PMID: 32467357; PMCID: PMC7329306.
111. Waterston RH, Lindblad-Toh K, Birney E, Rogers J, Abril JF, Agarwal P, Agarwala R, Ainscough R, Alexandersson M, An P, Antonarakis SE, Attwood J, Baertsch R, Bailey J, Barlow K, Beck S, Berry E, Birren B, Bloom T, Bork P, Botcherby M, Bray N, Brent MR, Brown DG, Brown SD, Bult C, Burton J, Butler J, Campbell RD, Carninci P, Cawley S, Chiaromonte F, Chinwalla AT, Church DM, Clamp M, Clee C, Collins FS, Cook LL, Copley RR, Coulson A, Couronne O, Cuff J, Curwen V, Cutts T, Daly M, David R, Davies J, Delehaunty KD, Deri J, Dermitzakis ET, Dewey C, Dickens NJ, Diekhans M, Dodge S, Dubchak I, Dunn DM, Eddy SR, Elnitski L, Emes RD, Esvara P, Eyraas E, Felsenfeld A, Fewell GA, Flicek P, Foley K, Frankel WN, Fulton LA, Fulton RS, Furey TS, Gage D, Gibbs RA, Glusman G, Gnerre S, Goldman N, Goodstadt L, Grafham D, Graves TA, Green ED, Gregory S, Guigó R, Guyer M, Hardison RC, Haussler D, Hayashizaki Y, Hillier LW, Hinrichs A, Hlavina W, Holzer T, Hsu F, Hua A, Hubbard T, Hunt A, Jackson I, Jaffe DB, Johnson LS, Jones M, Jones TA, Joy A, Kamal M, Karlsson EK, Karolchik D, Kasprzyk A, Kawai J, Keibler E, Kells C, Kent WJ, Kirby A, Kolbe DL, Korf I, Kucherlapati RS, Kulbokas EJ, Kulp D, Landers T, Leger JP, Leonard S, Letunic I, Levine R, Li J, Li M, Lloyd C, Lucas S, Ma B, Maglott DR, Mardis ER, Matthews L, Mauceli E, Mayer JH, McCarthy M, McCombie WR, McLaren S, McLay K, McPherson JD, Meldrim J, Meredith B, Mesirov JP, Miller W, Miner TL, Mongin E, Montgomery KT, Morgan M, Mott R, Mullikin JC, Muzny DM, Nash WE, Nelson JO, Nhan MN, Nicol R, Ning Z, Nusbaum C, O'Connor MJ, Okazaki Y, Oliver K, Overton-Larty E, Pachter L, Parra G, Pepin KH, Peterson J, Pevzner P, Plumb R, Pohl CS, Poliakov A, Ponce TC, Ponting CP, Potter S, Quail M, Reymond A, Roe BA, Roskin KM, Rubin EM, Rust AG, Santos R, Sapojnikov V, Schultz B, Schultz J, Schwartz MS, Schwartz S, Scott C, Seaman S, Searle S, Sharpe T, Sheridan A, Shownkeen R, Sims S, Singer JB, Slater G, Smit A, Smith DR, Spencer B, Stabenau A, Stange-Thomann N, Sugnet C, Suyama M, Tesler G, Thompson J, Torrents D, Trevaskis E, Tromp J, Ucla C, Ureta-Vidal A, Vinson JP, Von Niederhausern AC, Wade CM, Wall M, Weber RJ, Weiss RB, Wendl MC, West AP, Wetterstrand K, Wheeler R, Whelan S, Wierzbowski J, Willey D, Williams S, Wilson RK, Winter E, Worley KC, Wyman D, Yang S, Yang SP, Zdobnov EM, Zody MC, Lander ES. Initial sequencing and comparative analysis of the mouse genome. *Nature*. 2002;420(6915):520-62. Epub 2002/12/06. doi: 10.1038/nature01262. PubMed PMID: 12466850.
112. Nobile V, Pucci C, Chiurazzi P, Neri G, Tabolacci E. DNA Methylation, Mechanisms of FMR1 Inactivation and Therapeutic Perspectives for Fragile X Syndrome. *Biomolecules*. 2021;11(2). Epub 2021/03/07. doi: 10.3390/biom11020296. PubMed PMID: 33669384; PMCID: PMC7920310.
113. Dahlhaus R. Of Men and Mice: Modeling the Fragile X Syndrome. *Front Mol Neurosci*. 2018;11. doi: 10.3389/fnmol.2018.00041.

114. Willemsen R, Kooy RF. Mouse models of fragile X-related disorders. *Dis Model Mech.* 2023;16(2). Epub 2023/01/25. doi: 10.1242/dmm.049485. PubMed PMID: 36692473; PMCID: PMC9903145.
115. Drozd M, Bardoni B, Capovilla M. Modeling Fragile X Syndrome in *Drosophila*. *Front Mol Neurosci.* 2018;11:124. Epub 2018/05/02. doi: 10.3389/fnmol.2018.00124. PubMed PMID: 29713264; PMCID: PMC5911982.
116. den Broeder MJ, van der Linde H, Brouwer JR, Oostra BA, Willemsen R, Ketting RF. Generation and characterization of FMR1 knockout zebrafish. *PLoS One.* 2009;4(11):e7910. Epub 2009/11/26. doi: 10.1371/journal.pone.0007910. PubMed PMID: 19936290; PMCID: PMC2774943.
117. Curnow E, Wang Y. New Animal Models for Understanding FMRP Functions and FXS Pathology. *Cells.* 2022;11(10). Epub 2022/05/29. doi: 10.3390/cells11101628. PubMed PMID: 35626665; PMCID: PMC9140010.
118. Sakano H, Zorio DAR, Wang X, Ting YS, Noble WS, MacCoss MJ, Rubel EW, Wang Y. Proteomic analyses of nucleus laminaris identified candidate targets of the fragile X mental retardation protein. *J Comp Neurol.* 2017;525(15):3341-59. Epub 2017/07/08. doi: 10.1002/cne.24281. PubMed PMID: 28685837; PMCID: PMC5564178.
119. Wang X, Kohl A, Yu X, Zorio DAR, Klar A, Sela-Donenfeld D, Wang Y. Temporal-specific roles of fragile X mental retardation protein in the development of the hindbrain auditory circuit. *Development.* 2020;147(21). Epub 2020/08/05. doi: 10.1242/dev.188797. PubMed PMID: 32747436; PMCID: PMC7473654.
120. Bear MF, Huber KM, Warren ST. The mGluR theory of fragile X mental retardation. *Trends Neurosci.* 2004;27(7):370-7. Epub 2004/06/29. doi: 10.1016/j.tins.2004.04.009. PubMed PMID: 15219735.
121. Chen L, Toth M. Fragile X mice develop sensory hyperreactivity to auditory stimuli. *Neuroscience.* 2001;103(4):1043-50. Epub 2001/04/13. doi: 10.1016/s0306-4522(01)00036-7. PubMed PMID: 11301211.
122. Chapman AG, Nanan K, Williams M, Meldrum BS. Anticonvulsant activity of two metabotropic glutamate group I antagonists selective for the mGlu5 receptor: 2-methyl-6-(phenylethynyl)-pyridine (MPEP), and (E)-6-methyl-2-styryl-pyridine (SIB 1893). *Neuropharmacology.* 2000;39(9):1567-74. Epub 2000/06/16. doi: 10.1016/s0028-3908(99)00242-7. PubMed PMID: 10854901.
123. Graybiel AM. The basal ganglia and chunking of action repertoires. *Neurobiol Learn Mem.* 1998;70(1-2):119-36. Epub 1998/10/01. doi: 10.1006/nlme.1998.3843. PubMed PMID: 9753592.
124. Ade KK, Wan Y, Hamann HC, O'Hare JK, Guo W, Quian A, Kumar S, Bhagat S, Rodriguiz RM, Wetsel WC, Conn PJ, Dzirasa K, Huber KM, Calakos N. Increased Metabotropic Glutamate Receptor 5 Signaling Underlies Obsessive-Compulsive Disorder-like Behavioral and Striatal Circuit Abnormalities in Mice. *Biol Psychiatry.* 2016;80(7):522-33. Epub 2016/07/21. doi: 10.1016/j.biopsych.2016.04.023. PubMed PMID: 27436084; PMCID: PMC5536332.

125. Berry-Kravis E, Hessler D, Coffey S, Hervey C, Schneider A, Yuhas J, Hutchison J, Snape M, Tranfaglia M, Nguyen DV, Hagerman R. A pilot open label, single dose trial of fenobam in adults with fragile X syndrome. *J Med Genet.* 2009;46(4):266-71. Epub 2009/01/08. doi: 10.1136/jmg.2008.063701. PubMed PMID: 19126569; PMCID: PMC2658751.
126. Erickson CA, Mullett JE, McDougle CJ. Brief report: acamprosate in fragile X syndrome. *J Autism Dev Disord.* 2010;40(11):1412-6. Epub 2010/03/10. doi: 10.1007/s10803-010-0988-9. PubMed PMID: 20213249.
127. Grabb MC, Potter WZ. Central Nervous System Trial Failures: Using the Fragile X Syndrome-mGluR5 Drug Target to Highlight the Complexities of Translating Preclinical Discoveries Into Human Trials. *J Clin Psychopharmacol.* 2022;42(3):234-7. Epub 2022/05/01. doi: 10.1097/jcp.0000000000001553. PubMed PMID: 35489028; PMCID: PMC9060375.
128. Stoppel DC, McCamphill PK, Senter RK, Heynen AJ, Bear MF. mGluR5 Negative Modulators for Fragile X: Treatment Resistance and Persistence. *Front Psychiatry.* 2021;12:718953. Epub 2021/10/19. doi: 10.3389/fpsy.2021.718953. PubMed PMID: 34658956; PMCID: PMC8511445.
129. Scharf SH, Jaeschke G, Wettstein JG, Lindemann L. Metabotropic glutamate receptor 5 as drug target for Fragile X syndrome. *Curr Opin Pharmacol.* 2015;20:124-34. Epub 2014/12/10. doi: 10.1016/j.coph.2014.11.004. PubMed PMID: 25488569.
130. Swanson CJ, Bures M, Johnson MP, Linden AM, Monn JA, Schoepp DD. Metabotropic glutamate receptors as novel targets for anxiety and stress disorders. *Nat Rev Drug Discov.* 2005;4(2):131-44. Epub 2005/01/25. doi: 10.1038/nrd1630. PubMed PMID: 15665858.
131. Moghaddam B, Adams BW. Reversal of phencyclidine effects by a group II metabotropic glutamate receptor agonist in rats. *Science.* 1998;281(5381):1349-52. Epub 1998/08/28. doi: 10.1126/science.281.5381.1349. PubMed PMID: 9721099.
132. Ngomba RT, Santolini I, Salt TE, Ferraguti F, Battaglia G, Nicoletti F, van Luitelaar G. Metabotropic glutamate receptors in the thalamocortical network: strategic targets for the treatment of absence epilepsy. *Epilepsia.* 2011;52(7):1211-22. Epub 2011/05/17. doi: 10.1111/j.1528-1167.2011.03082.x. PubMed PMID: 21569017.
133. Bear MF. Therapeutic implications of the mGluR theory of fragile X mental retardation. *Genes Brain Behav.* 2005;4(6):393-8. Epub 2005/08/16. doi: 10.1111/j.1601-183X.2005.00135.x. PubMed PMID: 16098137.
134. Gibson JR, Bartley AF, Hays SA, Huber KM. Imbalance of Neocortical Excitation and Inhibition and Altered UP States Reflect Network Hyperexcitability in the Mouse Model of Fragile X Syndrome. *Journal of Neurophysiology.* 2008;100(5):2615-26. doi: 10.1152/jn.90752.2008. PubMed PMID: 18784272.
135. Antoine MW, Langberg T, Schnepel P, Feldman DE. Increased Excitation-Inhibition Ratio Stabilizes Synapse and Circuit Excitability in Four Autism Mouse Models. *Neuron.* 2019;101(4):648-61.e4. Epub 2019/01/27. doi: 10.1016/j.neuron.2018.12.026. PubMed PMID: 30679017; PMCID: PMC6733271.

136. Pfeiffer BE, Huber KM. The State of Synapses in Fragile X Syndrome. *The Neuroscientist*. 2009;15(5):549-67. doi: 10.1177/1073858409333075.
137. Aoto J, Nam CI, Poon MM, Ting P, Chen L. Synaptic signaling by all-trans retinoic acid in homeostatic synaptic plasticity. *Neuron*. 2008;60(2):308-20. Epub 2008/10/30. doi: 10.1016/j.neuron.2008.08.012. PubMed PMID: 18957222; PMCID: PMC2634746.
138. Zhang Z, Marro SG, Zhang Y, Arendt KL, Patzke C, Zhou B, Fair T, Yang N, Südhof TC, Wernig M, Chen L. The fragile X mutation impairs homeostatic plasticity in human neurons by blocking synaptic retinoic acid signaling. *Sci Transl Med*. 2018;10(452). Epub 2018/08/03. doi: 10.1126/scitranslmed.aar4338. PubMed PMID: 30068571; PMCID: PMC6317709.
139. Lee KY, Jewett KA, Chung HJ, Tsai NP. Loss of fragile X protein FMRP impairs homeostatic synaptic downscaling through tumor suppressor p53 and ubiquitin E3 ligase Nedd4-2. *Hum Mol Genet*. 2018;27(16):2805-16. Epub 2018/05/18. doi: 10.1093/hmg/ddy189. PubMed PMID: 29771335; PMCID: PMC6454515.
140. Woolsey TA, Van der Loos H. The structural organization of layer IV in the somatosensory region (SI) of mouse cerebral cortex. The description of a cortical field composed of discrete cytoarchitectonic units. *Brain Res*. 1970;17(2):205-42. Epub 1970/01/20. doi: 10.1016/0006-8993(70)90079-x. PubMed PMID: 4904874.
141. Staiger JF, Petersen CCH. Neuronal Circuits in Barrel Cortex for Whisker Sensory Perception. *Physiol Rev*. 2021;101(1):353-415. Epub 2020/08/21. doi: 10.1152/physrev.00019.2019. PubMed PMID: 32816652.
142. Morita T, Kang H, Wolfe J, Jadhav SP, Feldman DE. Psychometric curve and behavioral strategies for whisker-based texture discrimination in rats. *PLoS One*. 2011;6(6):e20437. Epub 2011/06/16. doi: 10.1371/journal.pone.0020437. PubMed PMID: 21673811; PMCID: PMC3106007.
143. Sofroniew NJ, Svoboda K. Whisking. *Curr Biol*. 2015;25(4):R137-40. Epub 2015/02/19. doi: 10.1016/j.cub.2015.01.008. PubMed PMID: 25689904.
144. Petersen CCH. Sensorimotor processing in the rodent barrel cortex. *Nat Rev Neurosci*. 2019;20(9):533-46. Epub 2019/08/02. doi: 10.1038/s41583-019-0200-y. PubMed PMID: 31367018; PMCID: PMC7116865.
145. Roohbakhsh A, Shamsizadeh A, Arababadi MK, Ayoobi F, Fatemi I, Allahtavakoli M, Mohammad-Zadeh M. Tactile learning in rodents: Neurobiology and neuropharmacology. *Life Sci*. 2016;147:1-8. Epub 2016/01/24. doi: 10.1016/j.lfs.2016.01.031. PubMed PMID: 26800784.
146. Takatoh J, Prevosto V, Wang F. Vibrissa sensory neurons: Linking distinct morphology to specific physiology and function. *Neuroscience*. 2018;368:109-14. Epub 2017/07/05. doi: 10.1016/j.neuroscience.2017.06.033. PubMed PMID: 28673712; PMCID: PMC5726905.
147. Petersen CC. The functional organization of the barrel cortex. *Neuron*. 2007;56(2):339-55. Epub 2007/10/30. doi: 10.1016/j.neuron.2007.09.017. PubMed PMID: 17964250.

148. Harding-Forrester S, Feldman DE. Chapter 4 - Somatosensory maps. In: Vallar G, Coslett HB, editors. *Handbook of Clinical Neurology*: Elsevier; 2018. p. 73-102.
149. Mo C, Petrof I, Viaene AN, Sherman SM. Synaptic properties of the lemniscal and paralemniscal pathways to the mouse somatosensory thalamus. *Proceedings of the National Academy of Sciences*. 2017;114(30):E6212-E21. doi: 10.1073/pnas.1703222114.
150. Constantinople CM, Bruno RM. Deep cortical layers are activated directly by thalamus. *Science*. 2013;340(6140):1591-4. Epub 2013/07/03. doi: 10.1126/science.1236425. PubMed PMID: 23812718; PMCID: PMC4203320.
151. Alloway KD. Information processing streams in rodent barrel cortex: the differential functions of barrel and septal circuits. *Cereb Cortex*. 2008;18(5):979-89. Epub 2007/08/19. doi: 10.1093/cercor/bhm138. PubMed PMID: 17702950.
152. Petersen Carl CH, Crochet S. Synaptic Computation and Sensory Processing in Neocortical Layer 2/3. *Neuron*. 2013;78(1):28-48. doi: 10.1016/j.neuron.2013.03.020.
153. Feldmeyer D, Egger V, Lubke J, Sakmann B. Reliable synaptic connections between pairs of excitatory layer 4 neurones within a single 'barrel' of developing rat somatosensory cortex. *J Physiol*. 1999;521 Pt 1(Pt 1):169-90. Epub 1999/11/24. doi: 10.1111/j.1469-7793.1999.00169.x. PubMed PMID: 10562343; PMCID: PMC2269646.
154. Jadhav SP, Wolfe J, Feldman DE. Sparse temporal coding of elementary tactile features during active whisker sensation. *Nat Neurosci*. 2009;12(6):792-800. Epub 2009/05/12. doi: 10.1038/nn.2328. PubMed PMID: 19430473.
155. Bale MR, Maravall M. Organization of sensory feature selectivity in the whisker system. *Neuroscience*. 2018;368:70-80. Epub 2017/09/18. doi: 10.1016/j.neuroscience.2017.09.014. PubMed PMID: 28918260; PMCID: PMC5798594.
156. Wang HC, LeMessurier AM, Feldman DE. Tuning instability of non-columnar neurons in the salt-and-pepper whisker map in somatosensory cortex. *Nat Commun*. 2022;13(1):6611. Epub 2022/11/05. doi: 10.1038/s41467-022-34261-1. PubMed PMID: 36329010; PMCID: PMC9633707.
157. Galvez R, Gopal AR, Greenough WT. Somatosensory cortical barrel dendritic abnormalities in a mouse model of the fragile X mental retardation syndrome. *Brain Res*. 2003;971(1):83-9. Epub 2003/04/15. doi: 10.1016/s0006-8993(03)02363-1. PubMed PMID: 12691840.
158. Nimchinsky EA, Oberlander AM, Svoboda K. Abnormal development of dendritic spines in FMR1 knock-out mice. *J Neurosci*. 2001;21(14):5139-46. Epub 2001/07/05. doi: 10.1523/jneurosci.21-14-05139.2001. PubMed PMID: 11438589; PMCID: PMC6762842.
159. Pan F, Aldridge GM, Greenough WT, Gan WB. Dendritic spine instability and insensitivity to modulation by sensory experience in a mouse model of fragile X syndrome. *Proc Natl Acad Sci U S A*. 2010;107(41):17768-73. Epub 2010/09/24. doi: 10.1073/pnas.1012496107. PubMed PMID: 20861447; PMCID: PMC2955121.

160. Bureau I, Shepherd GMG, Svoboda K. Circuit and Plasticity Defects in the Developing Somatosensory Cortex of *Fmr1* Knock-Out Mice. *The Journal of Neuroscience*. 2008;28(20):5178. doi: 10.1523/JNEUROSCI.1076-08.2008.
161. Harlow EG, Till SM, Russell TA, Wijetunge LS, Kind P, Contractor A. Critical period plasticity is disrupted in the barrel cortex of FMR1 knockout mice. *Neuron*. 2010;65(3):385-98. Epub 2010/02/18. doi: 10.1016/j.neuron.2010.01.024. PubMed PMID: 20159451; PMCID: PMC2825250.
162. Juczewski K, von Richthofen H, Bagni C, Celikel T, Fisone G, Krieger P. Somatosensory map expansion and altered processing of tactile inputs in a mouse model of fragile X syndrome. *Neurobiol Dis*. 2016;96:201-15. Epub 2016/10/19. doi: 10.1016/j.nbd.2016.09.007. PubMed PMID: 27616423.
163. He CX, Cantu DA, Mantri SS, Zeiger WA, Goel A, Portera-Cailliau C. Tactile Defensiveness and Impaired Adaptation of Neuronal Activity in the Fmr1 Knock-Out Mouse Model of Autism. *J Neurosci*. 2017;37(27):6475-87. Epub 2017/06/14. doi: 10.1523/jneurosci.0651-17.2017. PubMed PMID: 28607173; PMCID: PMC5511879.
164. Arnett MT, Herman DH, McGee AW. Deficits in tactile learning in a mouse model of fragile X syndrome. *PLoS One*. 2014;9(10):e109116. Epub 2014/10/09. doi: 10.1371/journal.pone.0109116. PubMed PMID: 25296296; PMCID: PMC4189789.
165. Todd PK, Malter JS, Mack KJ. Whisker stimulation-dependent translation of FMRP in the barrel cortex requires activation of type I metabotropic glutamate receptors. *Brain Res Mol Brain Res*. 2003;110(2):267-78. Epub 2003/02/20. doi: 10.1016/s0169-328x(02)00657-5. PubMed PMID: 12591163.
166. Hubel DH, Wiesel TN. Receptive fields, binocular interaction and functional architecture in the cat's visual cortex. *J Physiol*. 1962;160(1):106-54. Epub 1962/01/01. doi: 10.1113/jphysiol.1962.sp006837. PubMed PMID: 14449617; PMCID: PMC1359523.
167. Desai NS, Cudmore RH, Nelson SB, Turrigiano GG. Critical periods for experience-dependent synaptic scaling in visual cortex. *Nat Neurosci*. 2002;5(8):783-9. Epub 2002/06/25. doi: 10.1038/nn878. PubMed PMID: 12080341.
168. Wen W, Turrigiano GG. Developmental Regulation of Homeostatic Plasticity in Mouse Primary Visual Cortex. *The Journal of Neuroscience*. 2021;41(48):9891. doi: 10.1523/JNEUROSCI.1200-21.2021.
169. Goel A, Lee HK. Persistence of experience-induced homeostatic synaptic plasticity through adulthood in superficial layers of mouse visual cortex. *J Neurosci*. 2007;27(25):6692-700. Epub 2007/06/22. doi: 10.1523/jneurosci.5038-06.2007. PubMed PMID: 17581956; PMCID: PMC2601561.
170. Stern EA, Maravall M, Svoboda K. Rapid development and plasticity of layer 2/3 maps in rat barrel cortex in vivo. *Neuron*. 2001;31(2):305-15. Epub 2001/08/15. doi: 10.1016/s0896-6273(01)00360-9. PubMed PMID: 11502260.

171. Maravall M, Stern EA, Svoboda K. Development of intrinsic properties and excitability of layer 2/3 pyramidal neurons during a critical period for sensory maps in rat barrel cortex. *J Neurophysiol.* 2004;92(1):144-56. Epub 2004/02/20. doi: 10.1152/jn.00598.2003. PubMed PMID: 14973314.
172. Schierloh A, Eder M, Zieglgänsberger W, Dodt HU. Effects of sensory deprivation on columnar organization of neuronal circuits in the rat barrel cortex. *Eur J Neurosci.* 2004;20(4):1118-24. Epub 2004/08/13. doi: 10.1111/j.1460-9568.2004.03557.x. PubMed PMID: 15305882.
173. Schierloh A, Eder M, Zieglgänsberger W, Dodt HU. Sensory deprivation changes the pattern of synaptic connectivity in rat barrel cortex. *Neuroreport.* 2003;14(14):1787-91. Epub 2003/10/10. doi: 10.1097/00001756-200310060-00006. PubMed PMID: 14534421.
174. Glazewski S, Greenhill S, Fox K. Time-course and mechanisms of homeostatic plasticity in layers 2/3 and 5 of the barrel cortex. *Philosophical Transactions of the Royal Society B: Biological Sciences.* 2017;372:20160150. doi: 10.1098/rstb.2016.0150.
175. Gainey MA, Feldman DE. Multiple shared mechanisms for homeostatic plasticity in rodent somatosensory and visual cortex. *Philos Trans R Soc Lond B Biol Sci.* 2017;372(1715). Epub 2017/01/18. doi: 10.1098/rstb.2016.0157. PubMed PMID: 28093551; PMCID: PMC5247589.
176. Gainey MA, Aman JW, Feldman DE. Rapid Disinhibition by Adjustment of PV Intrinsic Excitability during Whisker Map Plasticity in Mouse S1. *The Journal of neuroscience : the official journal of the Society for Neuroscience.* 2018;38(20):4749-61. Epub 2018/04/20. doi: 10.1523/JNEUROSCI.3628-17.2018. PubMed PMID: 29678876.
177. Lakhani A, Gonzalez-Islas C, Sabra Z, Au Yong N, Wenner P. Homeostatic Regulation of Spike Rate within Bursts in Two Distinct Preparations. *eNeuro.* 2024;11(9):ENEURO.0259-24.2024. doi: 10.1523/ENEURO.0259-24.2024.
178. Hamood AW, Marder E. Animal-to-Animal Variability in Neuromodulation and Circuit Function. *Cold Spring Harb Symp Quant Biol.* 2014;79:21-8. Epub 2015/04/17. doi: 10.1101/sqb.2014.79.024828. PubMed PMID: 25876630; PMCID: PMC4610821.
179. Goaillard JM, Marder E. Ion Channel Degeneracy, Variability, and Covariation in Neuron and Circuit Resilience. *Annu Rev Neurosci.* 2021;44:335-57. Epub 20210326. doi: 10.1146/annurev-neuro-092920-121538. PubMed PMID: 33770451.
180. Liu Z, Golowasch J, Marder E, Abbott LF. A model neuron with activity-dependent conductances regulated by multiple calcium sensors. *J Neurosci.* 1998;18(7):2309-20. PubMed PMID: 9502792.
181. Hamood AW, Haddad SA, Otopalik AG, Rosenbaum P, Marder E. Quantitative Reevaluation of the Effects of Short- and Long-Term Removal of Descending Modulatory Inputs on the Pyloric Rhythm of the Crab, *Cancer borealis*. *eNeuro.* 2015;2(1). doi: 10.1523/ENEURO.0058-14.2015. PubMed PMID: 25914899; PMCID: PMC4408878.
182. Sakurai A, Tamvacakis AN, Katz PS. Hidden synaptic differences in a neural circuit underlie differential behavioral susceptibility to a neural injury. *Elife.* 2014;3. Epub 20140611. doi: 10.7554/eLife.02598. PubMed PMID: 24920390; PMCID: PMC4084405.

183. Niemeyer N, Schleimer JH, Schreiber S. Biophysical models of intrinsic homeostasis: Firing rates and beyond. *Curr Opin Neurobiol.* 2021;70:81-8. Epub 2021/08/29. doi: 10.1016/j.conb.2021.07.011. PubMed PMID: 34454303.
184. Buzsáki G, Csicsvari J, Dragoi G, Harris K, Henze D, Hirase H. Homeostatic maintenance of neuronal excitability by burst discharges in vivo. *Cereb Cortex.* 2002;12(9):893-9. Epub 2002/08/17. doi: 10.1093/cercor/12.9.893. PubMed PMID: 12183388.
185. Fong MF, Newman JP, Potter SM, Wenner P. Upward synaptic scaling is dependent on neurotransmission rather than spiking. *Nat Commun.* 2015;6:6339. Epub 2015/03/10. doi: 10.1038/ncomms7339. PubMed PMID: 25751516; PMCID: PMC4355957.
186. Weihberger O, Okujeni S, Mikkonen JE, Egert U. Quantitative examination of stimulus-response relations in cortical networks in vitro. *J Neurophysiol.* 2013;109(7):1764-74. Epub 2013/01/01. doi: 10.1152/jn.00481.2012. PubMed PMID: 23274313.
187. Corner MA, van Pelt J, Wolters PS, Baker RE, Nuytinck RH. Physiological effects of sustained blockade of excitatory synaptic transmission on spontaneously active developing neuronal networks--an inquiry into the reciprocal linkage between intrinsic biorhythms and neuroplasticity in early ontogeny. *Neurosci Biobehav Rev.* 2002;26(2):127-85. Epub 2002/02/22. doi: 10.1016/s0149-7634(01)00062-8. PubMed PMID: 11856557.
188. Gonzalez-Islas C, Sabra Z, Fong MF, Yilmam P, Au Yong N, Engisch K, Wenner P. GABAergic synaptic scaling is triggered by changes in spiking activity rather than AMPA receptor activation. *Elife.* 2024;12. Epub 20240628. doi: 10.7554/eLife.87753. PubMed PMID: 38941139.
189. Khawaled R, Bruening-Wright A, Adelman JP, Maylie J. Bicuculline block of small-conductance calcium-activated potassium channels. *Pflugers Arch.* 1999;438(3):314-21. doi: 10.1007/s004240050915. PubMed PMID: 10398861.
190. Wenner P, Bülow P. Homeostatic Plasticity in the CNS. Oxford University Press; 2019.
191. Gonzalez-Islas C, Wenner P, editors. Role of Spontaneous Activity in the Maturation of GABAergic Synapses in Embryonic Spinal Circuits 2010.
192. Blankenship AG, Feller MB. Mechanisms underlying spontaneous patterned activity in developing neural circuits. *Nat Rev Neurosci.* 2010;11(1):18-29. Epub 2009/12/03. doi: 10.1038/nrn2759. PubMed PMID: 19953103; PMCID: PMC2902252.
193. Turrigiano GG, Leslie KR, Desai NS, Rutherford LC, Nelson SB. Activity-dependent scaling of quantal amplitude in neocortical neurons. *Nature.* 1998;391(6670):892-6.
194. Bianchi D, Marasco A, Limongiello A, Marchetti C, Marie H, Tirozzi B, Migliore M. On the mechanisms underlying the depolarization block in the spiking dynamics of CA1 pyramidal neurons. *J Comput Neurosci.* 2012;33(2):207-25. Epub 20120205. doi: 10.1007/s10827-012-0383-y. PubMed PMID: 22310969.

195. Yang J, Prescott SA. Homeostatic regulation of neuronal function: importance of degeneracy and pleiotropy. *Front Cell Neurosci.* 2023;17:1184563. Epub 2023/06/19. doi: 10.3389/fncel.2023.1184563. PubMed PMID: 37333893; PMCID: PMC10272428.
196. Golowasch J, Goldman MS, Abbott LF, Marder E. Failure of averaging in the construction of a conductance-based neuron model. *J Neurophysiol.* 2002;87(2):1129-31. doi: 10.1152/jn.00412.2001. PubMed PMID: 11826077.
197. Sernagor E, Chub N, Ritter A, O'Donovan MJ. Pharmacological characterization of the rhythmic synaptic drive onto lumbosacral motoneurons in the chick embryo spinal cord. *J Neurosci.* 1995;15(11):7452-64.
198. Corner MA, Ramakers GJ. Spontaneous firing as an epigenetic factor in brain development--physiological consequences of chronic tetrodotoxin and picrotoxin exposure on cultured rat neocortex neurons. *Brain Res Dev Brain Res.* 1992;65(1):57-64. Epub 1992/01/17. doi: 10.1016/0165-3806(92)90008-k. PubMed PMID: 1551233.
199. Swensen AM, Bean BP. Robustness of burst firing in dissociated purkinje neurons with acute or long-term reductions in sodium conductance. *J Neurosci.* 2005;25(14):3509-20. doi: 10.1523/JNEUROSCI.3929-04.2005. PubMed PMID: 15814781; PMCID: PMC6725377.
200. He LS, Rue MCP, Morozova EO, Powell DJ, James EJ, Kar M, Marder E. Rapid adaptation to elevated extracellular potassium in the pyloric circuit of the crab, *Cancer borealis*. *J Neurophysiol.* 2020;123(5):2075-89. Epub 2020/04/23. doi: 10.1152/jn.00135.2020. PubMed PMID: 32319837; PMCID: PMC7444919.
201. O'Donovan MJ, Bonnot A, Wenner P, Mentis GZ. Calcium imaging of network function in the developing spinal cord. *Cell Calcium.* 2005;37(5):443-50. Epub 2005/04/12. doi: 10.1016/j.ceca.2005.01.012. PubMed PMID: 15820392.
202. Bakkum DJ, Radivojevic M, Frey U, Franke F, Hierlemann A, Takahashi H. Parameters for burst detection. *Front Comput Neurosci.* 2013;7:193. Epub 2014/01/13. doi: 10.3389/fncom.2013.00193. PubMed PMID: 24567714; PMCID: PMC3915237.
203. Ho J, Tumkaya T, Aryal S, Choi H, Claridge-Chang A. Moving beyond P values: data analysis with estimation graphics. *Nat Methods.* 2019;16(7):565-6. Epub 2019/06/21. doi: 10.1038/s41592-019-0470-3. PubMed PMID: 31217592.
204. Hagerman RJ, Berry-Kravis E, Hazlett HC, Bailey DB, Jr., Moine H, Kooy RF, Tassone F, Gantois I, Sonenberg N, Mandel JL, Hagerman PJ. Fragile X syndrome. *Nat Rev Dis Primers.* 2017;3:17065. Epub 2017/09/30. doi: 10.1038/nrdp.2017.65. PubMed PMID: 28960184.
205. Rais M, Binder DK, Razak KA, Ethell IM. Sensory Processing Phenotypes in Fragile X Syndrome. *ASN Neuro.* 2018;10:1759091418801092-. doi: 10.1177/1759091418801092. PubMed PMID: 30231625.
206. Liu X, Kumar V, Tsai N-P, Auerbach BD. Hyperexcitability and Homeostasis in Fragile X Syndrome. *Front Mol Neurosci.* 2022;14(359). doi: 10.3389/fnmol.2021.805929.

207. Bhakar AL, Dölen G, Bear MF. The pathophysiology of fragile X (and what it teaches us about synapses). *Annu Rev Neurosci.* 2012;35:417-43. Epub 20120405. doi: 10.1146/annurev-neuro-060909-153138. PubMed PMID: 22483044; PMCID: PMC4327822.
208. Turrigiano G. Homeostatic synaptic plasticity: local and global mechanisms for stabilizing neuronal function. *Cold Spring Harb Perspect Biol.* 2012;4(1):a005736. Epub 2011/11/17. doi: 10.1101/cshperspect.a005736. PubMed PMID: 22086977; PMCID: PMC3249629.
209. Tien N-W, Kerschensteiner D. Homeostatic plasticity in neural development. *Neural Dev.* 2018;13(1):9. doi: 10.1186/s13064-018-0105-x.
210. Monday HR, Wang HC, Feldman DE. Circuit-level theories for sensory dysfunction in autism: convergence across mouse models. *Front Neurol.* 2023;14:1254297. Epub 2023/09/25. doi: 10.3389/fneur.2023.1254297. PubMed PMID: 37745660; PMCID: PMC10513044.
211. Zhang L, Liang Z, Zhu P, Li M, Yi YH, Liao WP, Su T. Altered intrinsic properties and bursting activities of neurons in layer IV of somatosensory cortex from Fmr-1 knockout mice. *Exp Neurol.* 2016;280:60-9. Epub 2016/04/07. doi: 10.1016/j.expneurol.2016.03.025. PubMed PMID: 27048919.
212. Feldmeyer D. Excitatory neuronal connectivity in the barrel cortex. *Front Neuroanat.* 2012;6:24. Epub 2012/07/17. doi: 10.3389/fnana.2012.00024. PubMed PMID: 22798946; PMCID: PMC3394394.
213. Wen JA, Barth AL. Input-specific critical periods for experience-dependent plasticity in layer 2/3 pyramidal neurons. *J Neurosci.* 2011;31(12):4456-65. Epub 2011/03/25. doi: 10.1523/jneurosci.6042-10.2011. PubMed PMID: 21430146; PMCID: PMC3066457.
214. Zhang Y, Bonnan A, Bony G, Ferezou I, Pietropaolo S, Ginger M, Sans N, Rossier J, Oostra B, LeMasson G, Frick A. Dendritic channelopathies contribute to neocortical and sensory hyperexcitability in Fmr1(-/y) mice. *Nat Neurosci.* 2014;17(12):1701-9. Epub 20141110. doi: 10.1038/nn.3864. PubMed PMID: 25383903.
215. Kourdougli N, Suresh A, Liu B, Juarez P, Lin A, Chung DT, Graven Sams A, Gandal MJ, Martinez-Cerdeno V, Buonomano DV, Hall BJ, Mombereau C, Portera-Cailliau C. Improvement of sensory deficits in fragile X mice by increasing cortical interneuron activity after the critical period. *Neuron.* 2023;111(18):2863-80 e6. Epub 20230713. doi: 10.1016/j.neuron.2023.06.009. PubMed PMID: 37451263; PMCID: PMC10529373.
216. Goel A, Cantu DA, Guilfoyle J, Chaudhari GR, Newadkar A, Todisco B, de Alba D, Kourdougli N, Schmitt LM, Pedapati E, Erickson CA, Portera-Cailliau C. Impaired perceptual learning in a mouse model of Fragile X syndrome is mediated by parvalbumin neuron dysfunction and is reversible. *Nat Neurosci.* 2018;21(10):1404-11. Epub 2018/09/27. doi: 10.1038/s41593-018-0231-0. PubMed PMID: 30250263; PMCID: PMC6161491.
217. Kourdougli N, Nomura T, Wu M, Heuvelmans A, Dobler Z, Contractor A, Portera-Cailliau C. The NKCC1 inhibitor bumetanide restores cortical feedforward inhibition and lessens sensory hypersensitivity in early postnatal fragile X mice. *Biol Psychiatry.* 2024. Epub 20240629. doi: 10.1016/j.biopsych.2024.06.023. PubMed PMID: 38950809.

218. He Q, Nomura T, Xu J, Contractor A. The Developmental Switch in GABA Polarity Is Delayed in Fragile X Mice. *The Journal of Neuroscience*. 2014;34(2):446-50. doi: 10.1523/jneurosci.4447-13.2014.
219. Greenhill SD, Ranson A, Fox K. Hebbian and Homeostatic Plasticity Mechanisms in Regular Spiking and Intrinsic Bursting Cells of Cortical Layer 5. *Neuron*. 2015;88(3):539-52. Epub 2015/10/21. doi: 10.1016/j.neuron.2015.09.025. PubMed PMID: 26481037; PMCID: PMC4643308.
220. Li L, Gainey MA, Goldbeck JE, Feldman DE. Rapid homeostasis by disinhibition during whisker map plasticity. *Proc Natl Acad Sci U S A*. 2014;111(4):1616-21. Epub 20140113. doi: 10.1073/pnas.1312455111. PubMed PMID: 24474788; PMCID: PMC3910567.
221. Jacob V, Petreanu L, Wright N, Svoboda K, Fox K. Regular spiking and intrinsic bursting pyramidal cells show orthogonal forms of experience-dependent plasticity in layer V of barrel cortex. *Neuron*. 2012;73(2):391-404. doi: 10.1016/j.neuron.2011.11.034. PubMed PMID: 22284191; PMCID: PMC3524456.
222. Kubota J, Mikami Y, Kanemaru K, Sekiya H, Okubo Y, Iino M. Whisker experience-dependent mGluR signaling maintains synaptic strength in the mouse adolescent cortex. *Eur J Neurosci*. 2016;44(3):2004-14. Epub 2016/05/27. doi: 10.1111/ejn.13285. PubMed PMID: 27225340.
223. Jamann N, Dannehl D, Lehmann N, Wagener R, Thielemann C, Schultz C, Staiger J, Kole MHP, Engelhardt M. Sensory input drives rapid homeostatic scaling of the axon initial segment in mouse barrel cortex. *Nat Commun*. 2021;12(1):23. Epub 20210104. doi: 10.1038/s41467-020-20232-x. PubMed PMID: 33397944; PMCID: PMC7782484.
224. Breton JD, Stuart GJ. Loss of sensory input increases the intrinsic excitability of layer 5 pyramidal neurons in rat barrel cortex. *J Physiol*. 2009;587(Pt 21):5107-19. Epub 20090907. doi: 10.1113/jphysiol.2009.180943. PubMed PMID: 19736297; PMCID: PMC2790252.
225. Barnes SJ, Sammons RP, Jacobsen RI, Mackie J, Keller GB, Keck T. Subnetwork-Specific Homeostatic Plasticity in Mouse Visual Cortex In Vivo. *Neuron*. 2015;86(5):1290-303. doi: 10.1016/j.neuron.2015.05.010. PubMed PMID: 26050045; PMCID: PMC4460189.
226. Antar LN, Li C, Zhang H, Carroll RC, Bassell GJ. Local functions for FMRP in axon growth cone motility and activity-dependent regulation of filopodia and spine synapses. *Mol Cell Neurosci*. 2006;32(1-2):37-48. Epub 20060502. doi: 10.1016/j.mcn.2006.02.001. PubMed PMID: 16631377.
227. Jacob V, Estebanez L, Le Cam J, Tiercelin JY, Parra P, Parésys G, Shulz DE. The Matrix: a new tool for probing the whisker-to-barrel system with natural stimuli. *J Neurosci Methods*. 2010;189(1):65-74. Epub 2010/04/07. doi: 10.1016/j.jneumeth.2010.03.020. PubMed PMID: 20362614.
228. Pachitariu M, Steinmetz N, Kadir S, Carandini M, Kenneth D H. Kilosort: realtime spike-sorting for extracellular electrophysiology with hundreds of channels. *bioRxiv*. 2016:061481. doi: 10.1101/061481.
229. Rossant C, Kadir SN, Goodman DFM, Schulman J, Hunter MLD, Saleem AB, Grosmark A, Belluscio M, Denfield GH, Ecker AS, Tolias AS, Solomon S, Buzsaki G, Carandini M, Harris KD.

Spike sorting for large, dense electrode arrays. *Nat Neurosci.* 2016;19(4):634-41. Epub 2016/03/14. doi: 10.1038/nn.4268. PubMed PMID: 26974951.

230. Rodgers CC, Nogueira R, Pil BC, Greeman EA, Park JM, Hong YK, Fusi S, Bruno RM. Sensorimotor strategies and neuronal representations for shape discrimination. *Neuron.* 2021;109(14):2308-25.e10. doi: 10.1016/j.neuron.2021.05.019.

231. Wright NC, Borden PY, Liew YJ, Bolus MF, Stoy WM, Forest CR, Stanley GB. Rapid Cortical Adaptation and the Role of Thalamic Synchrony during Wakefulness. *J Neurosci.* 2021;41(25):5421-39. Epub 2021/05/15. doi: 10.1523/jneurosci.3018-20.2021. PubMed PMID: 33986072; PMCID: PMC8221593.

232. Sederberg AJ, Pala A, Zheng HJV, He BJ, Stanley GB. State-aware detection of sensory stimuli in the cortex of the awake mouse. *PLoS Comput Biol.* 2019;15(5):e1006716. Epub 2019/06/01. doi: 10.1371/journal.pcbi.1006716. PubMed PMID: 31150385; PMCID: PMC6561583.

233. Hooks BM, Hires SA, Zhang YX, Huber D, Petreanu L, Svoboda K, Shepherd GM. Laminar analysis of excitatory local circuits in vibrissal motor and sensory cortical areas. *PLoS Biol.* 2011;9(1):e1000572. Epub 2011/01/20. doi: 10.1371/journal.pbio.1000572. PubMed PMID: 21245906; PMCID: PMC3014926.

234. Isett BR, Feldman DE. Cortical Coding of Whisking Phase during Surface Whisking. *Current Biology.* 2020;30(16):3065-74.e5. doi: <https://doi.org/10.1016/j.cub.2020.05.064>.

235. Pape HC, McCormick DA. Noradrenaline and serotonin selectively modulate thalamic burst firing by enhancing a hyperpolarization-activated cation current. *Nature.* 1989;340(6236):715-8. doi: 10.1038/340715a0. PubMed PMID: 2475782.

236. Marder E. Variability, compensation, and modulation in neurons and circuits. *Proc Natl Acad Sci U S A.* 2011;108 Suppl 3(Suppl 3):15542-8. Epub 2011/03/09. doi: 10.1073/pnas.1010674108. PubMed PMID: 21383190; PMCID: PMC3176600.

237. Gross AS, Harry AC, Clifton CS, Della Pasqua O. Clinical trial diversity: An opportunity for improved insight into the determinants of variability in drug response. *Br J Clin Pharmacol.* 2022;88(6):2700-17. Epub 20220217. doi: 10.1111/bcp.15242. PubMed PMID: 35088432; PMCID: PMC9306578.

238. Tulloch JF. Bias and variability in clinical research. *Clin Orthod Res.* 1998;1(2):94-6. doi: 10.1111/ocr.1998.1.2.94. PubMed PMID: 10321136.

239. Li H, Chen Z, Zhu W. Variability: Human nature and its impact on measurement and statistical analysis. *J Sport Health Sci.* 2019;8(6):527-31. Epub 20190618. doi: 10.1016/j.jshs.2019.06.002. PubMed PMID: 31720063; PMCID: PMC6835034.

240. Whitacre JM. Degeneracy: a link between evolvability, robustness and complexity in biological systems. *Theoretical Biology and Medical Modelling.* 2010;7(1):6. doi: 10.1186/1742-4682-7-6.

241. Whitacre JM, Atamas SP. Degeneracy allows for both apparent homogeneity and diversification in populations. *Biosystems*. 2012;110(1):34-42. Epub 20120810. doi: 10.1016/j.biosystems.2012.08.003. PubMed PMID: 22910487; PMCID: PMC3722245.
242. Edelman GM, Gally JA. Degeneracy and complexity in biological systems. *Proc Natl Acad Sci U S A*. 2001;98(24):13763-8. Epub 20011106. doi: 10.1073/pnas.231499798. PubMed PMID: 11698650; PMCID: PMC61115.
243. Kepecs A, Wang X-J, Lisman J. Bursting Neurons Signal Input Slope. *The Journal of Neuroscience*. 2002;22(20):9053. doi: 10.1523/JNEUROSCI.22-20-09053.2002.
244. Zeldenrust F, Wadman WJ, Englitz B. Neural Coding With Bursts-Current State and Future Perspectives. *Front Comput Neurosci*. 2018;12:48. Epub 20180706. doi: 10.3389/fncom.2018.00048. PubMed PMID: 30034330; PMCID: PMC6043860.
245. Hanson MG, Milner LD, Landmesser LT. Spontaneous rhythmic activity in early chick spinal cord influences distinct motor axon pathfinding decisions. *Brain Res Rev*. 2008;57(1):77-85. Epub 20070801. doi: 10.1016/j.brainresrev.2007.06.021. PubMed PMID: 17920131; PMCID: PMC2233604.
246. Milner LD, Landmesser LT. Cholinergic and GABAergic inputs drive patterned spontaneous motoneuron activity before target contact. *J Neurosci*. 1999;19(8):3007-22. doi: 10.1523/jneurosci.19-08-03007.1999. PubMed PMID: 10191318; PMCID: PMC6782286.
247. Wenner PA. Chapter 10 - Development of the locomotor system—Chick embryo. In: Whelan PJ, Sharples SA, editors. *The Neural Control of Movement*: Academic Press; 2020. p. 221-36.
248. Friedenberger Z, Harkin E, Tóth K, Naud R. Silences, spikes and bursts: Three-part knot of the neural code. *The Journal of Physiology*. 2023;601(23):5165-93. doi: <https://doi.org/10.1113/JP281510>.
249. Slomowitz E, Styr B, Vertkin I, Milshtein-Parush H, Nelken I, Slutsky M, Slutsky I. Interplay between population firing stability and single neuron dynamics in hippocampal networks. *Elife*. 2015;4:e04378. doi: 10.7554/eLife.04378. PubMed PMID: 25556699.
250. Katsenelson M, Shapira I, Abbas E, Jevdokimenko K, Styr B, Ruggiero A, Aïd S, Fornasiero EF, Holzenberger M, Rizzoli SO, Slutsky I. IGF-1 receptor regulates upward firing rate homeostasis via the mitochondrial calcium uniporter. *Proc Natl Acad Sci U S A*. 2022;119(33):e2121040119. Epub 2022/08/10. doi: 10.1073/pnas.2121040119. PubMed PMID: 35943986; PMCID: PMC9388073.
251. De S, Balakrishnan J. Burst mechanisms and burst synchronization in a system of coupled type-I and type-II neurons. *Communications in Nonlinear Science and Numerical Simulation*. 2020;90:105391. doi: <https://doi.org/10.1016/j.cnsns.2020.105391>.
252. Ohta M, Asabuki T, Fukai T. Intrinsic bursts facilitate learning of Lévy flight movements in recurrent neural network models. *Scientific Reports*. 2022;12(1):4951. doi: 10.1038/s41598-022-08953-z.

253. Chen L, Li X, Tjia M, Thapliyal S. Homeostatic plasticity and excitation-inhibition balance: The good, the bad, and the ugly. *Curr Opin Neurobiol.* 2022;75:102553. doi: <https://doi.org/10.1016/j.conb.2022.102553>.
254. Smith-Dijak AI, Nassrallah WB, Zhang LYJ, Geva M, Hayden MR, Raymond LA. Impairment and Restoration of Homeostatic Plasticity in Cultured Cortical Neurons From a Mouse Model of Huntington Disease. *Front Cell Neurosci.* 2019;13:209. Epub 20190516. doi: [10.3389/fncel.2019.00209](https://doi.org/10.3389/fncel.2019.00209). PubMed PMID: 31156395; PMCID: PMC6532531.
255. Erzurumlu RS, Gaspar P. Development and critical period plasticity of the barrel cortex. *Eur J Neurosci.* 2012;35(10):1540-53. Epub 2012/05/23. doi: [10.1111/j.1460-9568.2012.08075.x](https://doi.org/10.1111/j.1460-9568.2012.08075.x). PubMed PMID: 22607000; PMCID: PMC3359866.
256. Zhang Y, Bonnan A, Bony G, Ferezou I, Pietropaolo S, Ginger M, Sans N, Rossier J, Oostra B, LeMasson G, Frick A. Dendritic channelopathies contribute to neocortical and sensory hyperexcitability in *Fmr1*-/*y* mice. *Nat Neurosci.* 2014;17(12):1701-9. doi: [10.1038/nn.3864](https://doi.org/10.1038/nn.3864).
257. Perche O, Lesne F, Patat A, Raab S, Twyman R, Ring RH, Briault S. Electroretinography and contrast sensitivity, complementary translational biomarkers of sensory deficits in the visual system of individuals with fragile X syndrome. *J Neurodev Disord.* 2021;13(1):45. Epub 20211008. doi: [10.1186/s11689-021-09375-0](https://doi.org/10.1186/s11689-021-09375-0). PubMed PMID: 34625026; PMCID: PMC8501595.
258. Van der Molen MJ, Van der Molen MW, Ridderinkhof KR, Hamel BC, Curfs LM, Ramakers GJ. Auditory change detection in fragile X syndrome males: a brain potential study. *Clin Neurophysiol.* 2012;123(7):1309-18. Epub 20111220. doi: [10.1016/j.clinph.2011.11.039](https://doi.org/10.1016/j.clinph.2011.11.039). PubMed PMID: 22192499.
259. Berzhanskaya J, Phillips MA, Shen J, Colonnese MT. Sensory hypo-excitability in a rat model of fetal development in Fragile X Syndrome. *Scientific Reports.* 2016;6(1):30769. doi: [10.1038/srep30769](https://doi.org/10.1038/srep30769).
260. Wheeler AC, Sideris J, Hagerman R, Berry-Kravis E, Tassone F, Bailey DB, Jr. Developmental profiles of infants with an FMR1 premutation. *J Neurodev Disord.* 2016;8:40. Epub 20161103. doi: [10.1186/s11689-016-9171-8](https://doi.org/10.1186/s11689-016-9171-8). PubMed PMID: 27822316; PMCID: PMC5095966.
261. Raspa M, Wylie A, Wheeler AC, Kolacz J, Edwards A, Heilman K, Porges SW. Sensory Difficulties in Children With an FMR1 Premutation. *Front Genet.* 2018;9:351. Epub 20180828. doi: [10.3389/fgene.2018.00351](https://doi.org/10.3389/fgene.2018.00351). PubMed PMID: 30233641; PMCID: PMC6127619.
262. Jewett KA, Lee KY, Eagleman DE, Soriano S, Tsai NP. Dysregulation and restoration of homeostatic network plasticity in fragile X syndrome mice. *Neuropharmacology.* 2018;138:182-92. Epub 2018/06/12. doi: [10.1016/j.neuropharm.2018.06.011](https://doi.org/10.1016/j.neuropharm.2018.06.011). PubMed PMID: 29890190; PMCID: PMC6349417.
263. Paoletti P, Bellone C, Zhou Q. NMDA receptor subunit diversity: impact on receptor properties, synaptic plasticity and disease. *Nat Rev Neurosci.* 2013;14(6):383-400. doi: [10.1038/nrn3504](https://doi.org/10.1038/nrn3504). PubMed PMID: 23686171.

264. Darnell JC, Klann E. The translation of translational control by FMRP: therapeutic targets for FXS. *Nat Neurosci.* 2013;16(11):1530-6. doi: 10.1038/nn.3379.
265. Yau S-Y, Bettio L, Chiu J, Chiu C, Christie BR. Fragile-X Syndrome Is Associated With NMDA Receptor Hypofunction and Reduced Dendritic Complexity in Mature Dentate Granule Cells. *Front Mol Neurosci.* 2019;11:495-. doi: 10.3389/fnmol.2018.00495. PubMed PMID: 30705620.
266. Yau SY, Bostrom CA, Chiu J, Fontaine CJ, Sawchuk S, Meconi A, Wortman RC, Truesdell E, Truesdell A, Chiu C, Hryciw BN, Eadie BD, Ghilan M, Christie BR. Impaired bidirectional NMDA receptor dependent synaptic plasticity in the dentate gyrus of adult female *Fmr1* heterozygous knockout mice. *Neurobiology of Disease.* 2016;96:261-70. doi: <https://doi.org/10.1016/j.nbd.2016.09.012>.
267. Bostrom CA, Majaess N-M, Morch K, White E, Eadie BD, Christie BR. Rescue of NMDAR-Dependent Synaptic Plasticity in *Fmr1* Knock-Out Mice. *Cerebral Cortex.* 2013;25(1):271-9. doi: 10.1093/cercor/bht237.
268. Breton J-D, Stuart GJ. Loss of sensory input increases the intrinsic excitability of layer 5 pyramidal neurons in rat barrel cortex. *The Journal of physiology.* 2009;587(Pt 21):5107-19. Epub 2009/09/07. doi: 10.1113/jphysiol.2009.180943. PubMed PMID: 19736297.
269. Gainey MA, Wolfe R, Pourzia O, Feldman DE. Whisker Deprivation Drives Two Phases of Inhibitory Synapse Weakening in Layer 4 of Rat Somatosensory Cortex. *PLoS One.* 2016;11(2):e0148227-e. doi: 10.1371/journal.pone.0148227. PubMed PMID: 26840956.
270. Bender KJ, Allen CB, Bender VA, Feldman DE. Synaptic basis for whisker deprivation-induced synaptic depression in rat somatosensory cortex. *The Journal of neuroscience : the official journal of the Society for Neuroscience.* 2006;26(16):4155-65. doi: 10.1523/JNEUROSCI.0175-06.2006. PubMed PMID: 16624936.
271. Uzunova G, Pallanti S, Hollander E. Excitatory/inhibitory imbalance in autism spectrum disorders: Implications for interventions and therapeutics. *World J Biol Psychiatry.* 2016;17(3):174-86. Epub 20151015. doi: 10.3109/15622975.2015.1085597. PubMed PMID: 26469219.
272. Cheetham CE, Fox K. The role of sensory experience in presynaptic development is cortical area specific. *J Physiol.* 2011;589(Pt 23):5691-9. Epub 20110926. doi: 10.1113/jphysiol.2011.218347. PubMed PMID: 21946850; PMCID: PMC3249043.
273. Popescu MV, Polley DB. Monaural deprivation disrupts development of binaural selectivity in auditory midbrain and cortex. *Neuron.* 2010;65(5):718-31. doi: 10.1016/j.neuron.2010.02.019. PubMed PMID: 20223206; PMCID: PMC2849994.